

AN ANALYSIS OF PRESSURE-TEMPERATURE-TIME
HISTORIES OF ERODING OROGENIC BELTS

by

Carol Jacqueline Bryan

B.S. California Institute of Technology
(1984)

Submitted to the Department of
Earth, Atmospheric, and Planetary Sciences
in Partial Fulfillment of the
Requirements of the Degree of

MASTER OF SCIENCE

at the

MASSACHUSETTS INSTITUTE OF TECHNOLOGY

February, 1987

© Massachusetts Institute of Technology, 1987

Signature of Author _____
Department of Earth, Atmospheric, and Planetary Sciences
February 9, 1987

Certified by _____
Leigh Royden
Thesis Supervisor

Accepted by _____
William Brace
Chairman, Department Committee on Graduate Studies



AN ANALYSIS OF PRESSURE-TEMPERATURE-TIME HISTORIES
OF ERODING OROGENIC BELTS

Carol J. Bryan

Submitted to the Department of Earth, Atmospheric, and Planetary Sciences
on February 9, 1987 in partial fulfillment of the requirements for the
degree of Master of Science in Geophysics

ABSTRACT

A linear-programming technique was used to invert temperature-depth (Tz) data generated by the upward movement of a single rock mass through an evolving temperature structure to obtain bounds on the temperature structure of the lithosphere at specified times. The linear-programming inversion scheme inverts a matrix of constraints while optimizing a specified function, e.g., temperature at a specified depth and time. This matrix includes constraints on the radiogenic contribution, steady-state contribution, and contribution from an infinite sum of transient terms to the temperature structure, as well as constraints on some of the physical parameters of the model. The ultimate goal of this exercise is to determine the resolution of this inversion scheme in recovering ancient geotherms in orogenic belts.

Synthetic temperature-depth (Tz) data were generated from three initial geotherms using a finite difference approximation to the heat conduction equation. They were then inverted subject to various assumptions regarding the quality of the data, uncertainties in the values of the physical parameters of the model (i.e., temperature at the base of the lithosphere, radiogenic heat productivity, thermal diffusivity, lithospheric thickness, and uplift rate), and error introduced into the inverse problem through truncation of the infinite sum in the mathematical model. Ten million years following the onset of uplift and erosion, uncertainty in the Tz data of $\pm 5^\circ\text{C}$ yields uncertainty in the extremal bounds of $\pm 175^\circ\text{C}$, while uncertainty in the data of $\pm 50^\circ\text{C}$ increases these bounds to $\pm 500^\circ\text{C}$. Within 30 m.y. of the onset of uplift and erosion, these bounds decrease to $\pm 25^\circ\text{C}$ for data of $\pm 5^\circ\text{C}$ uncertainty and to $\pm 350^\circ\text{C}$ for data of $\pm 50^\circ\text{C}$ uncertainty. These uncertainties are more significant than those due to either uncertainty in any of the physical parameters or error due to truncation of the mathematical model. Of the physical parameters, the most important are uplift rate and radiogenic heating. Uncertainty in the uplift rate may result in extremal bounds which do not include the actual geotherm while uncertainty in the radiogenic heating may affect significantly the bounds on the temperature structure of the upper lithosphere, the region of primary interest.

Forward modelling techniques reveal that within 20 m.y. of the onset of uplift and erosion, only the two longest wavelength transient contributions to the temperature structure are non-negligible. Hence, the ability of the extremal bound linear-programming method to recover

the temperature structure at various wavelengths was also investigated. The lowest order transient term in the temperature structure can be determined extremely well no matter what the quality of the data. The temperature structure of the second order term can be well determined only if the data are of good quality. Resolution of the third order term requires not only data of excellent quality, but also truncation of the mathematical model to three transient terms. In general, resolution of shorter wavelength contributions to the temperature structure ($n \geq 4$) are not possible even if the data are of excellent quality.

TABLE OF CONTENTS

Abstract	1
Table of Contents	3
Introduction	5
Chapter I: Mathematical model and data generation	9
Introduction	9
Mathematical model	9
Generation of synthetic data	14
The Inverse problem	18
The General linear-programming problem	21
Chapter II: Extremal bounds on temperature	41
Introduction	41
Forward model	41
Inverse model	46
Conclusions	61
Figure Captions	63
Figures	70
Chapter III: Extremal bounds on the temperature at various wavelengths	86
Introduction	86
Forward model	87
Inverse model	89
Conclusions	95
Figure Captions	98
Figures	103

Discussion	116
References	120
Appendix A	122
Acknowledgements	128

INTRODUCTION

Over large areas of the earth, the heat flux through the earth's surface provides important information about the amount of heat generated in the earth and the temperature structure of the crust and upper mantle. However, because surface heat flow measures only the present-day thermal structure at the earth's surface, it cannot be used to reconstruct the thermal history of the underlying mantle. Heat flow data can also be used to estimate the present near-surface temperature in orogenic belts; however, it may not provide a good indication of the deep temperature structure in young and recently eroded orogenic belts. In such areas, near-surface thermal gradients may be disturbed by convection (Oxburgh and Turcotte, 1971). Also, erosion quickly elevates surface gradients, but has little effect on the deeper temperature structure. Hence, the temperature gradients may vary rapidly as a function of depth so that near surface thermal gradients often are not indicative of temperatures present at greater depths. In addition, rapid changes in the temperature structure with time may produce abrupt spatial variation in geothermal gradients which become difficult to resolve as the geotherm relaxes by conductive cooling.

Within many orogenic belts, petrologic data from metamorphic rocks now found at the earth's surface can provide direct information about temperatures present at deep crustal levels. (Oxburgh and Turcotte, 1974; Albarède, 1976; England and Richardson, 1977; Royden and Hodges, 1984). Mineral assemblages found within these rocks serve as

geothermometers and geobarometers that can be used to reconstruct the temperatures present as these rocks were uplifted to the surface through erosion. When coupled with age-dating from mineral isotopic systems, a reasonably complete pressure-temperature-time (PTt) history can be reconstructed for individual rock parcels (Selverstone, 1985). This data is especially important because it is the only possible means of obtaining temperature measurements at great depths.

Geothermometers and geobarometers are often used as indicators of the maximum metamorphic temperature and equilibrium pressure attained by a rock. These maximum metamorphic temperatures are reached at different depths and times for different crustal horizons. Although knowledge of these temperatures is important in constraining the erosional and cooling histories of ancient metamorphic terrains, it is desirable to describe the temperature structure of an orogen at a specified time (the geotherm). Although it is not a geotherm itself, the PTt path, as defined by England and Richardson (1977), is useful in this respect. Whereas a geotherm describes the variation of temperature with depth at a fixed time, a PTt path represents temperatures recorded at different depths and times for a single crustal horizon. Because it is generated by the upward movement of a crustal horizon through a changing temperature structure, it reflects both the changes in the geotherm with time and the erosional history of the orogen. While PTt paths can be directly related to true geotherms through mathematical analysis, the metamorphic arrays traditionally used by metamorphic petrologists to estimate geotherms actually represent the maximum temperatures attained

along a suite of PTt paths. Hence, unlike PTt paths, they cannot easily be related to the evolution of a single geotherm.

England and Thompson (1984) have modelled extensively the PTt paths that would be followed by rocks under a variety of conditions resulting from crustal thickening. They found the thermal evolution of a metamorphic terrain to depend on relatively few large scale parameters. In particular, they found that the principal controls on the temperature experienced by a buried rock are the depth of its burial, the heat source distribution, and the conductivity of the overburden. They also found that the maximum temperature experienced by the rock was relatively insensitive to the erosion rate. The PTt paths followed by rocks in these environments are characterized by an initial period during which the temperature either decreases slightly or rises towards the higher geotherm that would be supported by the thickened crust. This is followed by a period of cooling as the rock approaches the cold surface of the earth.

Only more recently have attempts been made to invert pressure-temperature data for the geotherms present during and following an orogenic episode. Following Carslaw and Jaeger (1959), Royden and Hodges (1984) expanded the temperature structure of the orogen as a Fourier series, and showed that it is theoretically possible to recover geotherms from a PTt path. They developed an inversion scheme whereby P-T data is inverted through use of a truncated approximation to this expansion and used it to invert data from the Caledonides for a truncation to $n=2$. McNutt and Royden (1987) used a linear-programming algorithm to find

extremal bounds on geotherms present at any time following an orogenic episode. Because both of these inversion methods require truncation of the infinite sum, it is important both to understand the importance of the higher order terms and to determine criteria for their truncation. Because P-T data are not perfect and because the evolution of geotherms depend on several physical parameters, it is also important to understand how errors in these data and uncertainties in the values of these parameters affect the ability of the selected inversion scheme to recover the true geotherm. Clearly, a good way to approach the problem of determining the effects of those factors which influence the inversion process is to examine them under controlled circumstances such as by investigating their effects on synthetic data.

In this thesis, I propose to examine some of these problems using synthetic data. The data are generated using the mathematical framework developed by Royden and Hodges (1984) and are inverted by application of the linear-programming techniques as described by McNutt and Royden (1987).

CHAPTER I: MATHEMATICAL BACKGROUND AND DATA GENERATION

INTRODUCTION

In this chapter, the mathematical techniques used in this study and their limitations are discussed. In the first two sections of this chapter, the forward modelling technique is described, while in the last two sections, the inversion technique is outlined.

The physical model which formed the basis for earlier studies of the lithospheric temperature structure (England and Richardson, 1977; Royden and Hodges, 1984) is adopted in this study. A finite difference approximation to the heat conduction equation is used to calculate a series of successive geotherms from a known initial geotherm. From this set of successive geotherms, the temperature-depth paths for several crustal horizons are followed as they are brought to the surface by erosion. In this manner, "perfect" temperature-depth (T_z) data are synthesized. These T_z data are then used to test to ability of a linear-programming inversion scheme to recover the temperature structure of the lithosphere at any specified time.

MATHEMATICAL MODEL

Physically, the lithosphere is treated as a conductive slab of constant thickness with constant temperature at its surface and base. The slab is uplifted at a constant velocity, u , and is eroded at the

surface at the same rate. Material at a fixed temperature, T_m , is also added to the base of the lithosphere at this rate. The distribution of radiogenic heat sources is treated as either a slab of uniform heat productivity or a distribution of point sources. The temperature in the slab a function of depth and time is described by the equation of heat conduction in a moving medium:

$$(1/\alpha)(\partial T/\partial t) - (\partial^2 T/\partial z^2) - (u/\alpha)(\partial T/\partial z) = A(z+ut)/\kappa \quad (1.1)$$

where:

α = thermal diffusivity

κ = thermal conductivity

t = time

z = depth (relative to the surface)

u = uplift rate (positive for uplift)

$A(z+ut)$ = heat production

$T(z,t)$ = temperature as a function of depth and time

subject to the boundary conditions $T(0,t) = 0^\circ\text{C}$ and $T(\ell,t) = T_m$ where ℓ is the lithospheric thickness (Carslaw and Jaeger, 1959).

Following Royden and Hodges (1984), the equation may be solved by separation of variables to give:

$$T(z,t) = T_R(z,t) + T_m \cdot [(1 - \exp(-2Rz/\ell))/(1 - \exp(-2R))] + T_m \cdot \sum_{n=1}^{\infty} c_n \exp[-(n^2\pi^2 + R^2)\tau] \cdot \exp(-Rz/\ell) \cdot \sin(n\pi z/\ell) \quad (1.2)$$

where:

$T_R(z, t)$ = the contribution to $T(z, t)$ from radiogenic heat sources

$R = ul/2\alpha$ (Peclet number)

$\tau = \alpha t/\ell^2$.

The coefficients, c_n , in equation (1.2) are similar to Fourier coefficients and may be calculated for any initial temperature distribution, $T(z, 0)$, from the equation:

$$c_n = (2/\ell T_m) \int_0^\ell \{T(z, 0) - T_R(z, 0) - T_m \cdot [(1 - \exp(-2Rz/\ell))/(1 - \exp(-2R))]\} \cdot \exp(Rz/\ell) \cdot \sin(n\pi z/\ell) dz \quad (1.3)$$

The function T_R satisfies the equation:

$$(1/\alpha)(\partial T_R/\partial t) - (\partial^2 T_R/\partial z^2) - (u/\alpha)(\partial T_R/\partial z) = A(z+ut)/\kappa \quad (1.4)$$

subject to the boundary conditions $T_R(0, t) = T_R(\ell, t) = 0^\circ\text{C}$. For a layer of uniform heat productivity, A_0 , extending from depth $z=0$ to $z=a-ut$, $A(z+ut) = A_0 H(a-ut-z)$ where $H(a-ut-z)$ is the Heaviside function. The radiogenic contribution to the temperature structure is given by:

$$\begin{aligned} T_R(z, t) = & (A_0 \ell^2/\kappa) \{ -(a/\ell - 2R\tau - z/\ell)^2/2 \} H(a/\ell - 2R\tau - z/\ell) \\ & - (a/\ell - 2R\tau)^2 (B - A)C/2 + (a/\ell - 2R\tau)(z/\ell)(B + A)C \\ & - (z^2/\ell^2)(B - A)C/2 + (z/\ell)(B + A)C/2R \end{aligned}$$

$$\begin{aligned}
& - 2(a/\ell - 2R\tau)B(1 - A)C^2 + 2(z/\ell)B(1 + A)C^2 \\
& - B(1 - A)C^2/R - 2(1 + B)B(1 - A)C^3 \quad (1.5a)
\end{aligned}$$

where:

$$A = \exp(-2Rz/\ell) \quad (1.5b)$$

$$B = \exp(-2R) \quad (1.5c)$$

$$C = 1/(1 - B) \quad (1.5d)$$

provided that $a - ut \geq 0$ (Royden and Hodges, 1984).

For a point heat source at depth a , $A(z+ut) = A_0\delta(a-ut-z)$ where $\delta(a-ut-z)$ is the Kronecker delta. The radiogenic contribution to the temperature structure is then given by the equation:

$$\begin{aligned}
T_R(z, t) = (A_0\ell/\kappa) \{ & [-(a/\ell - 2R\tau - z/\ell)]H(a/\ell - 2R\tau - z/\ell) \\
& + (a/\ell - 2R\tau)(A - B)C + (z/\ell)(A + B)C - 2B(1 - A)C^2 \} \quad (1.6)
\end{aligned}$$

provided that $a - ut \geq 0$. A , B , and C are calculated from the expressions (1.5b-d).

The temperature-depth path ($S(z')$) for a given crustal horizon initially at depth z_0 at time t_0 may be traced:

$$\begin{aligned}
S(z') = T_R[z', (z_0 - z')/u + t_0] \\
+ T_m \cdot [(1 - \exp(-2Rz'/\ell))/(1 - \exp(-2R))] \\
+ T_m \cdot \sum_{n=1}^{\infty} a_n \cdot \exp[(n^2\pi^2/2R - R/2)z'/\ell] \sin(n\pi z'/\ell) \quad (1.7)
\end{aligned}$$

where its depth z' at time t is given by:

$$z' = z_0 - u(t - t_0) \quad (1.8)$$

and

$$a_n = c_n \cdot \exp[-(n^2\pi^2/2R + R/2)(z_0/\ell + 2R\tau_0)] \quad (1.9)$$

(Royden and Hodges, 1984). Thus, given a known initial geotherm, uplift rate, lithospheric thickness, distribution and magnitude of radiogenic heat production, thermal conductivity, and thermal diffusivity, one may calculate via equations 1.3, 1.2, and 1.7 the coefficients c_n , the geotherms at fixed times, and the temperature-depth paths followed by particular suites of rocks.

The expansion (1.2) consists of a term due to radiogenic heat sources, a steady-state term, and an infinite sum of time dependent terms. The time dependence of the n^{th} term of the infinite sum is given by:

$$\exp[-(n^2\pi^2 + R^2)\alpha t/\ell^2]. \quad (1.10)$$

For $u=0.6$ km/m.y., $\ell=120$ km, and $\alpha=6.4 \cdot 10^{-7}$ m²/s, the $n=2$ term decays to 10% of its initial value after 39 m.y. and to 1% of its initial value after 77 m.y.. The $n=3$ term decays to 10% of its initial value after 18 m.y. and to 1% of its initial value after 36 m.y.. The $n \geq 4$ terms decay to 10% of their initial values in 10 m.y. or less and to 1% of their initial values in less than 20 m.y.. Hence, after sufficiently long times, the infinite sum in (1.2) may be approximated by the sum of its first few terms. Because the accuracy of such an approximation is

critical for proper interpretation of the inversion of real Tz data to solve for ancient geotherms, one of the goals of this study is to bound the number of terms in the expansion (1.2) necessary to adequately approximate the true geotherm at any specified time.

GENERATION OF SYNTHETIC DATA

A finite difference approximation to the heat conduction equation, such as that of Zienkiewicz and Morgan (1983), can be used to generate geotherms at all depths and times from a known initial geotherm, uplift rate, lithospheric thickness, magnitude and distribution of heat sources, thermal conductivity, and thermal diffusivity. The finite difference formulation used to approximate equation (1.1) is:

$$\begin{aligned}
 T(z, t+dt) = & T(z, t) + (\alpha dt / (dz)^2) [T(z+dz, t) - 2T(z, t) \\
 & + T(z-dz, t)] + (u(t) dt / 2dz) [T(z+dz, t) - T(z-dz, t)] \\
 & + \alpha dt A(z, t) / \kappa
 \end{aligned}
 \tag{1.11}$$

in which:

dt = time spacing of grid points

dz = depth spacing of grid points

with the boundary conditions $T(0, t) = 0^\circ\text{C}$ and $T(\ell, t) = T_m$. The program which performed these calculations is given in Appendix A. Note that this formulation allows for variation in the uplift rate with time. It

also avoids the complications inherent in equations (1.5a) and (1.6) when $t > u/a$. Because temperature evolves with time, a forward difference must be used to approximate the partial derivative of temperature with respect to time; however, central differences may be used to approximate the first and second partial derivatives of temperature with respect to depth as two boundary conditions are specified by the model. Stability of the finite difference method requires that:

$$\alpha dt / (dz)^2 \leq .5 \quad (1.12)$$

(Richtmyer, 1957). The grid spacing used in this study ($dz = 2\text{km}$, $dt = .05 \text{ m.y.}$) was chosen in order both to satisfy this criterion and to simplify recovery of the desired output.

Three series of tests were run in order to check the accuracy of the finite difference approximation. The first series of tests was designed to check the decay rate of geotherms in both stationary and moving media in the absence of radiogenic heat sources. The second set of tests examined the effect of grid spacing on the finite difference approximation. The final series of tests was designed to check the radiogenic contribution to the temperature structure.

Decay of the initial geotherms in both stationary and moving media in the absence of radiogenic heat sources was examined first. Fortunately, there are several initial temperature distributions for which the analytic solution to the heat conduction equation may be easily calculated. Choosing the conditions:

$$u = 0 \text{ km/m.y.}; T(z, 0) = T_m \quad (1.13a)$$

$$u = .6 \text{ km/m.y.}; T(z, 0) = T_m \quad (1.13b)$$

$$\text{and } u = .6 \text{ km/m.y.}; T(z, 0) = T_m \cdot z/\ell, \quad (1.13c)$$

the respective analytic solutions to the heat conduction equation with the boundary conditions stated above are:

$$T(z, t) = T_m \cdot z/\ell + (2T_m/\pi) \cdot \sum_{n=1}^{\infty} (1/n) \exp(-n^2\pi^2\tau) \cdot \sin(n\pi z/\ell) \quad (1.14a)$$

$$\begin{aligned} T(z, t) = T_m \cdot [(1 - \exp(-2Rz/\ell))/(1 - \exp(-2R))] \\ + 2\pi T_m \cdot \sum_{n=1}^{\infty} [n/(n^2\pi^2 + R^2)] \cdot \exp[-(n^2\pi^2 + R^2)\tau] \\ \cdot \exp(-Rz/\ell) \cdot \sin(n\pi z/\ell) \end{aligned} \quad (1.14b)$$

$$\begin{aligned} T(z, t) = T_m \cdot [(1 - \exp(-2Rz/\ell))/(1 - \exp(-2R))] \\ + 4\pi R T_m \cdot \sum_{n=1}^{\infty} [n/(n^2\pi^2 + R^2)^2] [\exp(R) \cos(n\pi) - 1] \\ \cdot \exp[-(n^2\pi^2 + R^2)\tau] \cdot \exp(-Rz/\ell) \cdot \sin(n\pi z/\ell) \end{aligned} \quad (1.14c)$$

Geotherms representing 10 to 100 m.y. of decay of an initial geotherm were calculated using the finite difference method with the initial conditions and uplift rates given in (1.13a-c). These were then compared to the geotherms calculated from the first 20 terms of the corresponding analytic solutions. All agreed to within 1°C.

The second series of tests illustrated the sensitivity of the finite difference method to the grid spacing. Theoretically, choice of

$dt = (dz)^2/2\alpha$ yields errors of order $O(dt, (dz)^2)$ whereas choice of $dt = (dz)^2/6\alpha$ yields errors of order $O((dt)^2, (dz)^4)$ (Richtmyer, 1957). Fixing $dz=2\text{km}$ and choosing a range of values for dt with $\alpha=6.4 \times 10^{-7} \text{ m}^2/\text{s}$ such that $(dz)^2/6\alpha \leq dt \leq (dz)^2/2\alpha$, several initial geotherms were allowed to decay for periods of up to 100 m.y. in both stationary and moving media. For all subsets of the range of values of dt examined, the resulting geotherms always agreed to within .2%. On the other hand, choice of $dt \geq (dz)^2/2\alpha$ led to instability of the finite difference method.

The final series of tests compared the radiogenic contribution to the temperature structure calculated from the difference method for either a slab of uniform heat productivity or a distribution of point sources to that calculated from the appropriate analytic expression. The radiogenic contribution to the temperature structure satisfies the finite difference equation:

$$\begin{aligned}
 T_R(z, t+dt) = & T_R(z, t) + (\alpha dt / (dz)^2) [T_R(z+dz, t) - 2T_R(z, t) \\
 & + T_R(z-dz, t)] + (u(t) dt / 2dz) [T_R(z+dz, t) \\
 & - T_R(z-dz, t)] + \alpha dt A(z, t) / \kappa
 \end{aligned} \tag{1.15}$$

subject to the boundary conditions $T_R(0, t) = T_R(l, t) = 0^\circ\text{C}$. The heat production term $\alpha dt A(z, t) / \kappa$ corresponds to those heat sources within half a grid interval ($z-.5dz, z+.5dz$) about the grid point z . Hence, for a slab of uniform heat productivity, $A(z, t) = A_0 h$ where h scales the heat productivity by the percentage of the depth interval about the grid point

in which heat sources are distributed. For a point heat source, $A(z,t) = A_0(dz)h$ where h partitions the heat source between the grid points immediately above and below it. Temperature contributions determined from the finite difference method for the times 0, 10, 20, ..., 100 m.y. after the onset of uplift and erosion with model parameters thermal diffusivity (α) = 6.4×10^{-7} m²/s, thermal conductivity (κ) = 2.5 W/m³, lithospheric thickness (ℓ) = 120 km, thickness of the radiogenic layer (a) = 50 km, and density of heat sources (A_0) = .84 $\mu\text{W}/\text{m}^3$ agree with the contributions determined from the respective analytic solutions to within .1°C for slabs and to within .05°C for point sources.

THE INVERSE PROBLEM

Whereas the forward problem, i.e., the generation of geotherms and temperature-depth (Tz) paths forward in time from a known initial geotherm, is fairly straightforward, the inversion of pressure-temperature (P-T) data from one or more crustal horizons for either the temperature structure of the lithosphere or, equivalently, for the coefficients $\{c_n\}$ is much more complicated. These complications arise for many reasons, such as:

- (1) There are only a finite number of P-T measurements, but an infinite number of unknowns c_n ; therefore, there are an infinite number of solutions consistent with the data.
- (2) Some sets of coefficients $\{c_n\}$ fit the P-T data; yet they correspond to clearly physically unrealistic initial

temperature structures (e.g., they yield geotherms with either negative or excessively large temperatures (thousands of degrees Centigrade)).

- (3) Recovery of geotherms early in the orogenic history of a mountain belt requires the determination of high order coefficients, c_n . Because the terms of the infinite sum of expansion (1.2) decay as $\exp[-(n^2\pi^2+R^2)\alpha t/l]$ with time, P-T measurements corresponding to the later thermal evolution of an orogenic belt cannot recover these coefficients. This is a physical limitation of the inverse problem which can be improved upon only with the availability of many accurate P-T measurements at early times.
- (4) Many physical constraints on the problem are either unknown or poorly understood. Some may violate assumptions implicit in the inverse model.

(McNutt and Royden, 1987).

A linear programming technique is well-suited to handle difficulties of types (1) and (2) and can help to constrain or assess some of the errors inherent in the inversion scheme due to (3) and (4). Because the linear-programming scheme inverts a system of linear constraints subject to either minimization or maximization of an objective function, the extremal bounds on geotherms present during uplift of a mountain belt at a specified time or the extremal bounds on the coefficients $\{c_n\}$ may be found by suitable choice of the objective function. Using the revised simplex algorithm (Dantzig, 1953; Dantzig et al., 1954; Orchard-Hays,

1954), one solves for the solution vector

$$\vec{X} = (A_0, T_m, c_1, c_2, c_3, \dots, c_{\max}) \quad (1.16)$$

subject to the following constraints:

- (1) The resulting Tz path fits the observed Tz data to within a prescribed error $\pm\delta S$.
- (2) Temperatures along the entire Tz path are always less than or equal to $S(z'_{\max})$ where z'_{\max} corresponds to the depth at which the maximum grade of thermal metamorphism is observed.
- (3) The initial temperature is greater than or equal to zero but less than or equal to the maximum mantle temperature at all depths:

$$0 \leq T(z, 0) \leq T_m \quad (z: 0 \leq z \leq \ell)$$

This constraint is sufficient to ensure that $0 \leq T(z, t) \leq T_m$ for all depths $(z: 0 \leq z \leq \ell)$ at all times.

- (4) The radiogenic heat productivity, A_0 , lies within prescribed bounds:

$$A_{0\min} \leq A_0 \leq A_{0\max}$$

- (5) The temperature at the base of the lithosphere, T_m , lies within prescribed bounds:

$$T_{m\min} \leq T_m \leq T_{m\max}$$

(McNutt and Royden, 1987).

When solving for the extremal bounds on geotherms, the objective function is the total temperature as given by expansion (1.2). At a

given time t_b , the solution vector \vec{X} compatible with the above constraints is found such that temperature is either minimized or maximized at a specified depth z_b . Temperature bounds for all depths ($z: 0 \leq z \leq \ell$) at the specified time t_b are found by repeated application of the inversion algorithm. A complete series of inversions (both minimization and maximization of temperature at all depths at a specified time) thus yields an envelope of all possible geotherms consistent with the given constraints for that time. For example, if inversions are performed at four kilometer increments between depths of 2 km and 118 km inclusive, an envelope of all possible geotherms would require 60 inversions. The envelope found in this manner is usually not a possible geotherm, nor are all the geotherms within it feasible solutions; however, all geotherms which are compatible with the above constraints must lie within the envelope.

When solving for the extremal bounds on the coefficients $\{c_n\}$, each coefficient is taken in succession as the objective function. Because the coefficients are independent of depth and time, each series of inversions consists of only $2n$ inversions where n equals the number of coefficients one wishes to bound.

THE GENERAL LINEAR-PROGRAMMING PROBLEM

The general linear-programming problem is to find a vector

$$\vec{X} = (x_1, x_2, \dots, x_j, \dots, x_n)^t \quad (1.17)$$

where t denotes the transpose of the vector which maximizes a linear form

(i.e., the objective function)

$$z = \vec{c} \cdot \vec{X} \quad (1.18)$$

subject to the linear constraints

$$\underline{\underline{A}}\vec{X} \leq \vec{b} \quad (1.19)$$

and

$$\vec{X} \geq \vec{0} \quad (1.20)$$

where $\vec{c} = (c_1, c_2, \dots, c_n)$ is a row vector, \vec{X} is a column vector, $\underline{\underline{A}} = (a_{ij})$ is an $m \times n$ matrix, $\vec{b} = (b_1, b_2, \dots, b_m)^t$ is a column vector, and $\vec{0}$ is an n -dimensional null column vector. The constants a_{ij} , b_i , and c_j are known and $m < n$. Because for a linear form z , the maximum of z equals the negative of the minimum of $(-z)$, the linear-programming problem may be posed as an equivalent minimization problem.

For future reference, it is useful to restate the general linear-programming problem as:

maximize

$$z = \sum_{j=1}^n c_j x_j \quad (1.21)$$

subject to

$$\sum_{j=1}^n x_j \bar{P}_j \leq \bar{P}_0 \quad (1.22)$$

and

$$x_j \geq 0, \quad j=1,2,\dots,n \quad (1.23)$$

where \bar{P}_j is the j^{th} column of the matrix $\underline{\underline{A}}$ for $j=1,2,\dots,n$ and $\bar{P}_0 = \vec{b}$.

Every linear-programming problem has:

- (1) no solution in terms of nonnegative values of the variables x_j
- (2) a nonnegative solution that yields an infinite value for the objective function

or

- (3) a nonnegative solution that yields a finite value for the objective function.

The set of all feasible solutions to a linear programming problem, i.e., those vectors \vec{X} satisfying conditions (1.22) and (1.23), defines a convex region in n -dimensional space. The maximum value of the objective function occurs at an extreme point of this convex region. If this maximum value occurs at more than one extreme point, then it has the same value for every convex combination of these particular points. Furthermore, every feasible solution \vec{X} in which the difference $(n-m)$ between the number of variables x_j and the number of constraints is zero is called a basic feasible solution and corresponds to an extreme point of the convex set of feasible solutions. It can be shown that the vector \vec{X} is an extreme point of the convex set of feasible solutions if and only if the positive x_j are coefficients of linearly independent vectors \vec{P}_j in (1.22) (Gass, 1985). Hence, every extreme point of the set of feasible solutions has m linearly independent vectors of the set of n associated with it. Thus, it is necessary to consider only those feasible solutions generated by m linearly independent vectors. Since these m vectors are chosen from a set of n vectors, there are at most $\binom{n}{m}$ possible solutions of the problem. If n and m are large, the task of evaluating all possible solutions and selecting the one that maximizes

the objective function becomes very difficult. Hence, one seeks a computational scheme which selects a small subset of the possible solutions which converge to a maximum solution.

Because each basic feasible solution is associated with a basis (Chung, 1963), one first seeks an initial basis yielding a basic feasible solution. Assuming an initial basis can be found, movement from this basis to a basis associated with a basic feasible solution yielding an improved value of the objective function is accomplished by replacing one of the current basis vectors with a non-basis vector. The basis vector to be replaced is determined according to a rule which guarantees feasibility of the new solution. The new basis then forms a starting point for repetition of the same evaluative process to determine a "better" basic feasible solution. This iterative process continues until an optimal solution to the problem is found or until it can be shown that one does not exist.

Finding an initial solution implies the selection of a set of independent vectors to form a basis \underline{B} such that $\underline{B}^{-1}\vec{P}_0$ yields a unique feasible solution. For some problems, an initial basis can be easily guessed. More often, the requirements of simultaneous independence of the vectors and feasibility of the solution preclude guessing an initial basis; hence, an initial basis must be constructed.

Since any constraint i in which $b_i < 0$ may be transformed into a constraint in which $b_i > 0$ by multiplication of the constraint by -1 , one may assume that the constants b_i of the constraints are all non-negative. The constraints may be grouped into three categories:

- (1) All of the constraints are of the type \leq .
- (2) All of the constraints are of the type \geq .
- (3) The constraints are a mixture of types (1) and (2).

First consider equations of type (1) in which the b_i are non-negative. In general, it is more convenient to work with equalities than with inequalities. Therefore, inequality constraints in (1.19) are converted to equality constraints by the addition of non-negative variables, called slack variables, to obtain a set of simultaneous linear equations. For any inequality constraint i , the slack variable s_i is defined by:

$$s_i = b_i - \sum_{j=1}^n a_{ij}x_j \quad (1.24)$$

Thus, the system of equations may be written as:

$$\bar{P}_1x_1 + \bar{P}_2x_2 + \dots + \bar{P}_nx_n + \bar{P}_{n+1}s_1 + \dots + \bar{P}_{n+m}s_m = \bar{P}_0 \quad (1.25)$$

where $\bar{P}_{n+1}, \dots, \bar{P}_{n+m}$ are a set of m unit slack vectors which together form an identity matrix.

Let $\underline{B} = [\bar{P}_{n+1}, \dots, \bar{P}_{n+m}] = \underline{I}$ be the initial basis.

Associated with this basis is a vector \bar{Y}_0 , such that:

$$\bar{Y}_0 = \underline{B}^{-1}\bar{P}_0 = \underline{I}\bar{P}_0 = \bar{P}_0 = \bar{b} \geq 0. \quad (1.26)$$

Clearly, for this problem, $\bar{Y}_0 = (s_1, s_2, \dots, s_m)^t$ and the associated solution, $x_i = 0, i=1, \dots, n; s_i = b_i, i=1, \dots, m$, is feasible since \bar{P}_0 is assumed non-negative. Furthermore, it is a basic solution because it consists of at most m positive components. Hence, if all of the constraints are of the type \leq , a "natural" initial basis which immediately yields an initial basic feasible solution is the set of slack

vectors.

If all of the constraints are of type (2) and $\bar{P}_0 \geq \bar{0}$, the inequalities can be converted to equalities by the subtraction of non-negative slack variables as defined by equation (1.24). This gives a system of linear constraint equations:

$$\bar{P}_1 x_1 + \bar{P}_2 x_2 + \dots + \bar{P}_n x_n + \bar{P}_{n+1} s_1 + \dots + \bar{P}_{n+m} s_m = \bar{P}_0 \quad (1.27)$$

where $x_i \geq 0$, $i=1,2,\dots,n$; $s_i \geq 0$, $i=1,\dots,m$ and $\bar{P}_{n+1} = (-1, 0, \dots, 0)^t$; \dots ; $\bar{P}_{n+m} = (0, 0, \dots, 0, -1)^t$. The slack vectors \bar{P}_i , $i=n+1,\dots,n+m$ are linearly independent unit vectors. They form a basis

$\underline{B} = [\bar{P}_{n+1}, \dots, \bar{P}_{n+m}]$ which is associated with a vector

$\bar{Y}_0 = \underline{B}_0^{-1} \bar{P}_0 = (-\underline{I})^{-1} \bar{P}_0 = -\bar{P}_0$ which is not feasible and,

hence, unacceptable.

This difficulty may be overcome by the addition of a second set of non-negative variables, called artificial variables, to each of the m equations in (1.27) (Orden, 1952). This yields a set of constraints:

$$\begin{aligned} \bar{P}_1 x_1 + \bar{P}_2 x_2 + \dots + \bar{P}_n x_n + \bar{P}_{n+1} s_1 + \dots + \bar{P}_{n+m} s_m \\ + \bar{P}_{n+m+1} e_1 + \dots + \bar{P}_{n+2m} e_m = \bar{P}_0 \end{aligned} \quad (1.28)$$

where \bar{P}_i , $i=n+m+1,\dots,n+2m$ are the coefficient vectors of the artificial variables e_i , $i=1,\dots,m$; i.e., $\bar{P}_{n+m+1} = (1, 0, \dots, 0)^t$; \dots ; $\bar{P}_{n+2m} = (0, 0, \dots, 0, 1)^t$. Clearly, the set of m positive unit vectors $\bar{P}_{n+m+1}, \dots, \bar{P}_{n+2m}$ forms a basis which is an identity matrix; Associated with this basis is a non-negative basic solution $x_i = 0$, $i=1,\dots,n$; $s_i = 0$, $i=1,\dots,m$; and $e_i = b_i$, $i=1,\dots,m$.

Finally, consider constraints which are a mixture of types (1) and (2), or, equivalently, constraints of type (1) in which the b_i are not

restricted to be non-negative. As suggested by the above discussion, the set of equations:

$$\sum_{j=1}^n a_{ij} x_j \leq b_i \quad i = 1, 2, \dots, m \quad (1.19)$$

may be replaced by the augmented set of constraint equations:

$$\sum_{j=1}^n a_{ij} x_j + s_i = b_i \quad i = 1, 2, \dots, np \quad \text{if } b_i \geq 0 \quad (1.29a)$$

$$-\sum_{j=1}^n a_{ij} x_j - s_i + e_i = -b_i \quad i = np+1, \dots, ni \quad \text{if } b_i \leq 0 \quad (1.29b)$$

$$\pm \sum_{j=1}^n a_{ij} x_j + e_i = \pm b_i \quad i = ni+1, \dots, m \quad (1.29c)$$

where:

$$s_i \geq 0, \quad i=1, \dots, ni \text{ are slack variables}$$

and

$$e_i \geq 0, \quad i=np+1, \dots, m \text{ are artificial variables.}$$

The minus signs are taken in equation (1.29c) if the b_i are negative.

One immediately obvious basic feasible solution to the augmented set of constraint equations is:

$$x_j = 0, \quad j=1, \dots, n \quad (1.30a)$$

$$s_i = b_i, \quad i=1, \dots, np \quad (1.30b)$$

$$s_i = 0, \quad i=np+1, \dots, ni \quad (1.30c)$$

$$e_i = -b_i, \quad i=np+1, \dots, ni \quad (1.30d)$$

and

$$e_i = \pm b_i, \quad i=ni+1, \dots, m. \quad (1.30e)$$

This is not, however, a feasible solution to the original set of

constraints because any solution to the augmented constraint equations that is also a solution to the original set of constraint equations must have all artificial variables equal to zero. However, there exist methods of moving from this basic feasible solution to the augmented problem to an optimal solution of the original problem if one exists. These methods guarantee feasibility of successive basic solutions if the initial solution is feasible. The scheme employed in this study was selected in the interests of computational efficiency and is based on the revised simplex method (Dantzig, 1953; Dantzig et al., 1954; Orchard-Hays, 1954). It is described briefly below.

The revised simplex method is a two-phase method. In Phase 1, the artificial variables are driven to zero. In Phase 2, an optimal solution to the original problem is found.

For the purpose of illustration, assume that the constraint equations are all of the form of inequalities. Also, assume that all b_i , $i=1,2, \dots, m$ are positive. Because no artificial variables are necessary for this problem, it is solely a Phase 2 problem.

Hence, for the linear-programming problem:

maximize

$$z = \bar{c} \cdot \bar{X} \tag{1.18}$$

subject to

$$\underline{A}\bar{X} \leq \bar{P}_0 \tag{1.19}$$

and

$$\bar{X} \geq \bar{0} \tag{1.20}$$

where:

$$\underline{\underline{A}} = [\bar{P}_1, \bar{P}_2, \dots, \bar{P}_n] \tag{1.31}$$

$$= \begin{bmatrix} a_{11} & a_{12} & \cdot & \cdot & \cdot & a_{1n} \\ a_{21} & a_{22} & \cdot & \cdot & \cdot & a_{2n} \\ \cdot & \cdot & & & & \cdot \\ a_{m1} & a_{m2} & \cdot & \cdot & \cdot & a_{mn} \end{bmatrix} \tag{1.32}$$

$$\bar{X} = (x_1, x_2, \dots, x_n)^t \tag{1.33}$$

$$\bar{P}_0 = (b_1, b_2, \dots, b_m)^t \geq \bar{0} \tag{1.34}$$

and

$$\bar{c} = (c_1, c_2, \dots, c_n), \tag{1.35}$$

the simplex tableau may be set up as follows (1.36):

Equation	Admissible Variables	Slack Variables	z	constants
i	$x_1 \ x_2 \ \dots \ x_j \ \dots \ x_n$	$s_1 \ s_2 \ \dots \ s_m$		
1	$a_{11} \ a_{12} \ \dots \ a_{1j} \ \dots \ a_{1n}$	1 0 ... 0	0	b_1
2	$a_{21} \ a_{22} \ \dots \ a_{2j} \ \dots \ a_{2n}$	0 1 ... 0	0	b_2
·	· · · · ·	· · · · ·	·	·
·	· · · · ·	· · · · ·	·	·
·	· · · · ·	· · · · ·	·	·
m	$a_{m1} \ a_{m2} \ \dots \ a_{mj} \ \dots \ a_{mn}$	0 0 ... 1	0	b_m
z-form	$c_1 \ c_2 \ \dots \ c_j \ \dots \ c_n$	0 0 ... 0	-1	0

Unlike the simplex method, in which the entire tableau must be transformed between successive solutions, the link between successive solutions in the revised simplex method is the inverse of the basis

matrix; thus, it is necessary to keep only a portion of this tableau:

Basic Variables	-----				z	Value of Basic Variable
	s_1	s_2	\dots	s_m		
$x_{(1)}$	1	0	\dots	0	0	b_1
$x_{(2)}$	0	1	\dots	0	0	b_2
.	.	.	\dots	.	.	.
.	.	.	\dots	.	.	.
.	.	.	\dots	.	.	.
$x_{(m)}$	0	0	\dots	1	0	b_m
z-form	0	0	\dots	0	-1	0

(1.37)

Let there be a basis matrix $\underline{\underline{B}} = [\bar{P}_{(1)}, \bar{P}_{(2)}, \dots, \bar{P}_{(m)}]$ such that $\bar{Y}_0 = \underline{\underline{B}}^{-1} \bar{P}_0$. Note that the subscript in parenthesis refers to the order of the vector in the basis and not to the order in the structural constraints. This notation will be used whenever vectors or variables corresponding to the basis $\underline{\underline{B}}$ have counterparts in the structural constraints of matrix $\underline{\underline{A}}$ from which they must be distinguished.

An obvious solution to the augmented problem is :

$$x_j = 0 \quad j=1,2,\dots, n \quad (1.38a)$$

$$s_i = b_i \quad i=1,\dots,m \quad (1.38b)$$

$$z = 0. \quad (1.38c)$$

The corresponding basis matrix $\underline{\underline{B}}$ is the identity matrix $\underline{\underline{I}}$. Its inverse $\underline{\underline{B}}^{-1}$ is also the identity matrix. Thus, $\bar{Y}_0 = \bar{P}_0 = \bar{b}$.

Because $\underline{\underline{B}}$ is a basis, any vector \bar{P}_k , $k=1,2,\dots,m$ of matrix $\underline{\underline{A}}$

not in the basis can be expressed as a linear combination of the vectors in \underline{B} :

$$\bar{P}_k = y_{1k}\bar{P}_{(1)} + y_{2k}\bar{P}_{(2)} + \dots + y_{mk}\bar{P}_{(m)} = \underline{B}\bar{Y}_k \quad (1.39)$$

where $\bar{Y}_k = (y_{1k}, y_{2k}, \dots, y_{mk})^t$. Thus, the y_{ij} , $i, j=1, 2, \dots, m$ are the linear combination coefficients of the basis vectors $P_{(j)}$ and

$\bar{Y}_k = \underline{B}^{-1}\bar{P}_k$. Note that this implies that the matrix

$$\underline{Y} = [\bar{Y}_1, \bar{Y}_2, \dots, \bar{Y}_n] \quad (1.40a)$$

$$= \underline{B}^{-1}[\bar{P}_1, \bar{P}_2, \dots, \bar{P}_n] \quad (1.40b)$$

$$= \underline{B}^{-1}\underline{A}. \quad (1.40c)$$

Furthermore, for a transformation of the augmented basis matrix \underline{B} to the augmented basis matrix \underline{B}' , the elements of the inverse matrix

$\underline{B}'^{-1} = [\beta'_{ij}]$ can be obtained from the elements of the inverse matrix

$\underline{B}^{-1} = [\beta_{ij}]$ (Chung, 1963). Assume that

$\underline{B} = [\bar{V}_1, \bar{V}_2, \dots, \bar{V}_\ell, \dots, \bar{V}_{m+1}]$ where $\bar{V}_i = (\bar{P}_{(i)}, -c_{(i)})^t$,

$i=1, 2, \dots, m$ and $\bar{V}_{m+1} = (\bar{0}, 1)^t$ where $\bar{0}$ is an m -dimensional null

vector. Substitution of \bar{P}_k for $\bar{P}_{(\ell)}$ yields a new basis

$\underline{B}' = [\bar{V}_1, \bar{V}_2, \dots, \bar{V}'_\ell, \dots, \bar{V}_{m+1}]$ where $\bar{V}'_\ell = (\bar{P}_k, -c_k)^t$.

The transformation formulae relating the matrix elements β'_{ij} to the elements β_{ij} are:

$$\beta'_{ij} = (\beta_{ij})/(y_{\ell k}) \quad \text{for } i=\ell, \text{ all } j \quad (1.41a)$$

$$\beta'_{ij} = \beta_{ij} - [(y_{ik})/(y_{\ell k})]\beta_{\ell j} \quad \text{for } i \neq \ell, i=1, \dots, m+1; \text{ all } j. \quad (1.41b)$$

The revised simplex method employs a series of three steps to move from this initial solution of the augmented problem to a solution of the original problem if one exists. In the first step, the value of the objective function is examined. If it is optimal, the problem is solved;

if not, the vector which is to be entered into the basis is determined. In the second step, the vector which is to be removed from the basis is determined. In the final step, the elements of the simplex tableau are recalculated for return to the first step. These steps are examined in more detail below.

Step 1

The "cost" associated with a vector \vec{P}_k is given by:

$$z_k = \sum_{i=1}^m c_{(i)} y_{ik} = \tilde{c} \cdot \vec{Y}_k = \tilde{c}_B^{-1} \vec{P}_k = \vec{\pi} \cdot \vec{P}_k \quad (1.42)$$

where the m-dimensional row vector $\vec{\pi} = \tilde{c}_B^{-1}$ is called the pricing vector. The net effect on the objective function of an exchange of \vec{P}_k with one of the current basis vectors $\vec{P}_{(j)}$ is easily calculated from:

$$c'_k = z_k - c_k = \sum_{i=1}^m c_{(i)} y_{ik} - c_k = \vec{\pi} \cdot \vec{P}_k - c_k. \quad (1.43)$$

If $z_k - c_k$ is greater than zero, the introduction of \vec{P}_k into the basis will decrease the value of the objective function; however, if $z_k - c_k$ is less than zero, the effect of introducing \vec{P}_k into the basis is to increase the value of the objective function.

With the above as motivation, the value $z_k - c_k$ is calculated for all vectors \vec{P}_k of \underline{A} which are not also in \underline{B} . Two possibilities arise:

- (1) If $z_k - c_k \geq 0$ for all k, an optimal solution has been found.
- (2) If $z_k - c_k < 0$ for some k, the variable x_s for which

$$z_s - c_s = \underset{k}{\text{minimum}}(z_k - c_k) < 0 \text{ is chosen for insertion into the}$$

basis.

Step 2

In the second step, the vector which is to leave the basis is determined. First, the linear combination coefficients y_{is} , $i=1,2,\dots,m$ of the basis vector \bar{P}_s are calculated:

$$y_{is} = \sum_{j=1}^m \beta_{ij} a_{js} \quad (1.44)$$

where β_{ij} are the elements of the inverse of the basis matrix at any iteration. Next, the values of the basic variables are calculated:

$$b_{(i)} = \sum_{j=1}^m \beta_{ij} b_j. \quad (1.45)$$

Lastly, the values y_{is} are examined for all i .

- (1) If $y_{is} \leq 0$ for all i , the original problem has no solution.
- (2) If $y_{is} > 0$ for some i , the ratio $(b_{(i)})/(y_{is})$ is formed for all $y_{is} > 0$. The vector $\bar{P}_{(\ell)}$ with the minimum ratio is removed from the basis. If two or more vectors yield the same ratio, then of these vectors,
 - (A) that with the largest y_{is} is removed if the ratio is zero and
 - (B) that with the lowest (i) index is removed in all other cases.

Step 3

In the final step, the tableau entries for the next cycle of the

simplex method are calculated. At this point, for any iteration t , the simplex tableau has the following form:

Basic Variables	-----			z	Value of Basic Variable
	(1)	...	(m)		
$x_{(1)}$	β_{11}	...	β_{1m}	0	$b_{(1)}$
.
.
$x_{(\ell)}$	$\beta_{\ell 1}$...	$\beta_{\ell m}$.	$b_{(\ell)}$
.
$x_{(m)}$	β_{m1}	...	β_{mm}	0	$b_{(m)}$
z-form	$-\pi_1$...	$-\pi_m$	-1	$-z'_0$

(1.46)

where $z'_0 = \vec{\pi} \cdot \vec{b}$.

To prepare for the next iteration of the revised simplex method, the tableau is now transformed by means of equations (1.41a) and (1.41b).

Hence, at the start of iteration $t+1$, the tableau will have the form

(1.47):

Basic Variables	-----			z	Value of Basic Variable
	(1)	...	(m)		
$x_{(1)}$	$\beta_{11} - y_{1s} \beta'_{\ell 1}$...	$\beta_{1m} - y_{1s} \beta'_{\ell m}$	0	$b_{(1)} - y_{1s} b'_{(\ell)}$
.
.
x_s	$\beta'_{\ell 1}$...	$\beta'_{\ell m}$.	$b'_{(\ell)}$
.
$x_{(m)}$	$\beta_{m1} - y_{ms} \beta'_{\ell 1}$...	$\beta_{mm} - y_{ms} \beta'_{\ell m}$	0	$b_{(m)} - y_{ms} b'_{(\ell)}$
z-form	$-\pi_1 - c'_s \beta'_{\ell 1}$...	$-\pi_m - c'_s \beta'_{\ell m}$	-1	$-z'_0 - c'_s b'_{(\ell)}$

where $\beta'_{\ell j} = (\beta_{\ell j}) / (y_{\ell s})$, $j=1,2,\dots,m$ and $b'_{(\ell)} = (b_{(\ell)}) / (y_{\ell s})$.

The evaluative process as described above is repeated in this iteration.

Returning to the more general problem

maximize

$$z = \bar{c} \cdot \bar{X} \quad (1.18)$$

subject to

$$\underline{A} \bar{X} \leq \bar{P}_0 \quad (1.19)$$

and

$$\bar{X} \geq \bar{0} \quad (1.20)$$

the constraint equations may be modified as follows:

$$\sum_{j=1}^n a_{ij} x_j + s_i = b_i \quad i = 1, 2, \dots, np \quad \text{if } b_i \geq 0 \quad (1.29a)$$

$$-\sum_{j=1}^n a_{ij} x_j - s_i + e_i = -b_i \quad i = np+1, \dots, ni \quad \text{if } b_i \leq 0 \quad (1.29b)$$

$$\pm \sum_{j=1}^n a_{ij} x_j + e_i = \pm b_i \quad i = ni+1, \dots, m. \quad (1.29c)$$

Because the augmented problem contains artificial variables, the simplex tableau is modified to include a cost equation for these variables. This equation is:

$$\pm \sum_{i=ni+1}^m e_i = w \quad (1.48)$$

where w is the cost associated with the artificial variables.

The simplex tableau is set up as follows (1.49):

$$\left[\begin{array}{c|c|c|c|c|c|c|c} \underline{A}(np) & \underline{I}(np) & 0 & 0 & 0 & 0 & 0 & b(np) \\ \hline -\underline{A}(ni) & 0 & -\underline{I}(ni) & \underline{I}(ni) & 0 & 0 & 0 & -b(ni) \\ \hline \underline{A}(m) & 0 & 0 & 0 & \underline{I}(m) & 0 & 0 & \pm b(m) \\ \hline \bar{d} & 0 & 0 & 0 & 0 & 0 & 1 & -w_0 \\ \hline \bar{c} & 0 & 0 & 0 & 0 & -1 & 0 & 0 \end{array} \right]$$

where the elements of the m -dimensional row vector \bar{d} are:

$$d_i = -\sum_{j=1}^{np} a_{ij} + \sum_{j=np+1}^{ni} a_{ij} - \sum_{j=ni+1}^m a_{ij} \quad (1.50)$$

and

$$w_0 = \sum_{i=1}^m b_i. \quad (1.51)$$

The associated solution vector \bar{S} to the augmented problem is:

$$\bar{S} = (x_1, \dots, x_n, s_1, \dots, s_{ni}, e_{np+1}, \dots, e_m, z, w)^t. \quad (1.52)$$

An obvious initial solution \bar{S}_0 of this set of equations is:

$$x_j = 0 \quad j=1, \dots, n \quad (1.53a)$$

$$s_i = b_i \quad i=1, \dots, np \quad (1.53b)$$

$$s_i = 0 \quad i=np+1, \dots, ni \quad (1.53c)$$

$$e_i = -b_i \quad i=np+1, \dots, ni \quad (1.53d)$$

$$e_i = \pm b_i \quad i=ni+1, \dots, m \quad (1.53e)$$

$$z = 0 \quad (1.53f)$$

$$w = 0. \quad (1.53g)$$

For the revised simplex method, an $(m+2) \times (m+2)$ matrix analogous to that described above is set up to store the information pertaining to the non-zero variables as well as that pertaining to the two cost equations.

This is the matrix on which the computations are performed. At any iteration, it has the form:

Basic Variables	-----			z w	Value of Basic Variable
	(1)	...	(m)		
$x_{(1)}$	β_{11}	...	β_{1m}	0 0	$b_{(1)}$
.
.
$x_{(\ell)}$	$\beta_{\ell 1}$...	$\beta_{\ell m}$.	$b_{(\ell)}$
.
$x_{(m)}$	β_{m1}	...	β_{mm}	0 0	$b_{(m)}$
z-form	$-\pi_1$...	$-\pi_m$	-1 0	$-z'_0$
w-form	$-\sigma_1$		$-\sigma_m$	0 -1	$-w'_0$

(1.54)

where $\vec{\sigma} = \vec{d} \cdot \underline{B}^{-1}$ is an m -dimensional pricing vector relative to the artificial variables and

$$w'_0 = \sum_{i=1}^m \sigma_i b_i + w_0. \quad (1.55)$$

The computational procedure proceeds as explained above with the exception that Step 1 is modified as follows:

- (1) If all entries $d'_k = \vec{\sigma} \cdot \vec{P}_k - d_k \geq 0$ (Phase 1) or $c'_k \geq 0$ (Phase 2), then for
 - (A) Phase 1 with $w'_0 > 0$: terminate - no feasible solution exists
 - (B) Phase 1 with $w'_0 = 0$: initiate Phase 2 by:
 - (1) dropping all variables x_k with $d'_k > 0$
 - (2) dropping the w row of the tableau
 - (3) restarting the cycle with Phase 2 rules
 - (C) Phase 2: terminate - an optimal solution has been found
- (2) If some entry $d'_k < 0$ (Phase 1) or $c'_k < 0$ (Phase 2), choose x_s as the variable to enter the basis in the next cycle such that:

$$\text{Phase 1: } d'_s = \min_k d'_k < 0$$

$$\text{Phase 2: } c'_s = \min_k c'_k < 0.$$

The actual computational procedure of the linear-programming scheme employed in this study is a variation on that described above. The original tableau is set up in a slightly different fashion. It has the form (1.56):

$$\left[\begin{array}{c|c|c|c|c|c|c|c}
 g^t & -1 & -\bar{h}(np) & \bar{h}(ni) & 1 & 0 & 0 & 0 \\
 \hline
 -c & 1 & 0 & 0 & 0 & 0 & 0 & 0 \\
 \hline
 \underline{A}(np) & 0 & \underline{I}(np) & 0 & 0 & 0 & 0 & b(np) \\
 \hline
 -\underline{A}(ni) & 0 & 0 & -\underline{I}(ni) & 0 & \underline{I}(ni) & 0 & -b(ni) \\
 \hline
 \underline{A}(m) & 0 & 0 & 0 & 0 & 0 & \underline{I}(m) & \pm b(m)
 \end{array} \right]$$

where:

$$g_i = c_i - \sum_{j=1}^{np} a_{ji} + \sum_{j=np+1}^{ni} a_{ji} - \sum_{j=ni+1}^m a_{ji}. \quad (1.57)$$

$\bar{h}(np)$ is the np -dimensional row vector $(1, 1, \dots, 1)$

and

$\bar{h}(ni)$ is the $(ni-np)$ -dimensional row vector $(1, 1, \dots, 1)$.

The associated solution vector \bar{S} for this problem is:

$$\bar{S} = (x_1, \dots, x_n, z, s_1, \dots, s_{ni}, w, e_{np+1}, \dots, e_m)^t. \quad (1.58)$$

Again, an obvious initial solution \bar{S}_0 to this set of equations is:

$$x_j = 0 \quad j=1, \dots, n \quad (1.53a)$$

$$s_i = b_i \quad i=1, \dots, np \quad (1.53b)$$

$$s_i = 0 \quad i=np+1, \dots, ni \quad (1.53c)$$

$$e_i = -b_i \quad i=np+1, \dots, ni \quad (1.53d)$$

$$e_i = \pm b_i \quad i=ni+1, \dots, m \quad (1.53e)$$

$$z = 0 \quad (1.53f)$$

$$w = 0. \quad (1.53g)$$

As described earlier, a matrix is set up to store the information pertaining to the non-zero variables as well as to the two cost

equations. The decision-making process in moving from this solution of the augmented problem to a solution of the original problem then proceeds as outlined previously.

CHAPTER II: EXTREMAL BOUNDS ON TEMPERATURE

INTRODUCTION

In this chapter, I examine the resolution of a linear-programming technique in inverting temperature-depth data from a selected crustal horizon to obtain extremal bounds on evolving geotherms. In order to determine the resolution of the inversion scheme, extremal bounds are initially determined assuming no uncertainty in either the Tz data or in any of the physical parameters of the model. Uncertainty is later introduced into the data and into the value of each of these physical parameters in order to determine the extent to which these uncertainties degrade resolution of the extremal bounds.

FORWARD MODELGeotherms

Initial geotherms which correspond to three geologically "realistic" scenarios (Figure 2.1) were used with the finite difference scheme described in Chapter 1 to generate synthetic Tz data. These data were then used to investigate the resolution of the extremal bound linear-programming inversion scheme in recovering true geotherms calculated for various times in the history of an orogenic belt. Initial geotherms were chosen so as to span a wide range of possible geotherms. Model 1

corresponds to a 32 km thick thrust sheet with a thermal gradient of 10°C/km emplaced instantaneously above a 88 km thick plate with a thermal gradient of 15°C/km. Model 2 corresponds to an exponential dependence of temperature on depth. It might represent the temperature structure of an area which has been warmed by the advection of heat to the upper lithosphere by volcanism or intrusive activity. Model 3 corresponds to a 60 km thick thrust sheet with a thermal gradient of 10°C/km emplaced instantaneously above a 60 km thick plate with a thermal gradient of 22.5°C/km. Model 4 corresponds to the same initial geotherm as Model 3; however, unlike Models 1, 2, and 3 which assume a constant uplift rate (u) of .6 km/m.y., it assumes an uplift rate which varies linearly with time. This model will be considered only in a special context which will be discussed later. In all forward models, the values of maximum lithospheric temperature (T_m) = 1350°C, thermal diffusivity (α) = 6.4×10^{-7} m²/s, and lithospheric thickness (ℓ) = 120 km were used in the calculation of later geotherms from an initial geotherm. The radiogenic contribution to the temperature structure was always assumed to be that of a 50 km thick slab with a uniform density of heat sources of magnitude .84 $\mu\text{W}/\text{m}^3$.

Tz DATA

For each model, the temperature-depth history for the crustal horizon (i.e., the structural level parallel to the earth's surface which moves relative to the surface of the earth but is fixed with respect to an individual rock mass) initially at 50 km depth was followed as it was

brought to the surface by uplift and erosion. Three temperature-depth points from each Tz path were selected for use in a linear-programming inversion scheme to determine extremal bounds on either the geotherms at specified times or the coefficients $\{c_n\}$ of expansion (1.2). The first Tz point samples the temperature-depth path at a depth corresponding to a time early in the thermal history of the orogen; the second, at a depth near that at which the maximum temperature experienced by the crustal horizon occurs; and the third, at a near-surface depth (Figure 2.1). These data points were chosen because they correspond to temperatures and pressures often recorded by metamorphic minerals.

Effects of Parameter Variation

The extremal bounds that can be placed on the evolving geotherms through inversion of this synthetic Tz data are investigated in this chapter. In particular, the effects on the extremal bounds of uncertainties in the data and in various physical parameters as well as of errors introduced into the mathematical model are examined. Before proceeding, it is useful, while holding the initial geotherm fixed, to investigate the effects of variations in these parameters on the evolving temperature structure as determined by the forward model (Figures 2.2a-e). This exercise should provide additional insight into the effects of uncertainties in these parameters on the inversion scheme.

1) Temperature at the Base of the Lithosphere

Variations in the temperature at the base of the lithosphere

primarily affect the temperature structure of the lower lithosphere. Because the temperature at the base of the lithosphere (T_m) enters the forward problem linearly, a change in T_m results in changes in the temperature structure of the same magnitude in all models. Decreasing T_m to 1000°C results in a decrease in the temperature at all depths due to a decrease in the equilibrium temperature gradient. In the same fashion, increasing T_m to 1600°C results in an increase in the equilibrium temperature gradient, and, hence, an increase in the temperature at all depths. Because the effects of variations in the temperature at the base of the lithosphere propagate upwards into the lithosphere with time, at any specified depth, the magnitude of the changes in the temperature structure resulting from a change in T_m increases with passing time.

2) Radiogenic Heat Production

For a 50 km thick slab of uniformly distributed radiogenic heat sources, variations in the density of the heat sources, A_0 , primarily affect the temperature structure of the upper lithosphere, with the effects gradually penetrating deeper into the lithosphere through time. This effect is most pronounced during the first 50-60 m.y. following the onset of uplift and erosion; however, the magnitude of the change in the temperature at any depth due to a change in A_0 decreases with passing time beginning after about 30 m.y.. In addition, the change in the temperature at any depth due to a change in the density of the heat sources diminishes rapidly with depth. For example, increasing A_0 from $.84 \mu\text{W}/\text{m}^3$ to $2.0 \mu\text{W}/\text{m}^3$ results in perturbations in the temperature

structure of less than 135°C at any depth and of less than 10°C in the bottom quarter of the lithosphere. Because the forward problem is linear in A_0 , decreasing A_0 from $.84 \mu\text{W}/\text{m}^3$ to $.50 \mu\text{W}/\text{m}^3$ results in similar, but smaller, changes in the temperature structure.

3) Thermal Diffusivity

Variations in the thermal diffusivity (α) mainly affect the temperature structure at mid to upper-mid lithospheric depths. For early times, decreasing the thermal diffusivity from $6.4 \times 10^{-7} \text{ m}^2/\text{s}$ to $5.0 \times 10^{-7} \text{ m}^2/\text{s}$ results in a decrease in temperature (less than 30°C) in the upper lithosphere; however, after sufficiently long times, it results in an increase in the temperature at any depth (less than 70°C). Increasing the thermal diffusivity from $6.4 \times 10^{-7} \text{ m}^2/\text{s}$ to $8.0 \times 10^{-7} \text{ m}^2/\text{s}$ has the reverse effect on the temperature structure, although it results in slightly smaller changes in the temperature structure at most depths and times than does the decrease in α from $6.4 \times 10^{-7} \text{ m}^2/\text{s}$ to $5.0 \times 10^{-7} \text{ m}^2/\text{s}$.

4) Lithospheric Thickness

As with variations in the temperature at the base of the lithosphere, variations in the lithospheric thickness primarily affect the temperature structure of the deep lithosphere; however, they, too, propagate upwards into the lithosphere with time. Decreasing the lithospheric thickness from 120 km to 100 km results in warmer temperatures at all depths because the equilibrium temperature gradient

is increased if T_m is held constant. Increasing the lithospheric thickness from 120 km to 160 km decreases the temperature throughout the upper lithosphere; however, this change in the temperature structure is minimal (e.g., within 100 m.y. of the onset of uplift and erosion, it results in a perturbation of the temperature structure of less than 60°C at depths shallower than 100 km).

5) Uplift Rate

Examining the effects of uplift rates of .4 km/m.y., .6 km/m.y., and .8 km/m.y. reveals that faster uplift rates result in warmer temperatures at all depths at any fixed time. Viewed from a different perspective, comparison of the temperatures at times such that the structural level initially at a specified depth has been uplifted by a fixed amount for the uplift rates .4, .6, and .8 km/m.y. reveals that the temperature of this structural level increases as the uplift rate increases. Also, relative to the temperature calculated using an uplift rate of .6 km/m.y., the difference between the temperatures calculated for any structural level assuming uplift rates of .4 and .6 km/m.y. is slightly larger than that for uplift rates of .8 and .6 km/m.y..

INVERSE MODEL

Extremal bounds on the geotherms were determined from each set of T_z data using a linear-programming inversion scheme. These extremal bounds are either the maximum or minimum temperatures at a specified depth

determined for the set of all geotherms consistent with a given set of constraints. Thus, the set of these extremal temperatures determined for a specified set of constraints form an envelope which contains all possible geotherms. This envelope is usually not, however, a geotherm itself. The sensitivity of the inversion scheme to errors introduced into the mathematical model through truncation of the expansion (1.2), the quality of the Tz data, and to uncertainties in the values of the physical parameters, i.e., temperature at the base of the lithosphere, magnitude of the radiogenic heat productivity, thermal diffusivity, lithospheric thickness, and uplift rate was examined.

The linear programming method can solve only for parameters which enter the problem linearly; therefore, exact values must be assigned to those parameters which do not enter the problem linearly (i.e., thermal diffusivity, uplift rate, lithospheric thickness, and thickness of the radiogenic layer). Unless stated otherwise, inversions assume the same values for these physical parameters as were used in the forward model, i.e., thermal diffusivity (α) = 6.4×10^{-7} m²/s, uplift rate (u) = .6 km/m.y., lithospheric thickness (ℓ) = 120 km, and thickness of the radiogenic layer (a) = 50 km. Because finite difference solutions to the forward problem show that, to a large extent, the thickness of the radiogenic layer trades off with the radiogenic heat productivity (Hubbard, 1985), the effect on the extremal bounds of an incorrect choice for the thickness of this layer was not investigated. Values of the physical parameters which enter linearly into the problem (i.e., temperature at the base of the lithosphere and density of the radiogenic

heat sources) are required to lie within specified ranges. For most inversions, the temperature at the base of the lithosphere (T_m) was required to lie within the range ($1000 \leq T_m(^{\circ}\text{C}) \leq 1350$). The density of the radiogenic heat sources (A_0) was required to lie either within the range ($.83 \leq A_0(\mu\text{W}/\text{m}^3) \leq .85$) or within the range ($.50 \leq A_0(\mu\text{W}/\text{m}^3) \leq 2.0$). In addition, several assumptions were made regarding the quality of the Tz data. Inversions assumed uncertainties in the synthetic Tz data of $\delta S = \pm .5^{\circ}\text{C}$, $\pm 10^{\circ}\text{C}$, or $\pm 50^{\circ}\text{C}$. Uncertainty of $\pm .5^{\circ}\text{C}$ represents essentially no uncertainty in the Tz data. Uncertainty of $\pm 50^{\circ}\text{C}$ is probably larger than the uncertainty in experimental data. Hence, it should be sufficient to account for uncertainties in both temperature and pressure (depth) determined from metamorphic rocks.

Some very general conclusions may be drawn regarding the effects of the various types of uncertainties on the extremal bounds:

- (1) The bounds most sensitive to these uncertainties are the upper temperature bounds at depths above that of the reference horizon and the lower temperature bounds at depths below that of the reference horizon.
- (2) For most cases, a truncation of the mathematical model to $n_{\text{max}}=7$ is sufficient to ensure convergence of the extremal bounds. Thus, envelopes found for $n_{\text{max}}=7$ are very similar to those found for $n_{\text{max}}=12$.
- (3) There is a significant trade-off between the values assumed for the temperature at the base of the lithosphere (T_m) and the radiogenic heat productivity (A_0) with uncertainty in A_0 having a larger

effect on the extremal bounds than uncertainty in T_m ; however, uncertainty in either of these physical parameters is less important than that in the T_z data in reconstruction of geotherms at specified times in the history of the orogenic belt.

- (4) Overestimation of the thermal diffusivity leads to overly optimistic bounds while underestimation of the thermal diffusivity leads to overly pessimistic bounds; however, in all cases, the bounds include the true geotherm.
- (5) Underestimation of the lithospheric thickness requires warmer temperatures in the lower lithosphere than those observed for the correct value of the lithospheric thickness, while overestimation of the lithospheric thickness permits significantly cooler temperatures in the lower lithosphere than those observed for the correct lithospheric thickness. Temperatures at depths shallower than that of the reference horizon are not significantly affected by uncertainty in the lithospheric thickness.
- (6) In general, assumption of a slow uplift rate yields narrower bounds on the geotherms than does assumption of a more rapid uplift rate. However, if the assumed uplift rate is sufficiently slow, it may not be possible to find any geotherms which are consistent with the T_z data and the constraints on both the temperature structure and the physical parameters. In addition, when it is possible to find a solution, assumption of an inaccurate uplift rate may result in an envelope which does not include the true geotherm.

Truncation of Series

Extremal bounds were determined for a truncation of the mathematical model to $n_{\max}=3$ and $n_{\max}=7$ 30 m.y. after the onset uplift of erosion and to $n_{\max}=3, 7$, and 12 10 m.y. following the onset of erosion. Combinations of the inversion parameters $\delta S = \pm 5^\circ\text{C}$, $\pm 10^\circ\text{C}$, and $\pm 50^\circ\text{C}$ with $\{1000 \leq T_m(^{\circ}\text{C}) \leq 1350\}$ or $\{1340 \leq T_m(^{\circ}\text{C}) \leq 1350\}$ and $\{.83 \leq A_0(\mu\text{W}/\text{m}^3) \leq .85\}$ or $\{.50 \leq A_0(\mu\text{W}/\text{m}^3) \leq 2.0\}$ were examined. Figure 2.3 shows the geotherm calculated from the forward model for each of the models 10 m.y. and 30 m.y. after the onset of uplift and erosion (solid lines) and the corresponding envelopes found when $\delta S = \pm 50^\circ\text{C}$, $\{1000 \leq T_m(^{\circ}\text{C}) \leq 1350\}$, and $\{.83 \leq A_0(\mu\text{W}/\text{m}^3) \leq .85\}$. Truncations to $n_{\max}=3$ are shown by the small dashed lines, to $n_{\max}=7$ by the dotted lines, and to $n_{\max}=12$ by the large dashed lines. At $t_b=30$ m.y., the extremal bounds for $n_{\max}=3$ are found to approximate very closely those for $n_{\max}=7$. For $n_{\max}=7$, the temperature at any depth less than that of the reference horizon can be determined to within $\pm 75^\circ\text{C}$. The temperature at any depth greater than that of the reference horizon can be determined to within $\pm 350^\circ\text{C}$ with uncertainties of greater than approximately $\pm 250^\circ\text{C}$ resulting from the uncertainty in the temperature at the base of the lithosphere. A second set of inversions with identical parameters with the exception that $\{.50 \leq A_0(\mu\text{W}/\text{m}^3) \leq 2.0\}$ is shown in Figure 2.4. For $\{.50 \leq A_0(\mu\text{W}/\text{m}^3) \leq 2.0\}$, the temperature bounds expand to $\pm 150^\circ\text{C}$ for depths above that of the reference horizon and to $\pm 500^\circ\text{C}$ for depths below that of the reference horizon with uncertainties of greater than approximately $\pm 350^\circ\text{C}$ resulting from the uncertainty in the temperature at

the base of the lithosphere.

Because the terms of the infinite sum of expansion (1.2) decay exponentially with time, convergence of the bounding envelopes for the 10 m.y. geotherms requires more terms of this expansion than does convergence of the 30 m.y. envelopes. For example, for the values of the physical parameters used in the inversion, the $n=2$ term decays to 55% of its initial value after 10 m.y. and to 17% of its initial value after 30 m.y.. The $n=3$ term decays to 28% of its initial value after 10 m.y. and to 2% of its initial value after 30 m.y.. The $n=4$ term decays to 10% of its initial value after 10 m.y. and to 0.1% of its initial value after 30 m.y.. The $n=5$ term decays to 3% of its initial value after 10 m.y. and to 0.003% of its initial value after 30 m.y..

Examining the 10 m.y. envelopes in more detail reveals that although the lower bounds on temperature at depths above that of the reference horizon and the upper bounds on temperature at depths below that of this horizon are very similar for $n_{max}=3$ and $n_{max}=7$, convergence of the upper bounds on temperature at depths shallower than that of the reference horizon and of the lower bounds on temperature at depths deeper than that of the reference horizon does not occur until $3 < n_{max} \leq 7$. For $\{.83 \leq A_0 (\mu W/m^3) \leq .85\}$, the three and seven coefficient extremal temperatures differ by less than $90^\circ C$ at depths shallower than that of the reference horizon and by less than $150^\circ C$ at depths deeper than that of this horizon. Expanding the range of A_0 to $\{.50 \leq A_0 (\mu W/m^3) \leq 2.0\}$ yields differences between the three and seven coefficient extremal temperatures of as much as $\pm 120^\circ C$ in the upper lithosphere without

affecting the maximum difference in extremal temperatures in the lower lithosphere. These differences are small in comparison to those between the seven coefficient extremal temperatures and the actual temperature.

Uncertainty in Tz Data

For each model, inversions were performed assuming uncertainties in the Tz data of $\pm 0.5^\circ\text{C}$, $\pm 10^\circ\text{C}$, and $\pm 50^\circ\text{C}$. The $\pm 0.5^\circ\text{C}$ errors correspond to essentially perfect data, i.e., to almost no uncertainty in the data. Errors of $\pm 50^\circ\text{C}$ are assumed to include both the errors in temperature and depth inherent in petrologic data. Figure 2.5 shows the extremal bounds on the 10 m.y. and 30 m.y. geotherms (solid lines) for errors in the Tz data of $\pm 0.5^\circ\text{C}$ (small dashed lines), $\pm 10^\circ\text{C}$ (dotted lines), and $\pm 50^\circ\text{C}$ (large dashed lines) for a seven coefficient inversion with $\{1000 \leq T_m(^{\circ}\text{C}) \leq 1350\}$ and $\{.83 \leq A_0(\mu\text{W}/\text{m}^3) \leq .85\}$. Because the difference between the extremal temperature and the actual temperature must be less than or equal to the uncertainty in the the data at the depth of the reference horizon, all envelopes should pinch in to within $\pm \delta S$ of the actual geotherm at this depth (32 km for the 30 m.y. envelopes and 44 km for the 10 m.y. envelopes). This results in a characteristic broadening and constricting of the extremal bounds at depths shallower than that of the reference horizon. The envelopes then broaden again at depths below that of the reference horizon.

Recalling that the coefficients in expansion (1.2) decay with depth as $\exp(-Rz/\ell) \cdot \sin(n\pi z/\ell)$, it is clear that the $n=3$ term must vanish at depths $z=0, 40, 80$, and 120 km. Because the inversion scheme automatically

satisfies this condition, the pinching in of the envelopes at 40 km and 80 km depth is probably due to overestimation of c_3 which produces "swelling" of the envelopes at depths other than 40 and 80 km. This effect is not observed in the 30 m.y. envelopes because the decay with time of the $n=3$ term is sufficiently rapid that its contribution to the temperature structure is small. For $n \geq 4$, the higher order terms are negligible within 10 m.y. of the onset of uplift and erosion. Hence, the requirement that the n th term in the expansion (1.2) vanish at depths $z = k\ell/n$, $k=0,1,\dots,n-1$ exerts little or no influence on the inversion scheme.

At any specified time, the envelopes of all possible geotherms found using the three uncertainties in the Tz data have grossly similar shapes, with a widening of the extremal bounds as the uncertainty in the Tz data increases; however, the increases in the breadth of these bounds is not a simple function of the increase in uncertainty in the Tz data. For inversions at the bound time $t_b = 30$ m.y., the $\pm 5^\circ\text{C}$ envelopes bound the true geotherms to within $\pm 25^\circ\text{C}$; the $\pm 50^\circ\text{C}$ envelopes, on the other hand, differ from the true geotherms by as much as $\pm 350^\circ\text{C}$. For $\delta S = \pm 10^\circ\text{C}$, at depths shallower than that of the reference horizon, the upper bounds on temperature closely approximate those for $\delta S = \pm 50^\circ\text{C}$ while the lower bounds on temperature closely approximate those for $\delta S = \pm 5^\circ\text{C}$. For inversions at $t_b = 10$ m.y., the $\pm 5^\circ\text{C}$ envelopes bound the true geotherms to within $\pm 175^\circ\text{C}$ while the $\pm 50^\circ\text{C}$ extremal temperatures differ from the actual temperatures by up to $\pm 500^\circ\text{C}$.

Temperature at the Base of the Lithosphere

Envelopes were determined for two constraints on the temperature at the base of the lithosphere (T_m): $\{1340 \leq T_m(^{\circ}\text{C}) \leq 1350\}$ and $\{1000 \leq T_m(^{\circ}\text{C}) \leq 1600\}$. The first of these constraints is assumed to represent perfect knowledge of the temperature at the base of the lithosphere while the second is assumed to represent a realistic range of possible values for this parameter. Assuming $\delta S = \pm 50^{\circ}\text{C}$ and $\{.83 \leq A_0(\mu\text{W}/\text{m}^3) \leq .85\}$, Figure 2.6 shows the actual geotherm for Model 1 10 m.y. and 30 m.y. after the onset of uplift and erosion (solid lines) and the envelopes for these geotherms for $\{1000 \leq T_m(^{\circ}\text{C}) \leq 1600\}$ (dashed lines) and $\{1340 \leq T_m(^{\circ}\text{C}) \leq 1350\}$ (dotted lines).

At depths shallower than that of the reference horizon, imperfect knowledge of the temperature at the base of the lithosphere results in a broadening of the extremal bounds of less than 5°C for the 30 m.y. envelopes and less than 60°C for the 10 m.y. envelopes. These differences are negligible in comparison to the differences at any depth between the extremal temperatures and the actual temperature calculated from the forward model. At depths greater than that of the reference horizon, larger discrepancies are observed between these two sets of extremal temperatures. These are expected as there are fewer constraints on the allowable temperature structure in this region than in the upper part of the lithosphere.

The extremal temperatures allowed at the base of the lithosphere are very important in the determination of the extremal temperatures in the deep lithosphere. Because the effect of uplift is to increase the

temperature in the lower lithosphere with time, the range of depths for which the extremal bounds on temperature are relatively large propagates upward into the lower lithosphere with time.

Although heat flow studies have yielded estimates of the temperature at the base of the lithosphere of $1350 \pm 250^\circ\text{C}$ (Parsons and Sclater, 1977), petrologic studies find that the temperature at the base of the lithosphere should not exceed 1350°C . Because of this, and because allowing an increase in the temperature at the base of the lithosphere from 1350°C to 1600°C has a negligible effect on the bounds on the temperature structure of the upper lithosphere (the region of primary interest), future inversions will be restricted to the constraint $\{1000 \leq T_m(^{\circ}\text{C}) \leq 1350\}$.

Radiogenic Heat Production

Assuming $\delta S = 50^\circ\text{C}$, $\{1000 \leq T_m(^{\circ}\text{C}) \leq 1350\}$, and $n_{\text{max}}=7$, Figure 2.7 shows the extremal temperature bounds for two different constraints on the heat productivity: $\{.83 \leq A_0(\mu\text{W}/\text{m}^3) \leq .85\}$ (dashed lines) and $\{.50 \leq A_0(\mu\text{W}/\text{m}^3) \leq 2.0\}$ (dotted lines). At $t_b=30$ m.y., inversions assuming perfect knowledge of A_0 ($\{.83 \leq A_0(\mu\text{W}/\text{m}^3) \leq .85\}$) yield temperatures that differ from the true temperature by less than $\pm 80^\circ\text{C}$ at depths shallower than that of the reference horizon; however, in this region, inversions at $t_b=10$ m.y. return extremal temperatures which differ from the actual temperature by as much as $\pm 475^\circ\text{C}$. Swelling of the extremal bounds at depths greater than that of the reference horizon and uncertainty in the temperature at the base of the lithosphere contribute to larger

uncertainties in the temperature structure of the lower lithosphere.

Enlarging the allowable range of values for A_0 to $\{.50 \leq A_0 (\mu\text{W}/\text{m}^3) \leq 2.0\}$ primarily affects the lower bounds on temperature at depths deeper than that of the reference horizon. Differences between the lower bounds on temperatures when $.50 \leq A_0 (\mu\text{W}/\text{m}^3) \leq 2.0$ and the temperatures calculated from the forward model may be as large as $\pm 500^\circ\text{C}$ at $t_b=30$ m.y. and $\pm 800^\circ\text{C}$ at $t_b=10$ m.y..

The latitude in the range of values allowed for A_0 trades off with that allowed for T_m . At most depths, uncertainty in A_0 has a greater effect on the extremal bounds than does uncertainty in T_m ; however, the effect on the extremal bounds of the uncertainty in T_m becomes comparable to or exceeds that in A_0 at increasingly shallower depths as time progresses. In any case, the uncertainty in either T_m or A_0 is less important than that in the Tz data in determining the extremal bounds on all possible geotherms.

Thermal Diffusivity

Choosing $n_{\text{max}}=7$, $\delta S = 50^\circ\text{C}$, $\{1000 \leq T_m (^\circ\text{C}) \leq 1350\}$ and either $\{.83 \leq A_0 (\mu\text{W}/\text{m}^3) \leq .85\}$ or $\{.50 \leq A_0 (\mu\text{W}/\text{m}^3) \leq 2.0\}$, the effects on the extremal temperature bounds were investigated for several values of thermal diffusivity. As shown in Figure 2.8 underestimation of the thermal diffusivity ($\alpha=5.0 \times 10^{-7} \text{ m}^2/\text{s}$) (small dashed lines) yields extremal bounds which are larger than those determined for the true value of the thermal diffusivity ($\alpha=6.4 \times 10^{-7} \text{ m}^2/\text{s}$) (dotted lines) while overestimation of the thermal diffusivity ($\alpha=8.0 \times 10^{-7} \text{ m}^2/\text{s}$) (large dashed

lines) underestimates these bounds. The envelope of all possible geotherms appears to converge on the true geotherm as the value assumed for the thermal diffusivity increases; however, this is not what is actually occurring. If the conductivity were infinite, diffusion would result in instantaneous loss of all excess heat in the lithosphere and one would expect to recover a linear steady-state geotherm. For small conductivities, the terms in the expansion (1.2) decay slowly with time; hence, as the conductivity becomes smaller, the extremal bounds converge more slowly on a steady-state geotherm. It is fortunate that for the range of thermal diffusivities believed to be representative of those present in the lithosphere, convergence on the linear steady-state geotherm is sufficiently slow that it is unlikely that the true geotherm will lie outside the extremal bounds.

Lithospheric Thickness

Figure 2.9 shows the effect of uncertainty in the lithospheric thickness (ℓ) on inversions in which $n_{\max}=7$, $\delta S = 50^\circ\text{C}$, $\{1000 \leq T_m(^{\circ}\text{C}) \leq 1350\}$ and $\{.83 \leq A_0(\mu\text{W}/\text{m}^3) \leq .85\}$. Extremal bounds are shown for $\ell = 100$ km (small dashed lines), $\ell = 120$ km (dotted lines), and $\ell = 160$ km (large dashed lines). Uncertainty in the lithospheric thickness has a negligible effect on the extremal bounds at depths above that of the reference horizon. Below this depth, the extremal bounds on maximum temperature found for a lithospheric thickness of 160 km are very similar to those found for the lithospheric thickness for which the T_z data were generated (120 km), while the bounds on minimum temperature

allow significantly cooler temperatures than those allowed by a correct choice of ℓ . Underestimation of the lithospheric thickness primarily affects the extremal bounds on minimum temperature in the lower lithosphere. Warmer temperatures than those found for a correct choice of lithospheric thickness are required in order to maintain the boundary condition at the base of the lithosphere.

Uplift Rate

The effect of uplift rate on the inversion of Tz data for extremal bounds was also investigated. Synthetic Tz data were inverted assuming an uplift rate which differed from that of the forward model by $\pm 33\%$. Tz data synthesized with a variable uplift rate were also inverted assuming a constant uplift rate.

Tz data generated assuming $u=.6$ km/m.y. were inverted for the three models with uplift rates of .4, .6, and .8 km/m.y.. The resulting bounds on the temperature structure found when the reference horizon initially at 50 km depth has been uplifted to 26 km for inversions in which $\{1000 \leq T_m (^{\circ}\text{C}) \leq 1350\}$, $\{.83 \leq A_0 (\mu\text{W}/\text{m}^3) \leq .85\}$, and $\delta S = 50^{\circ}\text{C}$ are shown in Figure 2.10. In each plot, the geotherm calculated from the forward model is shown by the solid line, the .4 km/m.y. envelope by the small dashed lines, the .6 km/m.y. envelope by the dotted lines, and the .8 km/m.y. envelope by the large dashed lines. Note that it takes more time for the reference horizon to reach 26 km depth as the uplift rate decreases. For example, the reference horizon initially at 50 km depth reaches 26 km when $t_b=30$ m.y. if $u=.8$ km/m.y., when $t_b = 40$ m.y. if

$u = .6$ km/m.y., and when $t_b = 60$ m.y. if $u = .4$ km/m.y.. Because the terms of the infinite sum of expansion (1.2) decay with time, at a fixed depth, the infinite sum in (1.2) contributes less to the temperature structure for slower uplift rates than for faster uplift rates. Hence, the extremal bounds on the temperature tighten as the uplift rate decreases.

The effect of an incorrect assumption of the value of the uplift rate becomes more important as time progresses. Extremal bounds found when the reference horizon initially at 50 km has reached a depth of 2 km are shown in Figure 2.11 for uplift rates of .4 km/m.y. (small dashed lines), .6 km/m.y. (dotted lines), and .8 km/m.y. (large dashed lines). The extremal bounds contain the true geotherm at all depths when the uplift rate assumed for the inversion is either .6 km/m.y. or .8 km/m.y.. However, the extremal bounds underestimate the true temperature at all depths for Models 1 and 2 when the uplift rate is .4 km/m.y.. This results from the longer time required for the reference horizon to reach 2 km, and subsequently, the greater decay of the terms of the infinite sum, for an uplift rate of .4 km/m.y. than for a correct choice of the uplift rate (.6 km/m.y.).

If the inversion scheme assumes an uplift rate which is slower than that assumed in the forward model, fitting the T_z data at any depth allows only a small number of sets of values of the coefficients $\{c_n\}$. This occurs because a slower uplift rate implies a longer elapsed time before the reference horizon reaches a particular depth; hence, each term in expansion (1.2) will have decayed to a smaller fraction of its initial value than for the correct uplift rate. Because of the rate of

decay with depth of the terms of the sum, it may be impossible to fit the remaining Tz data subject to the other constraints on the temperature structure with any of these sets of coefficients. Because the terms of the sum decay more slowly with depth as uplift rate increases, more interplay among the coefficients is allowed in the inversion of the Tz data if faster uplift rates are assumed for the inversion than were assumed for the forward model. Thus, for any datum, a larger number of sets of possible values for the coefficients is allowed, and, hence, unlike inversions which assume slower uplift rates, inversions which assume faster uplift rates may be able to find a set of coefficients which fit all of the Tz data and which also satisfy the other constraints on the temperature structure.

Variable Uplift Rate

Tz data generated from the finite difference method assuming an uplift rate which varies linearly with time ($u(t) = .2 + .008t$ km/m.y.) for a 60-km thick thrust sheet model (Model 4) were inverted assuming constant uplift rates $u = .4, .6,$ and $.8$ km/m.y. for $n_{max}=7$, $\delta S = \pm .5^\circ\text{C}, \pm 10^\circ\text{C},$ or $\pm 50^\circ\text{C}$, $\{1000 \leq T_m(^\circ\text{C}) \leq 1350\}$ and $\{.83 \leq A_0(\mu\text{W}/\text{m}^3) \leq .85\}$. The extremal bounds on the temperature found when the reference horizon has reached 26 km depth for inversions in which $\{1000 \leq T_m(^\circ\text{C}) \leq 1350\}$, $\{.83 \leq A_0(\mu\text{W}/\text{m}^3) \leq .85\}$, and $\delta S = 50^\circ\text{C}$ are shown in Figure 2.12. Again, the geotherm calculated from the finite difference method when the reference horizon has been uplifted 14 km to a depth of 26 km is shown by the solid line, the .4 km/m.y. envelope by the small dashed lines, the

.6 km/m.y. envelope by the dotted lines, and the .8 km/m.y. envelope by the large dashed lines. Because the Tz data generated for this model do not differ significantly from those generated for Model 3, these envelopes are almost identical to those discussed above for corresponding inversions. As with the envelopes found for Model 3, these envelopes broaden with increasing uplift rate and each envelope contains the actual geotherm found from the forward model.

CONCLUSIONS

The extremal bound linear-programming technique can be used to invert metamorphic temperature-depth data for bounds on ancient geotherms in orogenic belts. Uncertainty in the Tz data has a much more important effect on the extremal bounds than does either uncertainty in any of the physical parameters of the model or error introduced into the mathematical model through truncation of the sum of expansion (1.2). The most important of the physical parameters is the uplift rate, because an incorrect choice of uplift rate can result in extremal bounds which do not include the true geotherm. Fortunately, petrologic techniques make it possible to assign an average uplift rate with a reasonable amount of confidence. Because it primarily affects the extremal bounds in the upper two-thirds of the lithosphere, the next most important of the physical parameters is the radiogenic heat productivity. Because the region of primary interest is the upper lithosphere, and because the temperature at the base of the lithosphere and the lithospheric thickness

primarily affect the temperatures in the deep lithosphere, these parameters are relatively unimportant. Unfortunately, because these parameters have negligible effects on the temperature structure of the upper lithosphere, this inversion scheme cannot be used to place any constraints on the values of these parameters, and thus will not contribute significantly to our knowledge of the nature of the lower lithosphere.

FIGURE CAPTIONS

Figures 2.1a-d: Initial geotherms (solid lines) and the temperature-depth path (dotted lines) for the crustal horizon initially at 50 km depth for Models 1-4. Models 1-3 assume a constant uplift rate of .6 km/m.y.. Model 4 assumes a linearly varying uplift rate $u(t) = .2 + .008t$ km/m.y.. Large circles show the T_z data points used in the inversions.

Figure 2.2a-e: Effects of variations in the physical parameters on evolving geotherms for Models 1-3. In each case, the initial geotherm was held fixed, and the evolving geotherms calculated by allowing variation in only one physical parameter. Unless stated otherwise, geotherms are calculated assuming the following values for the physical parameters: temperature at the base of the lithosphere: 1350°C, density of radiogenic heat sources: $.84 \mu\text{W}/\text{m}^3$, thermal diffusivity: $6.4 \times 10^{-7} \text{ m}^2/\text{s}$, lithospheric thickness: 120 km, and uplift rate: .6 km/m.y.. Plots are shown for Model 1 10 m.y. (Figure 2.2a), 30 m.y. (Figure 2.2b), and 50 m.y. (Figure 2.2c) after the onset of uplift and erosion, and for Models 2 and 3 30 m.y after the onset of uplift and erosion (Figures 2.2d, 2.2e). In the upper left-hand plots, geotherms are shown for temperatures at the base

of the lithosphere of 1000°C (dashed lines), 1350°C (solid lines), and 1600°C (dotted lines). In the upper center plots, geotherms are shown for a 50 km thick slab of uniformly distributed heat sources. Densities of these heat sources are $.50 \mu\text{W}/\text{m}^3$ (dashed lines), $.84 \mu\text{W}/\text{m}^3$ (solid lines), and $2.0 \mu\text{W}/\text{m}^3$ (dotted lines). The upper right-hand plots show the effect of variations in thermal diffusivity. Geotherms are plotted for thermal diffusivities of $5.0 \times 10^{-7} \text{ m}^2/\text{s}$ (dashed lines), $6.4 \times 10^{-7} \text{ m}^2/\text{s}$ (solid lines), and $8.0 \times 10^{-7} \text{ m}^2/\text{s}$ (dotted lines). The effects of lithospheric thicknesses of 100 km (dashed lines), 120 km (solid lines), and 160 km (dotted lines) on the evolving geotherms are shown in the lower left-hand plots. The lower right-hand plots show geotherms calculated for uplift rates of $.4 \text{ km}/\text{m.y.}$ (dashed lines), $.6 \text{ km}/\text{m.y.}$ (solid lines), and $.8 \text{ km}/\text{m.y.}$ (dotted lines).

Figure 2.3: Geotherms and extremal bounds on the geotherms for Models 1-3 30 m.y. after the onset of uplift and erosion and 10 m.y. after the onset of uplift and erosion determined for several different truncations of the mathematical model. Geotherms calculated from the forward model are shown by the solid lines. Extremal bounds on the 30 m.y. geotherms are shown for truncations

of the infinite sum to $n_{\max}=3$ (small dashed lines) and to $n_{\max}=7$ (dotted lines). Extremal bounds on the 10 m.y. geotherms are shown for truncations of the sum to $n_{\max}=3$ (small dashed lines), to $n_{\max}=7$ (dotted lines), and to $n_{\max}=12$ (large dashed lines). Other inversion parameters are: uncertainty in the T_z data $\delta S = \pm 50^\circ\text{C}$, temperature at the base of the lithosphere, T_m : $\{1000 \leq T_m(^{\circ}\text{C}) \leq 1350\}$, radiogenic heat productivity, A_0 : $\{.83 \leq A_0(\mu\text{W}/\text{m}^3) \leq .85\}$, uplift rate, u : .6 km/m.y., thermal diffusivity, α : $6.4 \times 10^{-7} \text{ m}^2/\text{s}$, and lithospheric thickness, ℓ : 120 km. The radiogenic layer was assumed to have a thickness of 50 km.

Figure 2.4: Geotherms and extremal bounds on the geotherms for Models 1-3 30 m.y. and 10 m.y. after the onset of uplift and erosion determined for several different truncations of the mathematical model. Geotherms calculated from the forward model are shown by the solid lines. Extremal bounds on the 30 m.y. geotherms are shown for truncations of the infinite sum to $n_{\max}=3$ (small dashed lines) and to $n_{\max}=7$ (dotted lines). Extremal bounds on the 10 m.y. geotherms are shown for truncations of the expansion to $n_{\max}=3$ (small dashed lines), to $n_{\max}=7$ (dotted lines), and to $n_{\max}=12$ (large dashed lines). Inversion parameters are the same of those of Figure 2.3 except

that $(.50 \leq A_0 (\mu\text{W}/\text{m}^3) \leq 2.0)$.

Figure 2.5: Geotherms and extremal bounds on the geotherms for Models 1-3 30 m.y. and 10 m.y. after the onset of uplift and erosion assuming three different uncertainties in the Tz data. Geotherms calculated from the forward model are shown by the solid lines. Also shown are the extremal bounds on these geotherms for uncertainties in the Tz data of $\pm 5^\circ\text{C}$ (small dashed lines), $\pm 10^\circ\text{C}$ (dotted lines), and $\pm 50^\circ\text{C}$ (large dashed lines) for a seven coefficient inversion ($n_{\text{max}}=7$). Other inversion parameters are: temperature at the base of the lithosphere, T_m : $(1000 \leq T_m (^\circ\text{C}) \leq 1350)$, radiogenic heat productivity, A_0 : $(.83 \leq A_0 (\mu\text{W}/\text{m}^3) \leq .85)$, uplift rate, u : .6 km/m.y., thermal diffusivity, α : $6.4 \times 10^{-7} \text{ m}^2/\text{s}$, and lithospheric thickness, ℓ : 120 km. The radiogenic layer was assumed to have a thickness of 50 km.

Figure 2.6: Geotherms and extremal bounds in the geotherms for Model 1 30 m.y. after the onset of uplift and erosion and 10 m.y. after the onset of uplift and erosion for two constraints on the temperature at the base of the lithosphere. The actual geotherms are shown by the solid lines. The envelopes for these geotherms are shown for $(1000 \leq T_m (^\circ\text{C}) \leq 1600)$ (dashed lines) and

$\{1340 \leq T_m(^{\circ}\text{C}) \leq 1350\}$ (dotted lines). Other inversion parameters have the values: $n_{\text{max}}=7$, uncertainty in the Tz data $\delta S = \pm 50^{\circ}\text{C}$, density of radiogenic heat sources, A_0 : $\{.83 \leq A_0(\mu\text{W}/\text{m}^3) \leq .85\}$, thickness of the radiogenic layer, a : 50 km, uplift rate, u : .6 km/m.y., thermal diffusivity, α : $6.4 \times 10^{-7} \text{ m}^2/\text{s}$, and lithospheric thickness, l : 120 km.

Figure 2.7: Geotherms and extremal bounds on the geotherms for Models 1-3 30 m.y. after the onset of uplift and erosion and 10 m.y. after the onset of uplift and erosion for two constraints on the magnitude of the radiogenic heating. Geotherms calculated from the forward model are shown by the solid lines. Extremal bounds on these geotherms assuming perfect knowledge of A_0 , i.e., $\{.83 \leq A_0(\mu\text{W}/\text{m}^3) \leq .85\}$ are shown by the dashed lines. Extremal bounds for an expanded range of values of A_0 : $\{.50 \leq A_0(\mu\text{W}/\text{m}^3) \leq 2.0\}$ are shown by the dotted lines.

Figure 2.8: Geotherms and extremal bounds for a range of values of thermal diffusivity. The geotherms calculated from the forward model for a thermal diffusivity of $6.4 \times 10^{-7} \text{ m}^2/\text{s}$ are shown by the solid lines. Extremal bounds are shown for thermal diffusivities of $5.0 \times 10^{-7} \text{ m}^2/\text{s}$ (small dashed lines), $6.4 \times 10^{-7} \text{ m}^2/\text{s}$ (dotted lines), and $8.0 \times 10^{-7} \text{ m}^2/\text{s}$

(large dashed lines).

Figure 2.9: Effect of uncertainty in the lithospheric thickness on the extremal bounds. Forward model geotherms are shown by the solid lines. Extremal bounds are shown for $\ell = 100$ km (small dashed lines), $\ell = 120$ km (dotted lines), and $\ell = 160$ km (large dashed lines). Other inversion parameters are: uncertainty in the Tz data $\delta S = \pm 50^\circ\text{C}$, temperature at the base of the lithosphere, $T_m: \{1000 \leq T_m (\text{°C}) \leq 1350\}$, radiogenic heat productivity, $A_0: \{.83 \leq A_0 (\mu\text{W}/\text{m}^3) \leq .85\}$, thickness of the radiogenic layer $a: 50$ km, uplift rate, $u: .6$ km/m.y., thermal diffusivity, $\alpha: 6.4 \times 10^{-7}$ m²/s, lithospheric thickness, $\ell: 120$ km, and $n_{\text{max}}=7$.

Figure 2.10: Effect of uplift rate on the extremal bounds obtained for the reference horizon initially at 50 km depth after it has been uplifted to 26 km depth. In each plot, the geotherm calculated from the forward model is shown by the solid line, the .4 km/m.y. envelope by the small dashed lines, the .6 km/m.y. envelope by the dotted lines, and the .8 km/m.y. envelope by the large dashed lines.

Figure 2.11: Effect of uplift rate on the extremal bounds determined

for the reference horizon initially at 50 km depth after it has been uplifted 48 km to a depth of 2 km. In each plot, the geotherm calculated from the forward model is shown by the solid line, the .4 km/m.y. envelope by the small dashed lines, the .6 km/m.y. envelope by the dotted lines, and the .8 km/m.y. envelope by the large dashed lines.

Figure 2.12: Effect on the extremal bounds of inverting data generated for a 60 km thick thrust sheet model with a linearly varying uplift rate ($u(t) = .2 + .008t$ km/m.y.) with a constant uplift rate. The geotherm calculated from the forward model when the reference horizon initially at 50 km depth has reached 26 km is shown by the solid line. Envelopes are shown for constant uplift rates of .4 km/m.y. (small dashed lines), .6 km/m.y. (dotted lines), and .8 km/m.y. (large dashed lines).

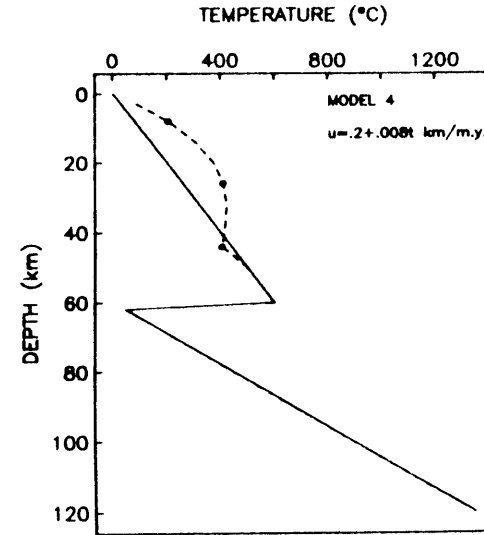
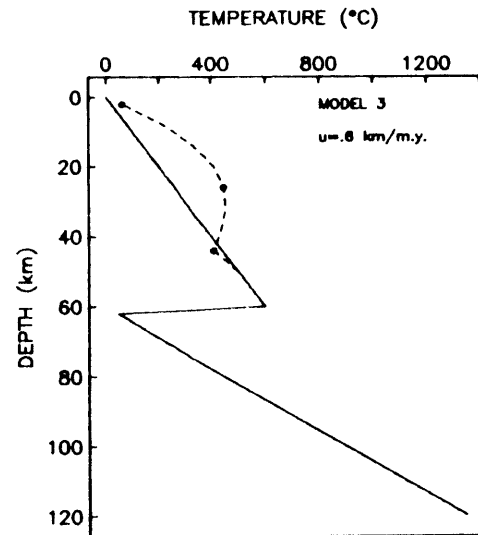
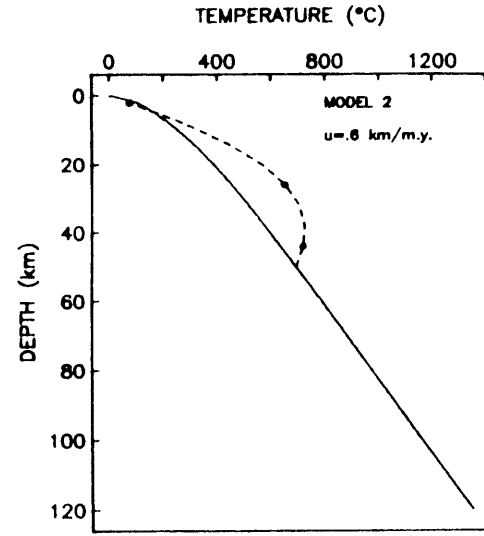
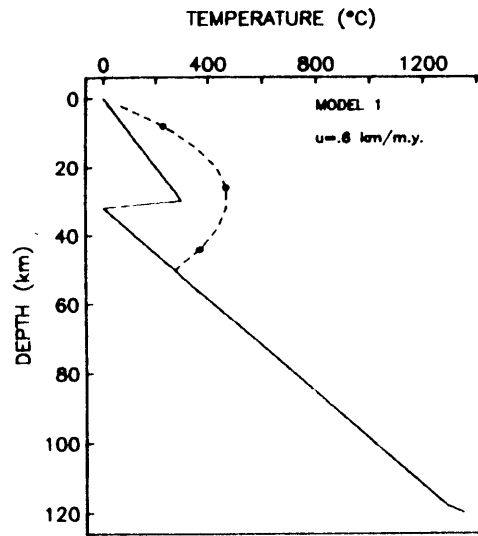


Figure 2.1

MODEL 1
10 m.y.

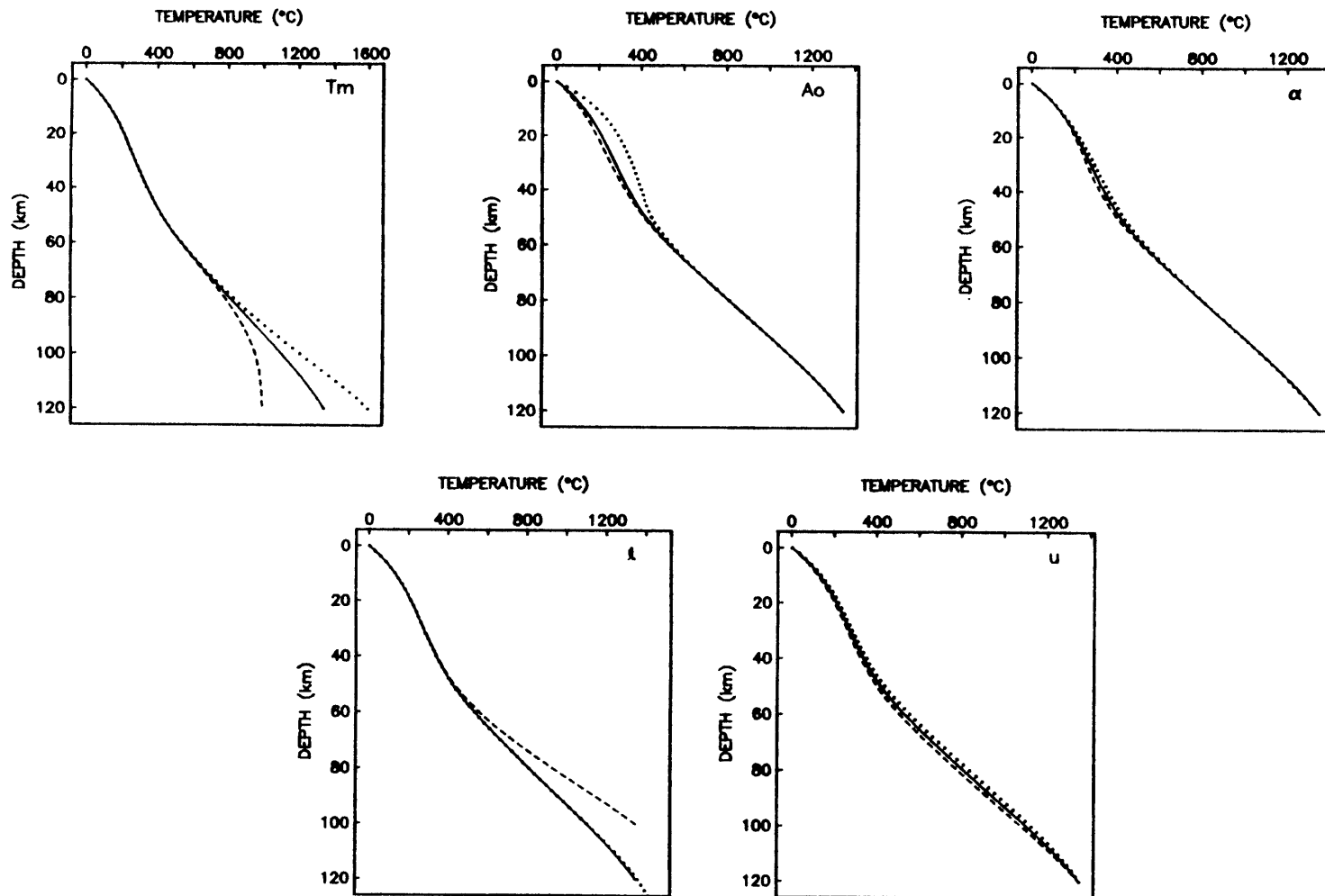


Figure 2.2a

MODEL 1
30 m.y.

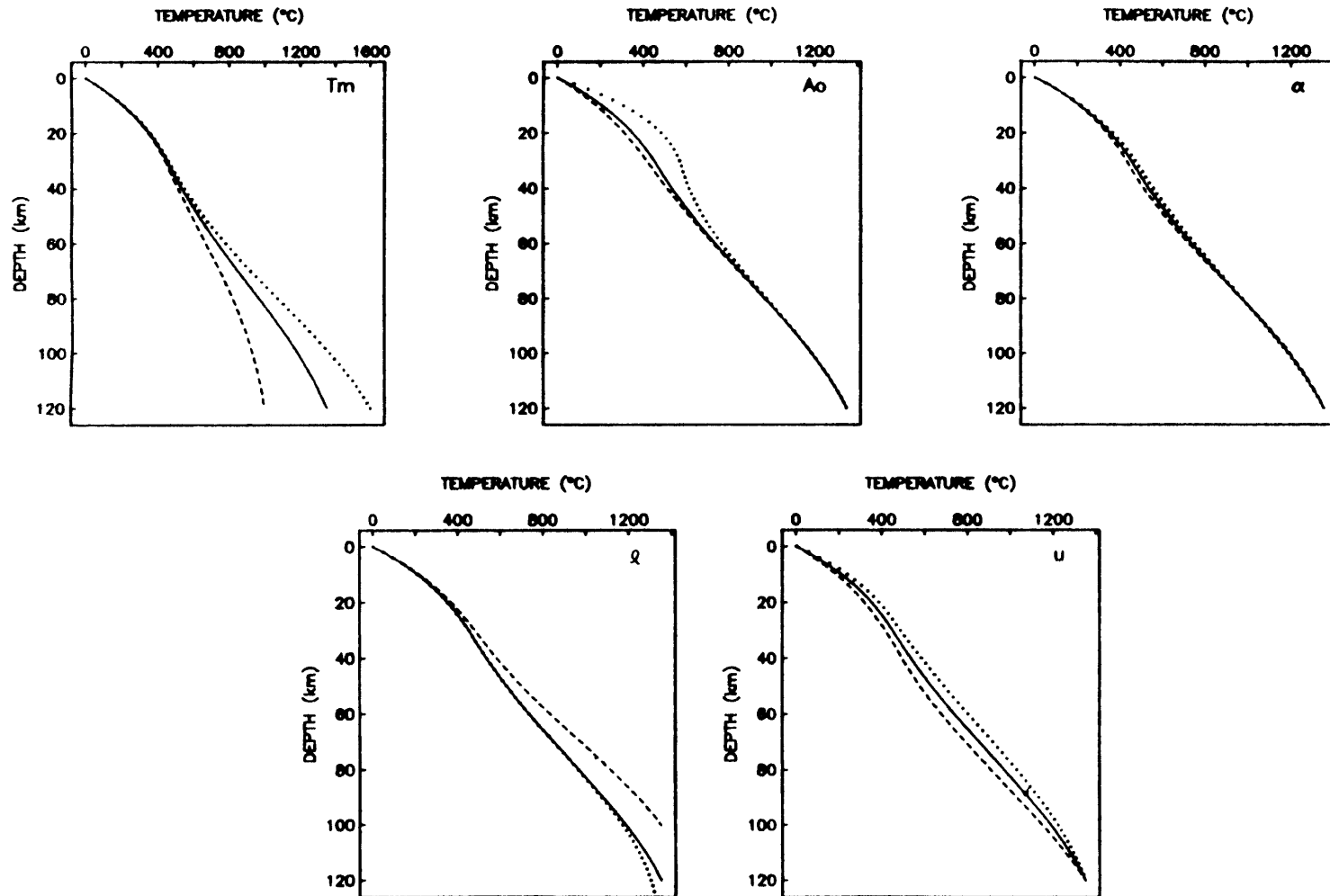


Figure 2.2b

MODEL 1
50 m.y.

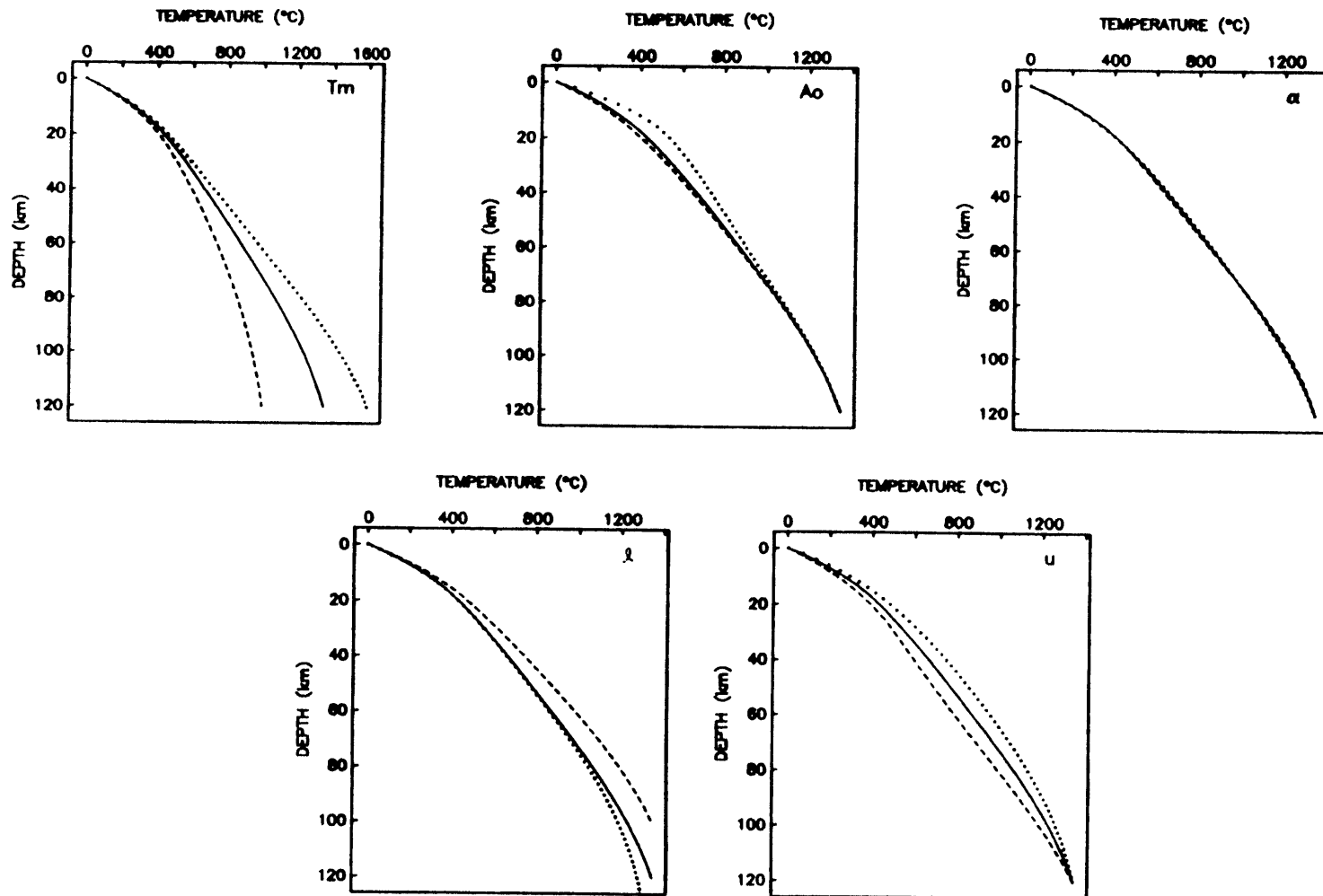


Figure 2.2c

MODEL 2
30 m.y.

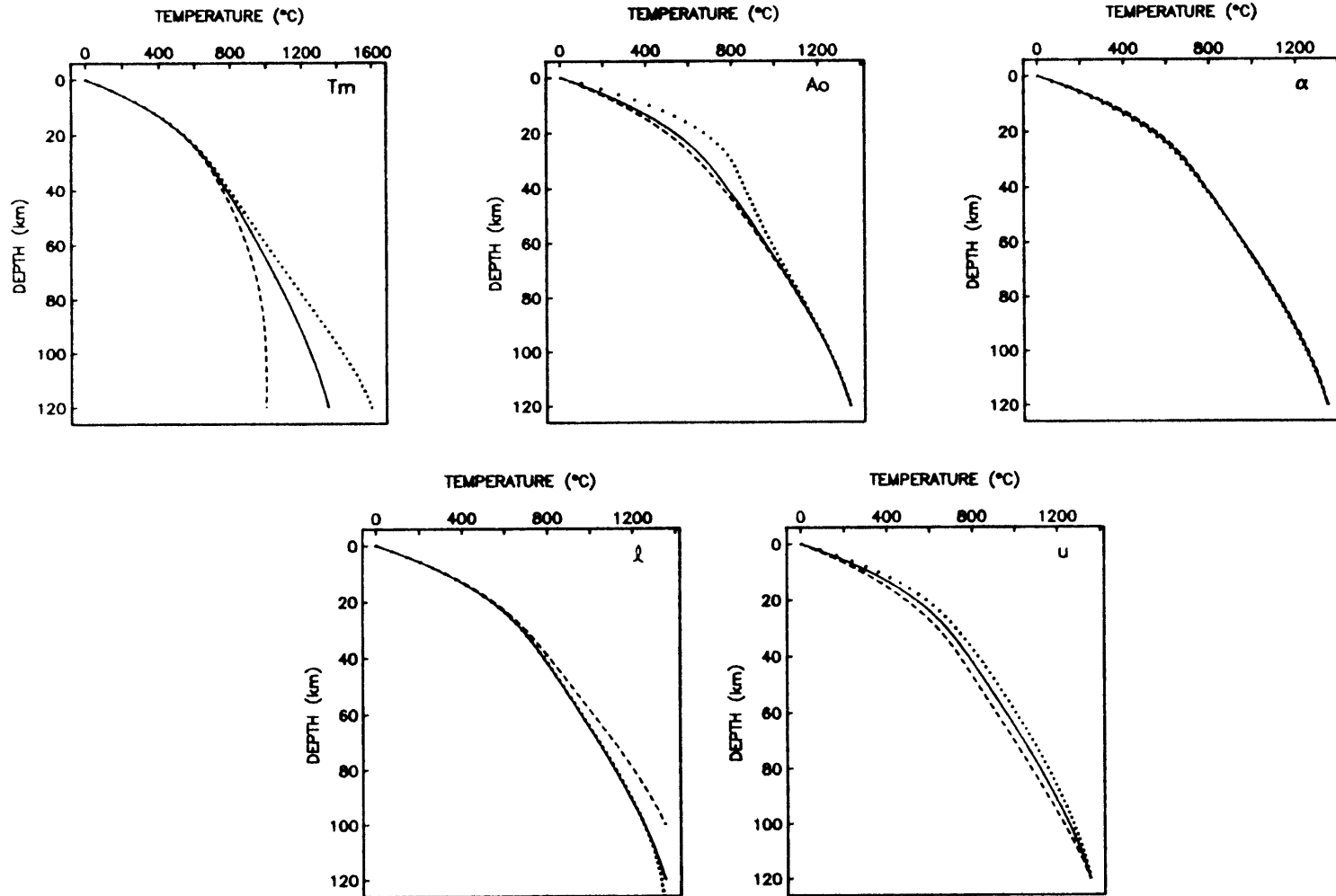


Figure 2.2d

MODEL 3
30 m.y.

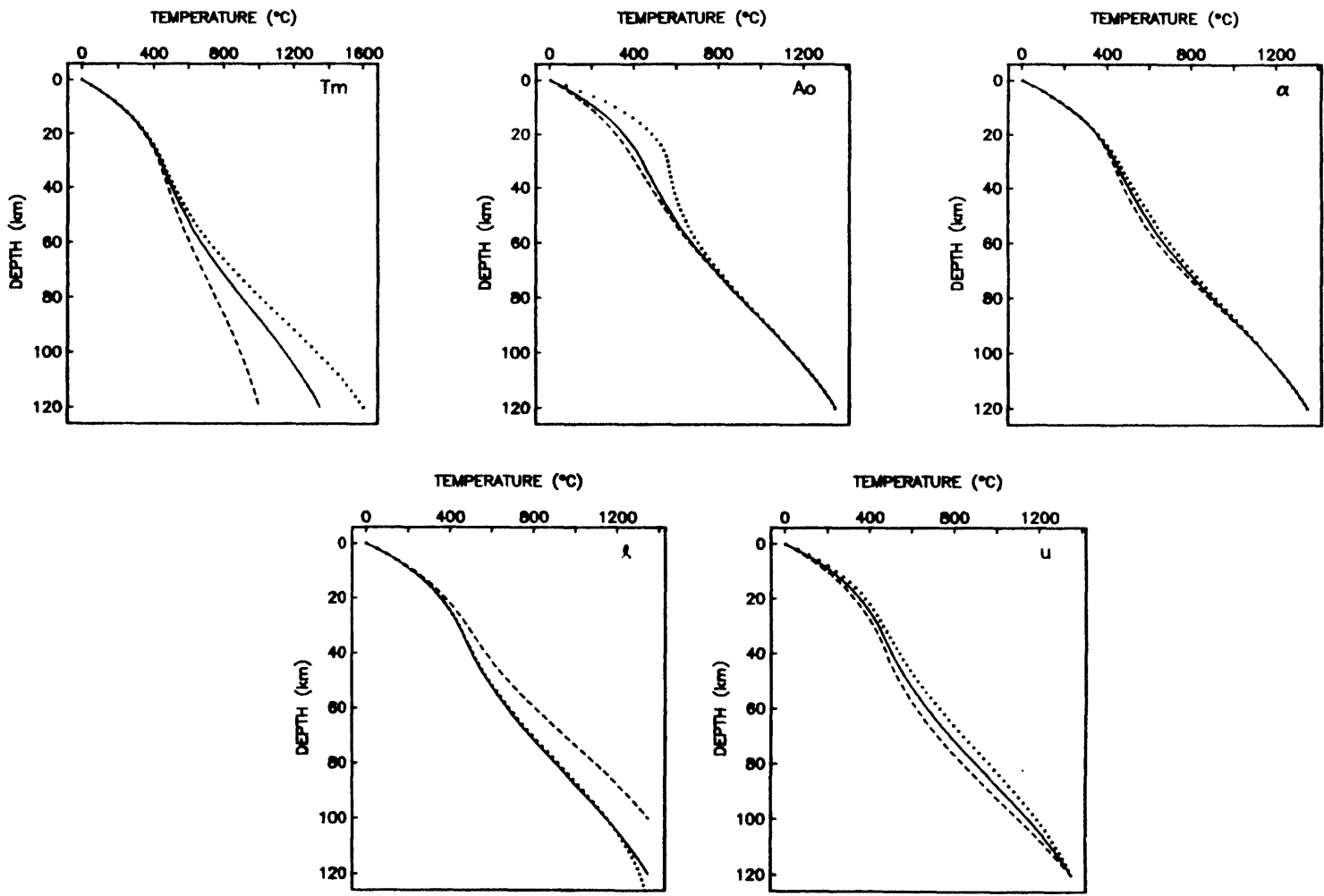


Figure 2.2e

TRUNCATION OF SERIES

$$.83 \leq A_0 (\mu W / m^2) \leq .85$$

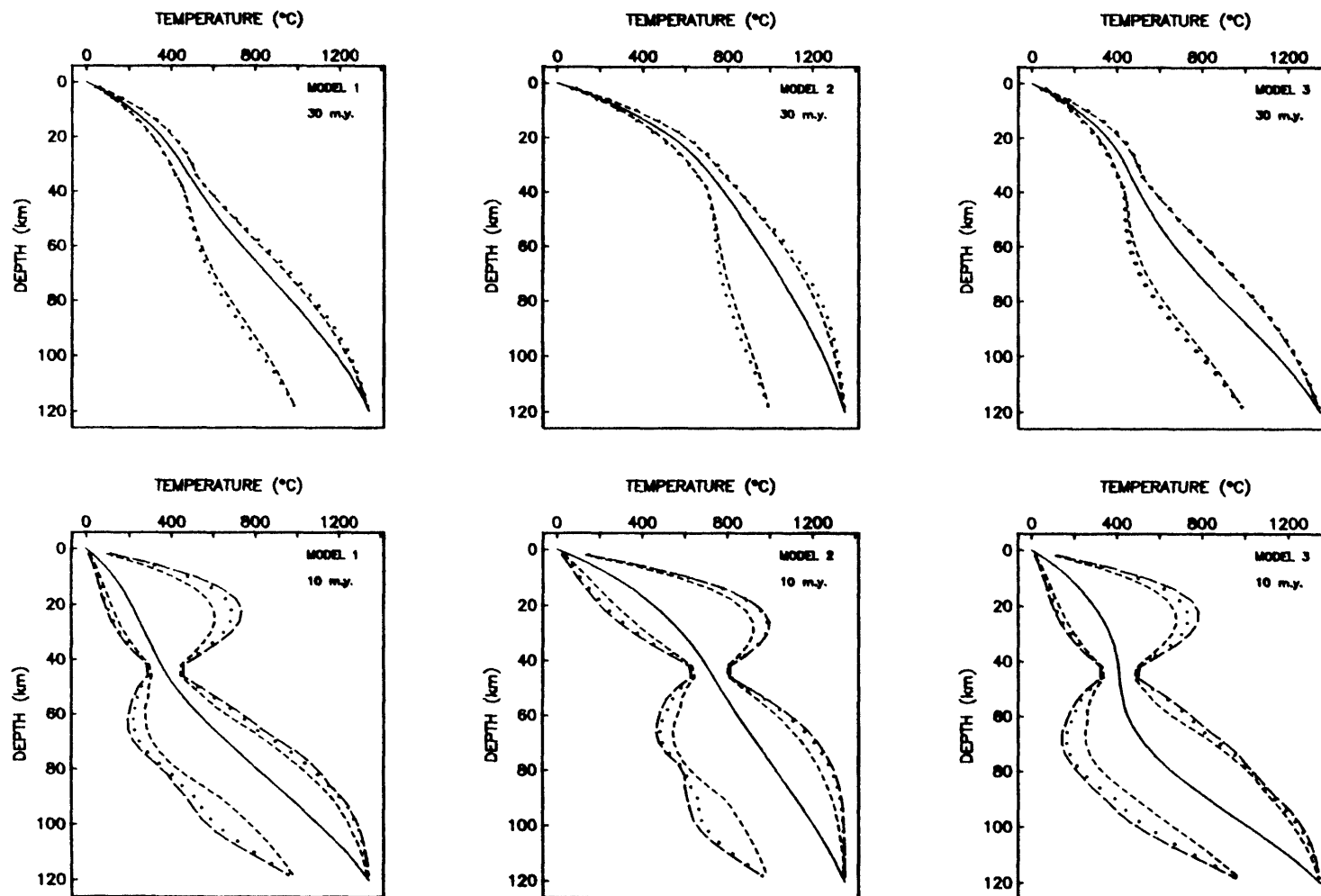


Figure 2.3

TRUNCATION OF SERIES

$$.50 \leq A_0 (\mu W / m^2) \leq 2.0$$

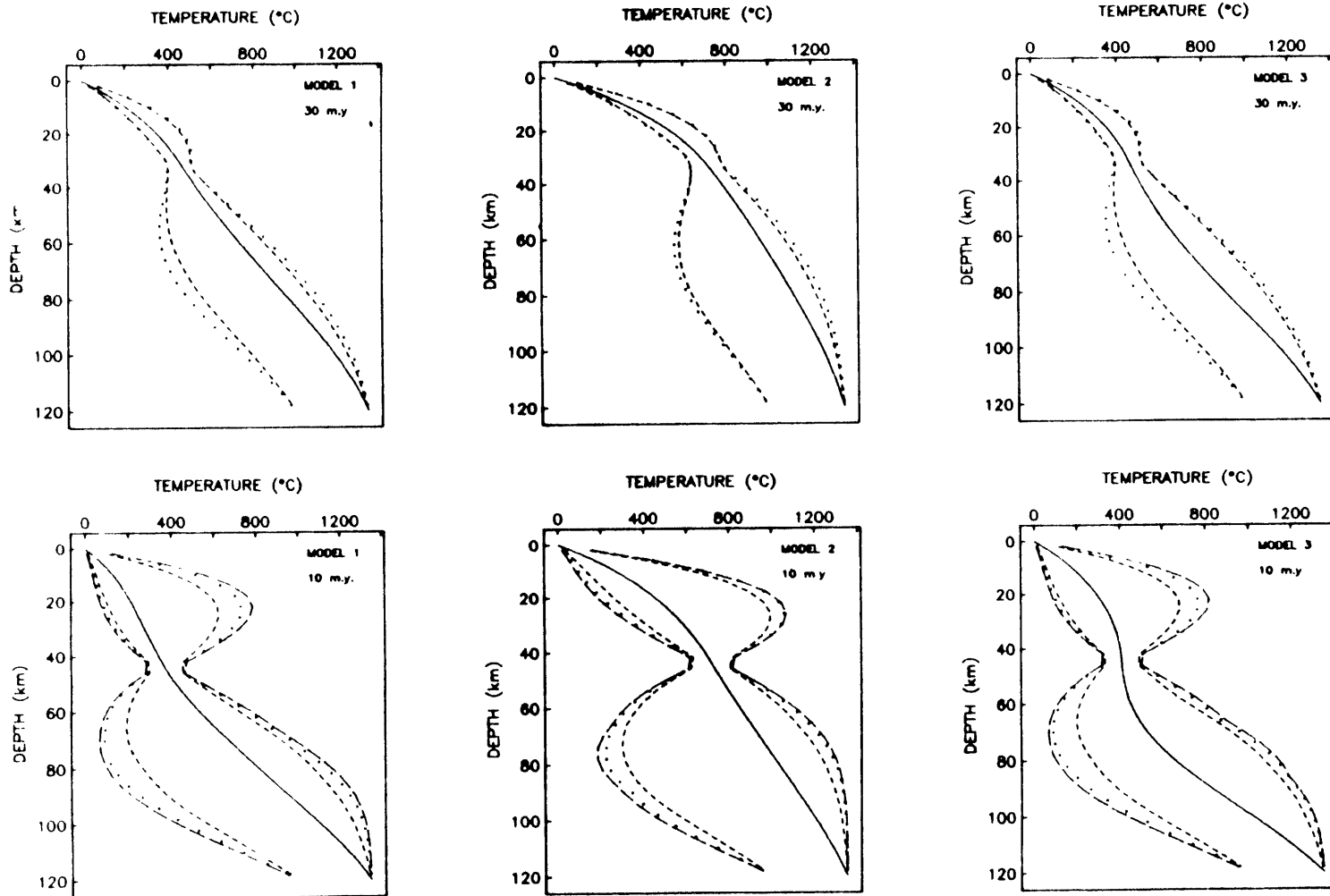


Figure 2.4

Tz DATA

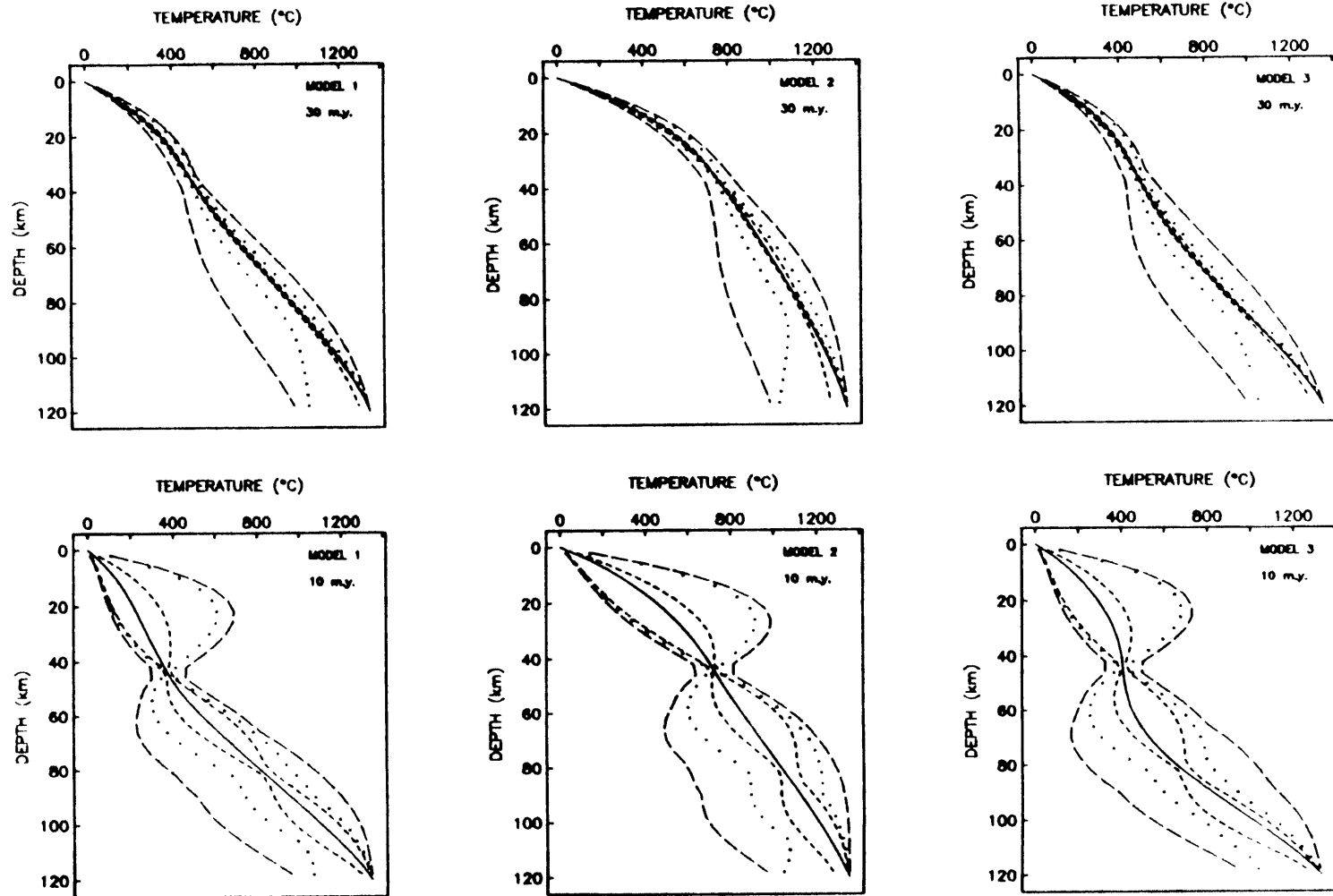


Figure 2.5

TEMPERATURE

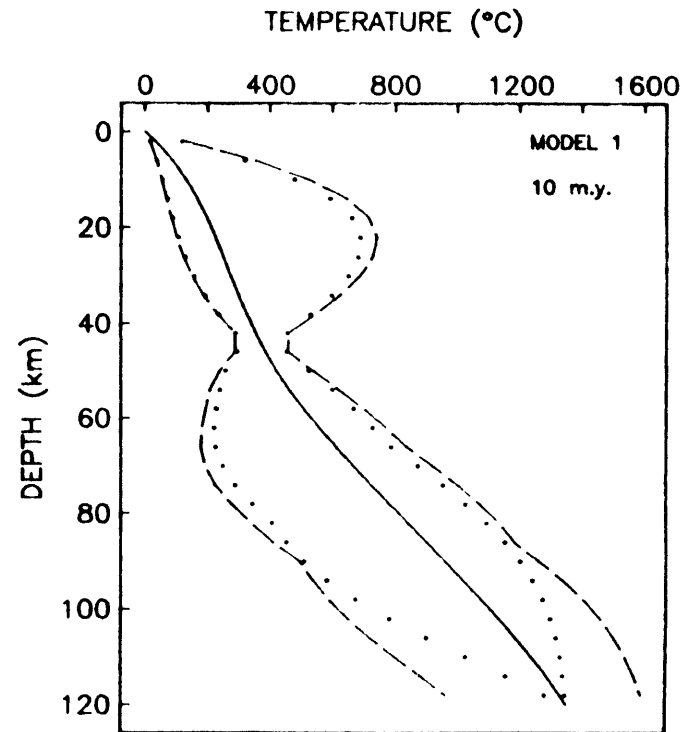
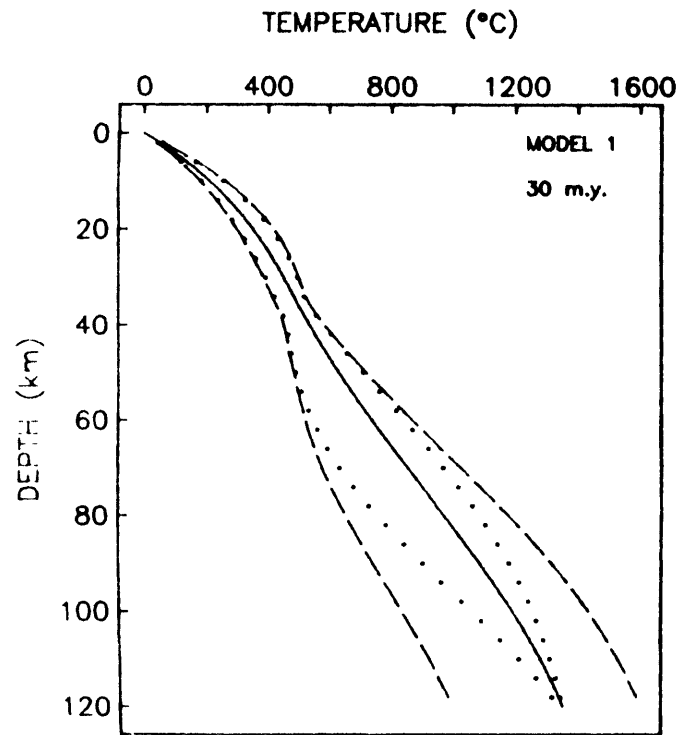


Figure 2.6

RADIOACTIVITY

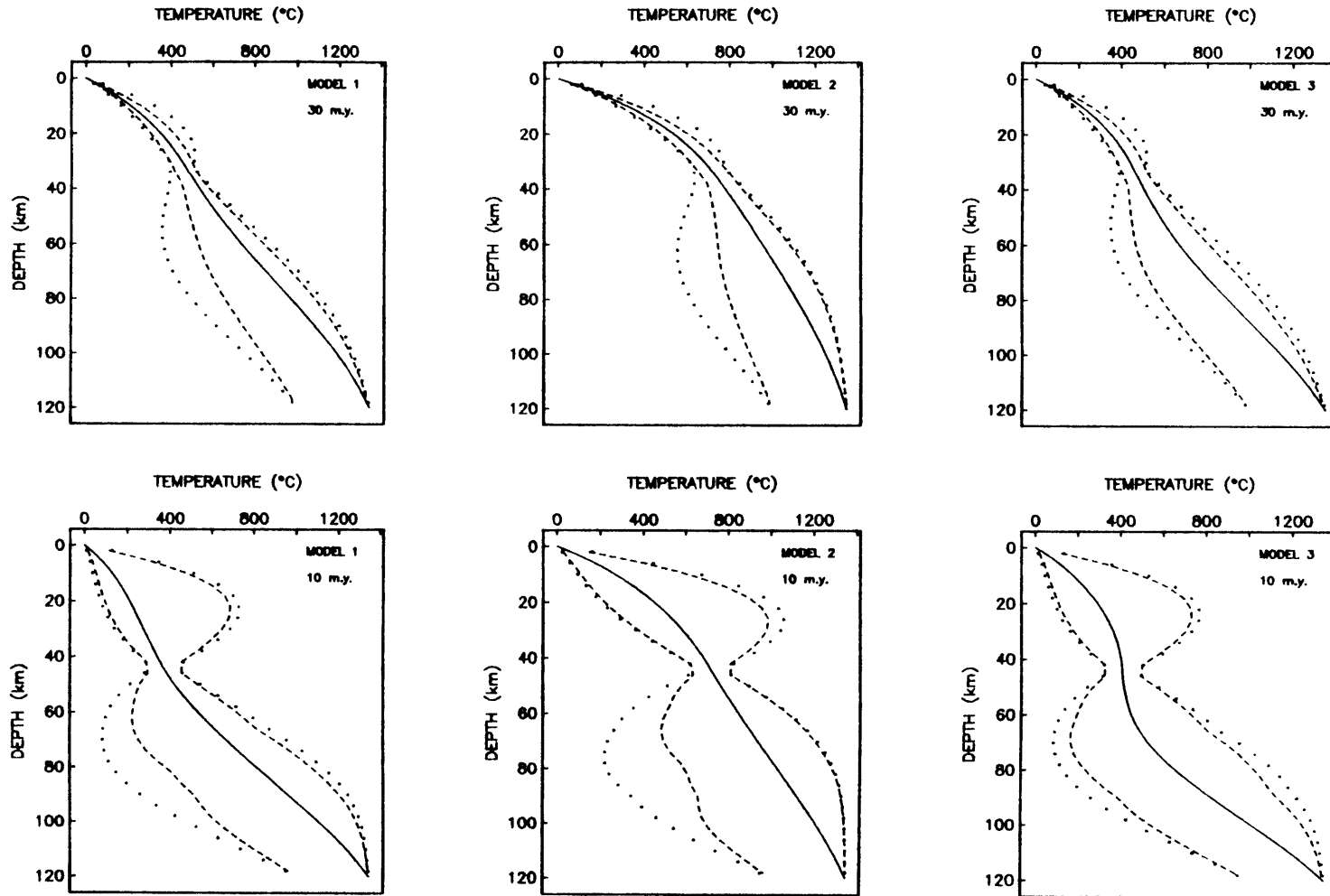


Figure 2.7

THERMAL DIFFUSIVITY

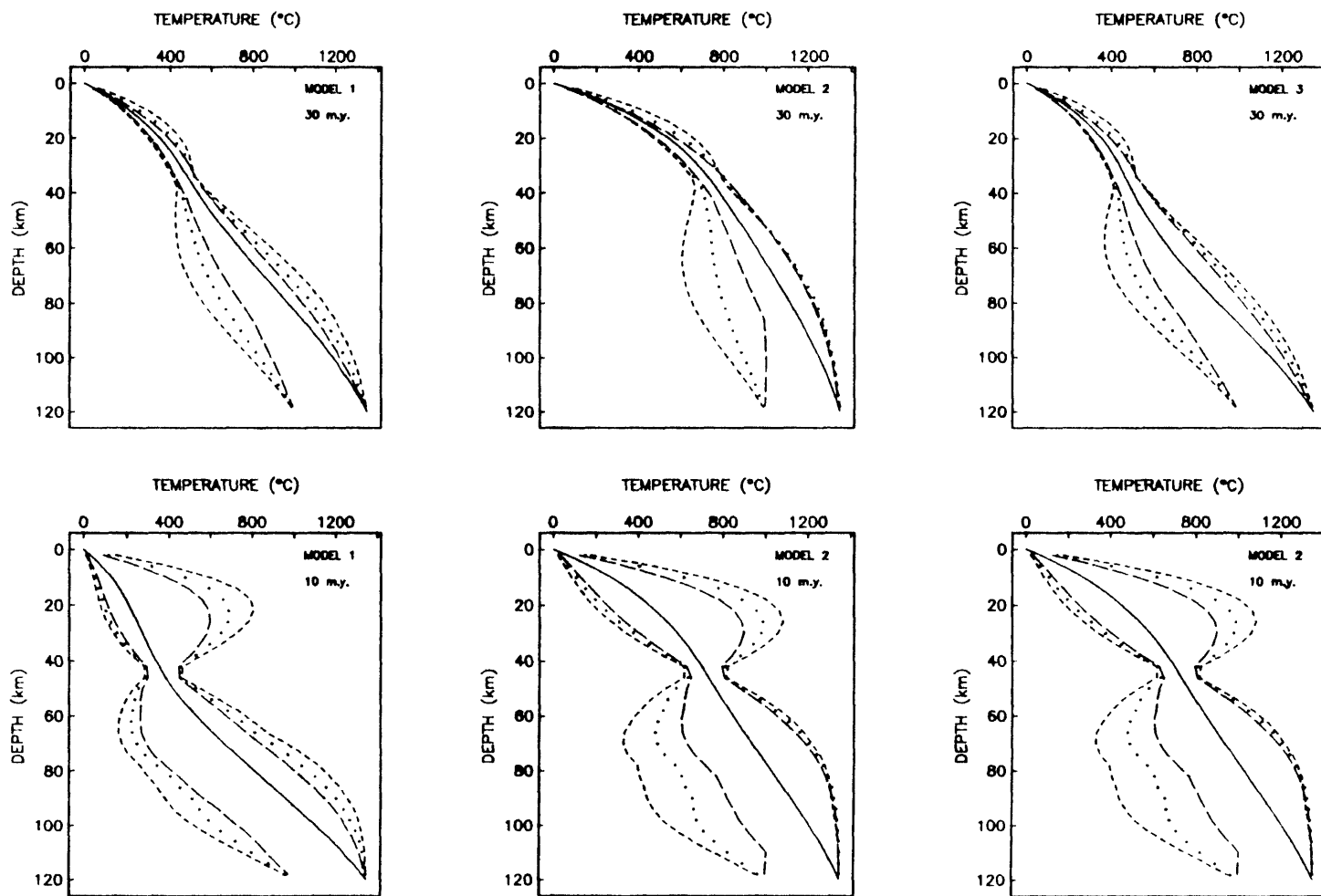


Figure 2.8

LITHOSPHERIC THICKNESS

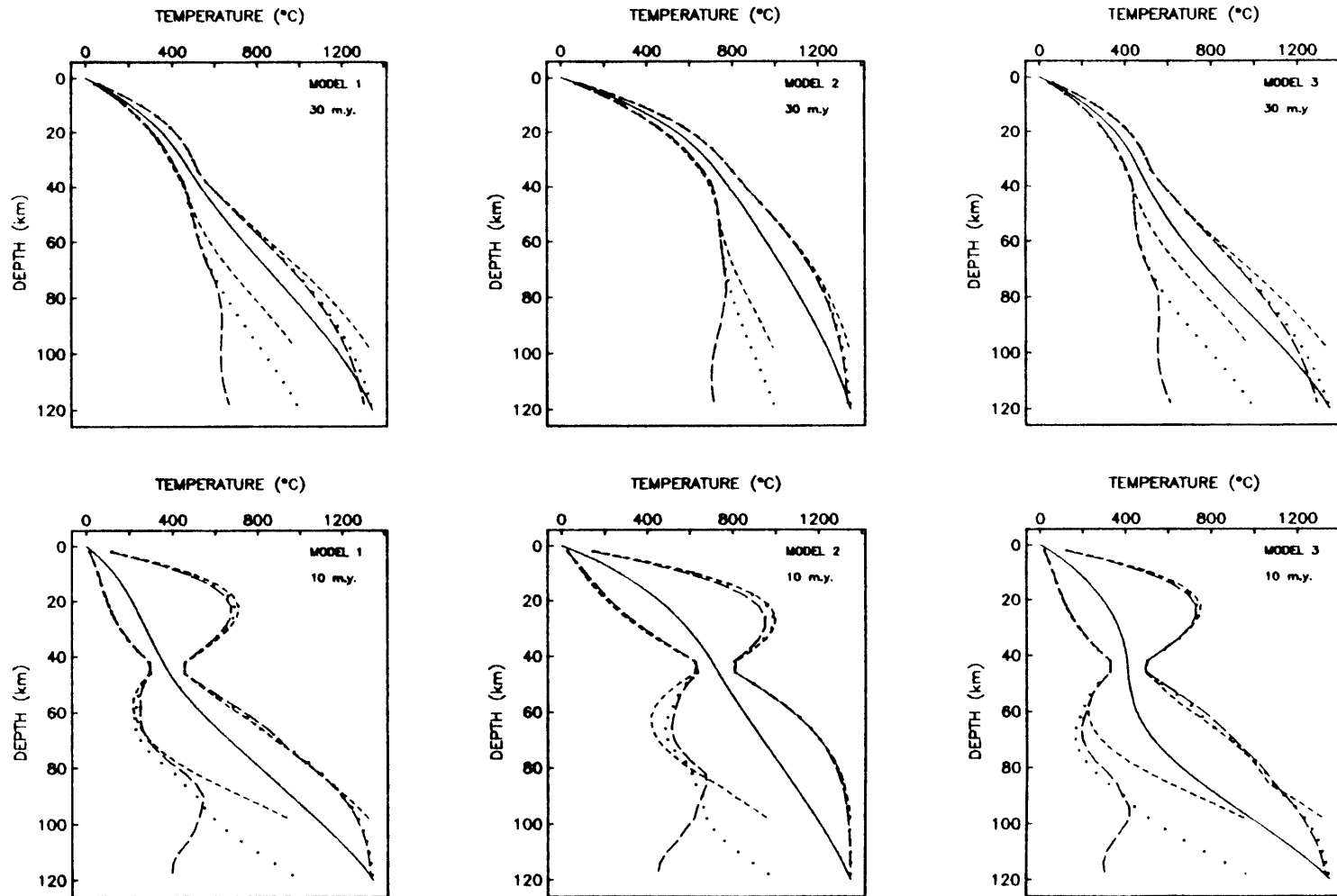


Figure 2.9

UPLIFT RATE

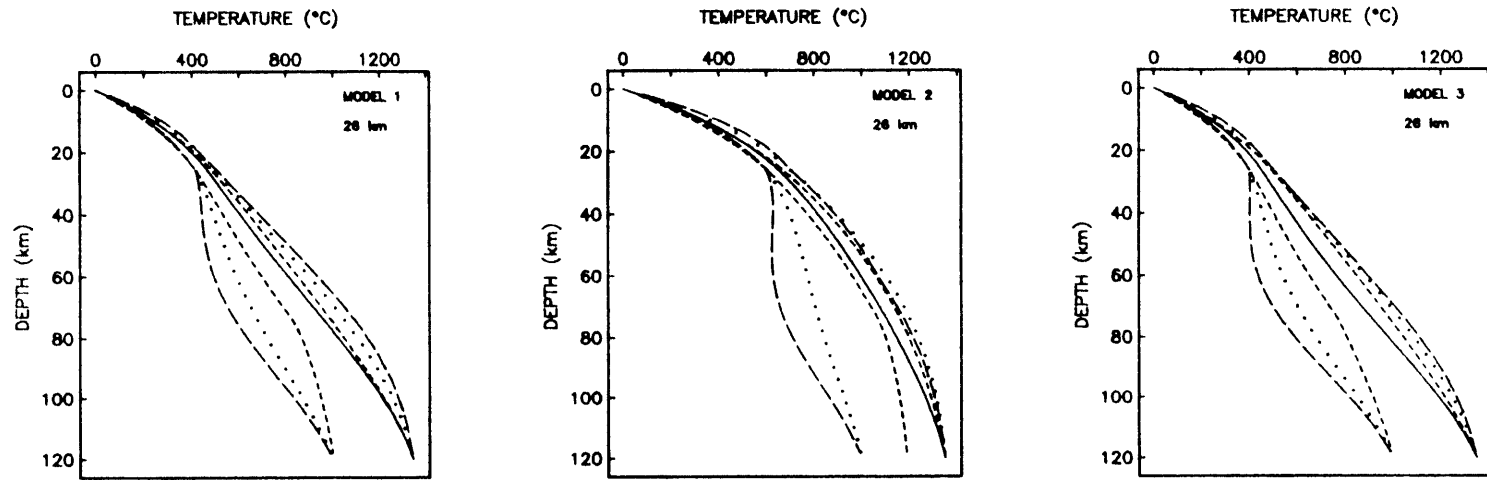


Figure 2.10

UPLIFT RATE

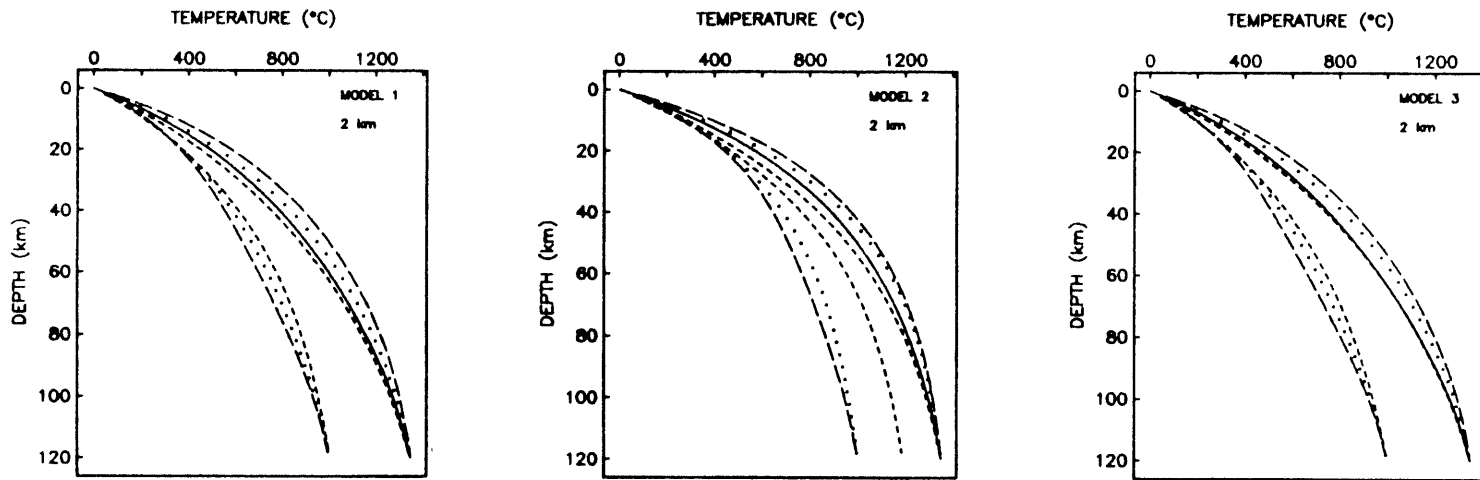


Figure 2.11

VARIABLE UPLIFT RATE

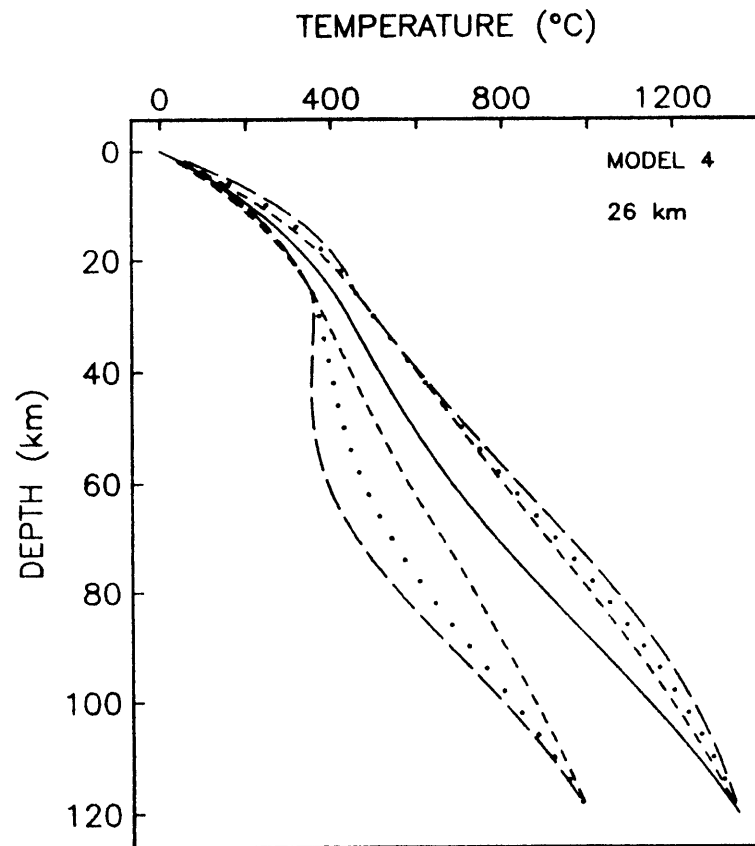


Figure 2.12

CHAPTER III: EXTREMAL BOUNDS ON THE TEMPERATURE
STRUCTURE AT VARIOUS WAVELENGTHS

INTRODUCTION

In the previous chapter, it was shown that the linear-programming method can be used to bound the temperature structure of the lithosphere. The quality of the Tz data appear to be more important than exact knowledge of the values of the physical parameters of the inversion model; hence, if the Tz data are of good quality, it is possible to closely bound the actual temperature structure of the lithosphere. However, if the data are of poor quality, as is likely to be the case with real data determined from metamorphic rocks, uncertainty in the temperature structure may increase significantly. Hence, it may be useful to seek an alternative approach to bounding the temperature structure of the lithosphere. One possible method for doing so is to bound each coefficient in the expansion (1.2)

In this chapter, the extremal bounds on each coefficient, as determined by a linear-programming technique similar to that used in Chapter 2, are investigated. These bounds may be compared to the values of the appropriate coefficients obtained from the forward models. Hence, the ability of the inversion scheme to recover the temperature structure at different wavelengths may be examined.

FORWARD MODEL

Decay of Terms of the Infinite Series

The terms of the infinite sum of expansion (1.2) decay as $\exp[-(n^2\pi^2 + R^2)\alpha t/\ell^2]$ with time. Reiterating an earlier discussion of this thesis, whereas 126 m.y. are required for decay of the $n=1$ term to 10% of its initial value when $u=.6$ km/Ma, $\ell=120$ km, and $\alpha=6.4 \cdot 10^{-7}$ m²/s, decay of higher order terms is significantly faster. For example, the $n=2$ term decays to 10% of its initial value after 39 m.y., the $n=3$ term after 18 m.y., and the $n=4$ term after 10 m.y.. Figure 3.1 shows the decay with time of the function $f(t)=\exp[-(n^2\pi^2 + R^2)\alpha t/\ell^2]$ for $n=1$ (solid line), $n=2$ (small dashed line), $n=3$ (medium dashed line), and $n=4$ (large dashed line). After 10 m.y, for $n=2$, this function has 66% of its corresponding value for $n=1$; for $n=3$, 33%; and for $n=4$, 13%. After 20 m.y, for $n=2$, $f(t)$ has 44% of its corresponding value for $n=1$; for $n=3$, 11%; and for $n=4$, 2%. After 30 m.y, for $n=2$, $f(t)$ has 29% of its corresponding value for $n=1$; for $n=3$, 4%; and for $n=4$, 0.2%. Clearly, if the value of each coefficient c_n is taken to be one, the time decay of the terms of the sum is such that after 20 m.y., contributions to the temperature structure for terms of order $n \geq 3$ are negligible relative to that for $n=1$. On the other hand, decay of the second term is such that the contribution to the temperature structure from the $n=2$ term is significant relative to that for $n=1$ for a much longer time.

The depth and time dependence of each term of the infinite sum of

expansion (1.2) is given by

$$g(z,t)=\exp[-(n^2\pi^2 + R^2)\alpha t/\ell^2]\cdot\exp[-Rz/\ell]\cdot\sin(n\pi z/\ell). \quad (3.1)$$

Figures 3.2a-d show the dependence of $g(z,t)$ on depth for $n=1$ (Figure 3.2a), $n=2$ (Figure 3.2b), $n=3$ (Figure 3.2c), and $n=6$ (Figure 3.2d) when $t=0$ m.y. (solid line), $t=10$ m.y. (small dashed line), $t=20$ m.y. (medium dashed line), and $t=30$ m.y. (large dashed line).

For fixed n , the exponential depth decay of $g(z,t)$ results in a decreasing maximum magnitude of this function in each half period of the sinusoid. Thus, the contribution to the temperature structure of $T_m \cdot c_n \cdot g(z,t)$ becomes progressively smaller for depths $z+k\ell/n$, $k=0,1,\dots,n-1$ as k increases. For sufficiently large depths and long times, the contribution of the infinite sum of (1.2) to the temperature structure is negligible relative to that of the steady-state term.

Forward Model Coefficients

Figure 3.3 shows the absolute values of the first eleven coefficients for Models 1-3 and for the two additional initial geotherms of Figure 3.4 as calculated from numerical integration of equation (1.3). Clearly, c_1 is of much greater magnitude than (has an absolute value greater than twice that of) any other coefficient for all of the five models. Moreover, the values of most coefficients for any model are less than 10% of c_1 . Hence, the time decay of the terms of the infinite sum is such that within 10 m.y. of the onset of uplift and erosion, at most, only the first two terms of the sum (1.2) contribute significantly to the temperature structure. Furthermore, within 30 m.y. of the onset of

uplift and erosion, the contribution to the temperature structure of the second term of the series is less than 10% of that of the first term at any specified depth. This suggests that for reconstruction of ancient geotherms, it may be more useful to use only the first few coefficients to bound the temperature structure of the lithosphere rather than to bound the total temperature structure of the lithosphere with a very large number of coefficients. This hypothesis can be examined through comparison of the values of the coefficients found for the initial geotherms of Figure 3.4 with the extremal bounds on these same coefficients as determined from inversion of appropriate Tz data for each model.

INVERSE MODEL

It was shown in the previous chapter that the extremal bounds on the lithospheric temperature structure are more sensitive to the quality of the Tz data than to uncertainty in the values of the physical parameters; therefore, in this chapter, extremal bounds on the coefficients $\{c_n\}$ are determined only as a function of the uncertainty in the Tz data with no uncertainty in the values of the various physical parameters. Extremal bounds on the coefficients are also determined for several different truncations of the mathematical model. Unless otherwise stated, inversions assume the same values for the physical parameters as were assumed in the forward model, i.e., temperature at the base of the lithosphere (T_m) = 1350°C, thermal diffusivity (α) = 6.4×10^{-7} m²/s,

lithospheric thickness (ℓ) = 120 km, and thickness of the radiogenic layer (a) = 50 km. Inversions assume exact knowledge of those parameters which enter the problem linearly, i.e., ($1340 \leq T_m(^{\circ}\text{C}) \leq 1350$) and ($.83 \leq A_0(\mu\text{W}/\text{m}^3) \leq .85$). Because the coefficients c_n are independent of depth and time, it is irrelevant at which depth and time the extremal bounds on the coefficients are determined.

Effects of Parameter Variation

1) Truncation of Series

The extremal bounds on the coefficients for truncations of the mathematical model to $n_{\text{max}}=3$ (triangles), $n_{\text{max}}=7$ (circles), and $n_{\text{max}}=12$ (ends of bars) are plotted in Figure 3.5. Also plotted are the values of each coefficient as calculated from numerical integration of equation (1.3). The bounds on each coefficient broaden as the number of terms of the sum (1.2) used in the inversion increases, with the true value of the coefficient contained within the extremal bounds for all models.

For Models 1-3, the first coefficient can be well bounded regardless of the number of terms of the expansion (1.2) kept in the inversion. Truncations of the mathematical model to $n_{\text{max}}=3$ and $n_{\text{max}}=7$ yield very similar bounds on c_1 for uncertainties in the Tz data of both $\delta S = \pm 1.5^{\circ}\text{C}$ and $\delta S = \pm 50^{\circ}\text{C}$; however, increasing n_{max} to 12 leads to larger bounds on c_1 if the data are of poor quality. The second coefficient, c_2 , can also be well bounded if the uncertainty in the Tz data is small. However, the extremal bounds on c_2 widen with n_{max} and span a fairly large range of possible values if the data are of poor quality. The

third coefficient can be well determined only for truncations of the mathematical model to $n_{\max}=3$ and if the Tz data are of excellent quality. Coefficients of order $n \geq 4$ cannot be well bounded for any of the combinations of inversion parameters examined.

2) Tz Data

The extremal bounds on the coefficients are plotted for uncertainty in the Tz data of $\pm 0.5^\circ\text{C}$ (triangles), $\pm 10^\circ\text{C}$ (circles), and $\pm 50^\circ\text{C}$ (ends of bars) in Figure 3.6. The extremal bounds on each coefficient broaden as the uncertainty in the Tz data increases. If either $n_{\max}=7$ or $n_{\max}=12$, coefficients of order $n \geq 3$ cannot be well determined even if the Tz data are of superb quality. Furthermore, increases in the uncertainty in the Tz data from $\pm 0.5^\circ\text{C}$ to $\pm 10^\circ\text{C}$ to $\pm 50^\circ\text{C}$ result in unimportant changes in the extremal bounds on these coefficients. This suggests that the values of these coefficients do not depend on the Tz data; rather, they probably depend on the boundary conditions of the problem.

The extremal bounds on c_1 and c_2 broaden significantly as the uncertainty in the Tz data increases from $\pm 0.5^\circ\text{C}$ to $\pm 10^\circ\text{C}$ to $\pm 50^\circ\text{C}$. However, the first coefficient, c_1 , can be quite well determined even if the Tz data are of poor quality. The second coefficient, c_2 , can only be well determined if the uncertainty in the Tz data is small. This dependence of the extremal bounds on c_1 and c_2 on the quality of the Tz data suggests that the values of these coefficients are tightly linked to the Tz data.

Resolution of Coefficients

In a further effort to investigate the resolution of the inversion scheme, the product {extremal c_n /actual c_n } was examined. Figure 3.7 shows this product for Models 1-3 for uncertainties in the Tz data of both $\pm 5^\circ\text{C}$ and $\pm 50^\circ\text{C}$ for truncations of the mathematical model to $n_{\text{max}}=3$ (triangles), $n_{\text{max}}=7$ (circles), and $n_{\text{max}}=12$ (squares). Other inversion parameters are assigned the same values as were used in the forward models. In general, coefficients of larger absolute magnitude can be better constrained than those of smaller magnitude. For example, those of absolute magnitude of greater than 1.0, can be determined to within a factor of two, those with absolute values in the range 0.1-0.99 to within a factor of twenty, and those with absolute values in the range 0.01-0.099 to within approximately two orders of magnitude. Coefficients of absolute magnitude of less than about 0.01 cannot, in general, be meaningfully constrained. Thus, for Models 1-3, c_1 can be extremely well determined. The second coefficient, c_2 , can be resolved to within a order of magnitude if the Tz data are of decent quality ($\pm 10^\circ\text{C}$) while coefficients c_3 and c_4 can be resolved only to within two orders of magnitude. Coefficients c_n , $n \geq 5$ cannot, in general, be resolved.

Resolution of the Temperature Structure at Various Wavelengths

The effects of various uncertainties in the parameters necessary for the inversion of Tz data to determine extremal bounds on the coefficients, c_n , may also be viewed in terms of the resulting uncertainty in the contributions of the temperature structure at various

wavelengths to the total temperature structure. Thus, equivalently, one may desire to determine at which wavelengths the temperature structure can be resolved. Because it was shown above that, in general, only the low order coefficients can be well determined, only the longer wavelength contributions to the temperature structure should be recoverable. These contributions are plotted at $t_b=10$ m.y. in Figures 3.8 (c_1), 3.9 (c_2), and 3.10 (c_3) for combinations of the inversion parameters $n_{max}=3,7,$ and 12 and uncertainty in the Tz data of $\pm 5^\circ\text{C}$, $\pm 10^\circ\text{C}$, and $\pm 50^\circ\text{C}$. For fixed n_{max} , the bounds on the temperature contribution from each of the first two terms of the sum show drastic broadening as the quality of the data worsens. However, for fixed uncertainty in the data, there is negligible change in the uncertainty in the temperature contribution at any depth as n_{max} increases. This is not, however, true for the temperature contribution of the third term of the sum. It is sensitive to both n_{max} and the uncertainty in the Tz data. Thus, while the first two terms of the sum of (1.2) depend primarily on the Tz data, the third term is sensitive to other constraints.

Optimization of Temperature vs. Optimization of Coefficients

In order to tie together the results of Chapters 2 and 3, it is appropriate to ask how the coefficients found when the total temperature at any depth is optimized compare with the extremal bounds on these same coefficients. Figure 3.11 shows both the extremal bounds on the coefficients for Model 1 determined by taking each coefficient successively as the objective function and the coefficients found when

the temperature at a range of depths is optimized at $t_b=10$ m.y.. All inversions assume exact knowledge of all physical parameters. Extremal bounds on the coefficients are shown by triangles, values of the coefficients found by optimizing the temperature by circles, and the actual values of these coefficients as determined by numerical integration of the forward model by X's. Because determining extremal bounds on the total temperature requires a series of inversions, numerous values are possible for each coefficient, one for each depth at which the temperature is optimized. For inversions in which the uncertainty in the Tz data is $\pm 5^\circ\text{C}$, the coefficients c_n , $n \leq 6$ found by optimizing the total temperature sample most of the space spanned by the extremal bounds on these same coefficients. For coefficients c_n , $n=7,8,\dots,11$ optimizing the temperature yields a smaller range of possible values for these coefficients than does optimizing each coefficient in succession. For inversions in which the uncertainty in the Tz data is $\pm 50^\circ\text{C}$, the coefficients found when the temperature is optimized sample most of the space spanned by the extremal bounds on these same coefficients for $n \leq 3$. Values of the higher order coefficients are roughly centered between the extremal bounds on these coefficients; however, most are smaller than the actual values of the coefficients calculated from numerical integration of the forward models.

An alternate means of examining the importance of each coefficient is to investigate how uncertainty in the extremal bounds on these coefficients translates into uncertainty in the total temperature. However, performing this exercise is probably only useful if the

coefficient is one whose value is strongly controlled by the Tz data rather than one whose value depends primarily on the other constraints of the problem. Thus, the forward model was used to calculate the temperature structure from the coefficients found when c_1 was optimized (Figure 3.12). The top three plots show the bounds on the temperature structure for fixed n_{max} and uncertainties in the Tz data of $\pm 5^\circ\text{C}$ (small dashed lines), $\pm 10^\circ\text{C}$ (dotted lines), $\pm 50^\circ\text{C}$ (large dashed lines). The bottom three plots show the bounds on the temperature structure for fixed uncertainty in the Tz data and truncations of the mathematical model to three (small dashed lines), seven (dotted lines), and twelve (large dashed lines). As seen in the last chapter, it is clear that uncertainty in the Tz data has a much greater effect on the uncertainty in the temperature structure than error due to truncation of the mathematical model.

CONCLUSIONS

Forward modelling techniques for initial geotherms chosen to span a range of geotherms likely to exist in real orogenic belts show that within 20 m.y. of the onset of uplift and erosion, only the two lowest order transient terms in the description of the temperature structure (1.2) are non-negligible. This suggests that as an alternative to bounding the total temperature structure of the lithosphere by retaining a large number of these transient terms, perhaps it is wise to bound the contribution to the temperature structure of each of these transients.

Bounding each of these transients is equivalent to bounding each of the coefficients of the sum of expansion (1.2). Because extremal bounds on the total temperature structure show that the uncertainties in the physical parameters of the model have a much smaller effect on the temperature bounds than does uncertainty in the T_z data, it is extremely unlikely that uncertainties in these physical parameters would have a greater effect on the bounds on the transient contributions to the temperature structure than would uncertainty in the T_z data. Hence, bounds on these transients were determined only for various assumptions regarding the quality of the T_z data and the error introduced into the inversion scheme through truncation of the mathematical model.

Resolution of the longest wavelength transient is possible with the linear-programming technique even if the data are of poor quality; however, resolution of higher order transients degrades quickly. The second order transient can only be well resolved if the data are of good quality while resolution of the third order transient requires both data of excellent quality and truncation of the mathematical model to three. The fourth order term can be resolved only to within two orders of magnitude even if the data are of excellent quality. Resolution of transients of order $n \geq 5$ cannot, in general, be guaranteed even to within two orders of magnitude. Because terms of order $n \geq 4$ cannot be well resolved, and since forward modelling shows that these terms are negligible compared to lower order terms, perhaps the contributions of these terms should be set to zero in the inverse problem. This will not jeopardize the ability of the inversion scheme to recover the actual

temperature structure of the lithosphere, yet it will disallow inclusion of unwarranted uncertainty in the extremal bounds on the temperature structure.

FIGURE CAPTIONS

Figure 3.1: Decay of the terms of the infinite sum of expansion (1.2) with time. Time decay of the function

$$f(t) = \exp[-(n^2\pi^2 + R^2)\alpha t / \ell^2]$$

is shown for $n=1$ (solid line), $n=2$ (small dashed line), $n=3$ (medium dashed line), and $n=4$ (large dashed line). Values of other parameters are: uplift rate, $u=0.6$ km/m.y., thermal diffusivity, $\alpha=6.4 \times 10^{-7}$ m²/s, and lithospheric thickness, $\ell=120$ km.

Figure 3.2a-d: Depth and time dependence of each term of the infinite sum of expansion (1.2). The function

$$g(z,t) = \exp[-(n^2\pi^2 + R^2)\alpha t / \ell^2] \cdot \exp[-Rz/\ell] \cdot \sin(n\pi z/\ell)$$

is plotted for $n=1$ (Figure 3.2a), $n=2$ (Figure 3.2b), $n=3$ (Figure 3.2c), and $n=6$ (Figure 3.2d) when $t=0$ m.y. (solid line), $t=10$ m.y. (small dashed line), $t=20$ m.y. (medium dashed line), and $t=30$ m.y. (large dashed line). Other parameters are: uplift rate, $u=0.6$ km/m.y., thermal diffusivity, $\alpha=6.4 \times 10^{-7}$ m²/s, and lithospheric thickness, $\ell=120$ km.

Figure 3.3: Absolute values of the first eleven coefficients for the initial geotherms of Figure 3.4 as calculated from numerical integration of equation (1.3).

Figure 3.4: Initial geotherms of Models 1-3 of the previous chapter and two additional "possible" geotherms.

Figure 3.5: Coefficients and extremal bounds on these coefficients for Models 1-3 determined for various truncations of the mathematical model. The extremal bounds on the coefficients are plotted for truncations of the infinite sum to $n_{max}=3$ (triangles), $n_{max}=7$ (circles), and $n_{max}=12$ (ends of bars). The value of each coefficient calculated from numerical integration of equation (1.3) is shown by an X. All inversions assume perfect knowledge of all physical parameters.

Figure 3.6: Coefficients and extremal bounds on these coefficients for Models 1-3 determined for several uncertainties in the T_z data. The extremal bounds on the coefficients are plotted for uncertainty in the T_z data of $\pm 5^\circ\text{C}$ (triangles), $\pm 10^\circ\text{C}$ (circles), and $\pm 50^\circ\text{C}$ (ends of bars). Again, the value of each coefficient calculated from numerical integration of equation 1.3 is shown by an X.

Figure 3.7: The product $\{\text{extremal } c_n / \text{actual } c_n\}$ calculated for Models 1-3 for uncertainties in the T_z data of $\pm 5^\circ\text{C}$ (upper plots) and $\pm 50^\circ\text{C}$ (lower plots) for truncations of

the infinite sum to three (triangles), seven (circles), and twelve (squares).

Figure 3.8: Temperature contribution of the first term of the sum (1.2) at $t_b = 10$ m.y.. The top plots show the uncertainty in the temperature contribution of the longest wavelength transient of expansion (1.2) for fixed n_{max} (3, 7, and 12) and uncertainty in the T_z data of $\pm 0.5^\circ\text{C}$ (small dashed lines), $\pm 1^\circ\text{C}$ (dotted lines), and $\pm 5^\circ\text{C}$ (large dashed lines). The bottom plots show the uncertainty in the temperature contribution of this transient for fixed uncertainty in the T_z data ($\pm 0.5^\circ\text{C}$, $\pm 1^\circ\text{C}$, and $\pm 5^\circ\text{C}$) and truncations of the infinite sum to $n_{max}=3$ (small dashed lines), $n_{max}=7$ (dotted lines), and $n_{max}=12$ (large dashed lines).

Figure 3.9: Temperature contribution of the second term of the sum (1.2) at $t_b = 10$ m.y.. The top plots show the uncertainty in the temperature contribution of the second term of the expansion (1.2) for fixed n_{max} (3, 7, and 12) and uncertainty in the T_z data of $\pm 0.5^\circ\text{C}$ (small dashed lines), $\pm 1^\circ\text{C}$ (dotted lines), and $\pm 5^\circ\text{C}$ (large dashed lines). The bottom plots show the uncertainty in this temperature contribution for fixed uncertainty in the T_z data ($\pm 0.5^\circ\text{C}$, $\pm 1^\circ\text{C}$, and $\pm 5^\circ\text{C}$) and truncations of the infinite sum to

$n_{\max}=3$ (small dashed lines), $n_{\max}=7$ (dotted lines), and $n_{\max}=12$ (large dashed lines).

Figure 3.10: Temperature contribution of the third term of the sum (1.2) at $t_b = 10$ m.y.. The top plots show the uncertainty in the temperature contribution of the third term of the sum of expansion (1.2) for fixed n_{\max} (3, 7, and 12) and uncertainty in the T_z data of $\pm 0.5^\circ\text{C}$ (small dashed lines), $\pm 10^\circ\text{C}$ (dotted lines), and $\pm 50^\circ\text{C}$ (large dashed lines). The bottom plots show the uncertainty in this temperature contribution fixed uncertainty in the T_z data ($\pm 0.5^\circ\text{C}$, $\pm 10^\circ\text{C}$, and $\pm 50^\circ\text{C}$) and truncations of the infinite sum to $n_{\max}=3$ (small dashed lines), $n_{\max}=7$ (dotted lines), and $n_{\max}=12$ (large dashed lines).

Figure 3.11: Comparison of extremal bounds on coefficients for Model 1 with those coefficients found by optimizing the temperature at a series of depths at $t_b=10$ m.y.. Extremal bounds on the coefficients are shown by triangles, values of the coefficients found by optimizing the temperature at $t_b=10$ m.y. by circles, and actual values by X's. All inversions assume perfect knowledge of all physical parameters.

Figure 3.12: Temperature structure for Model 1 at $t_b=10$ m.y. calculated

from the coefficients found when c_1 was optimized. The top three plots show the bounds on the temperature structure for fixed n_{max} and uncertainties in the T_z data of $\pm 0.5^\circ\text{C}$ (small dashed lines), $\pm 10^\circ\text{C}$ (dotted lines) and $\pm 50^\circ\text{C}$ (large dashed lines). The actual geotherm calculated from the forward model is shown by a solid line. The bottom three plots show the bounds on the temperature structure calculated for fixed uncertainty in the T_z data and truncations of the mathematical model to three (small dashed lines), seven (dotted lines), and twelve (large dashed lines). Again, the actual geotherm is shown by a solid line.

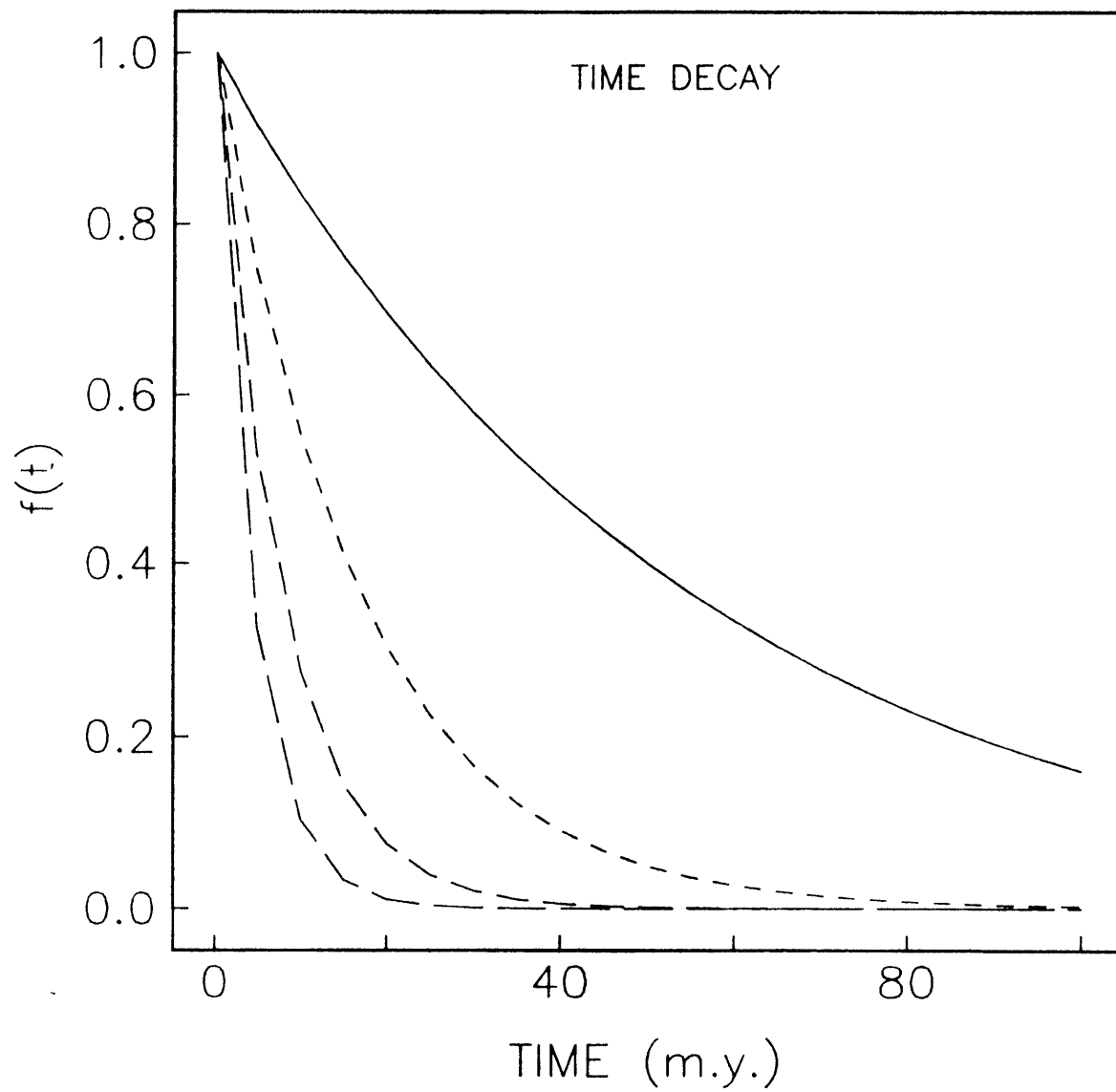


Figure 3.1

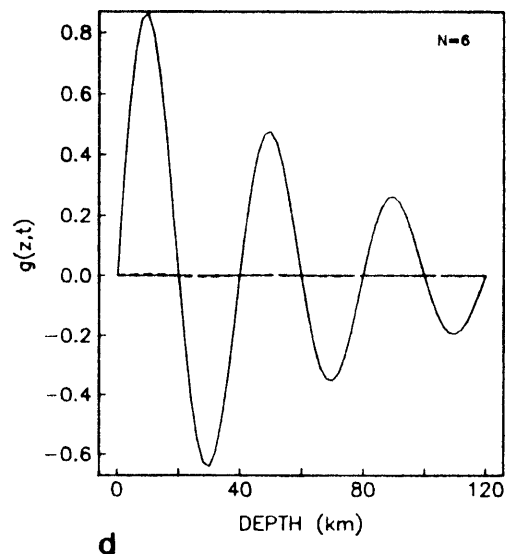
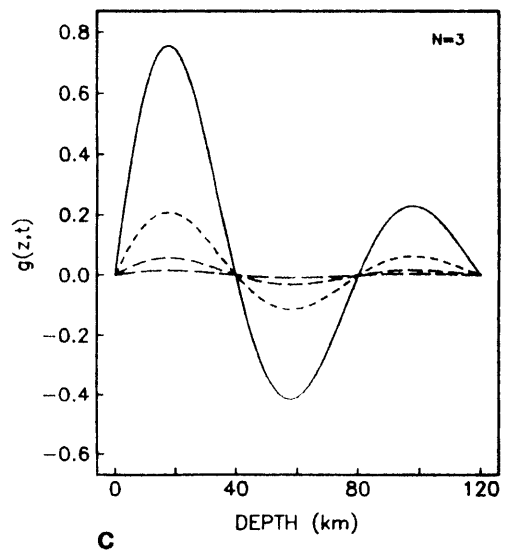
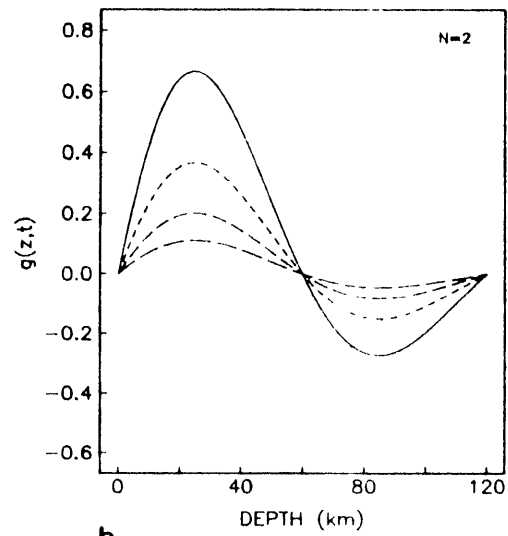
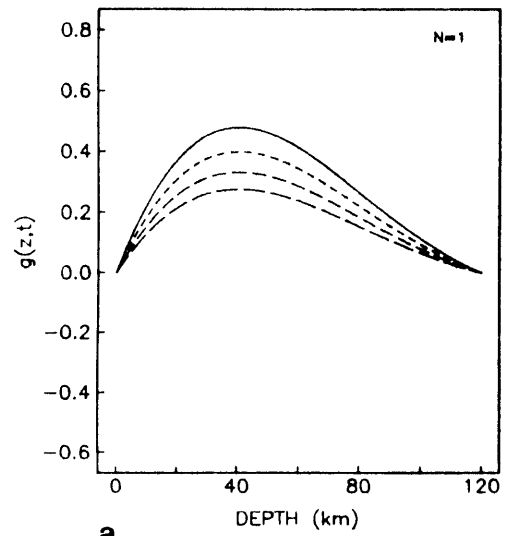


Figure 3.2

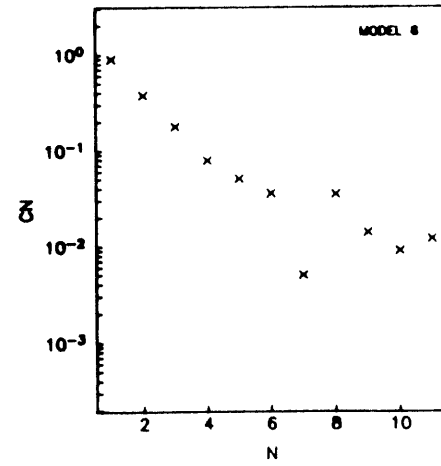
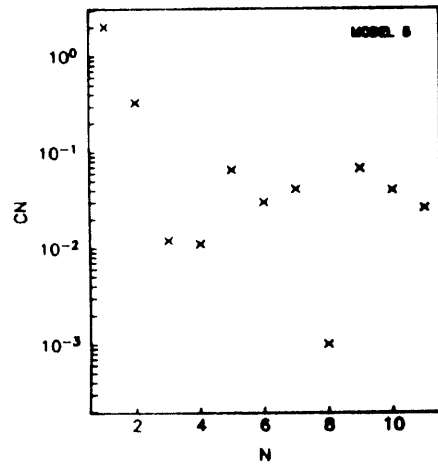
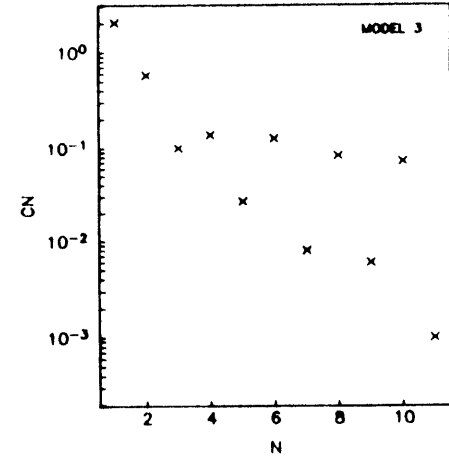
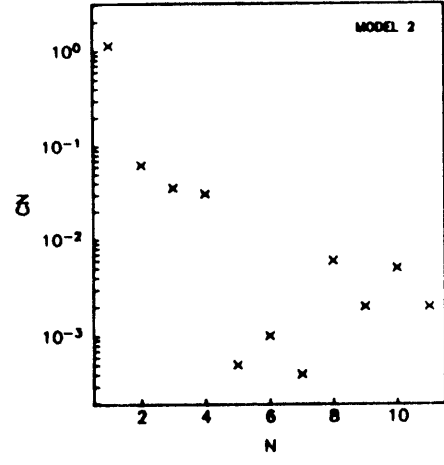
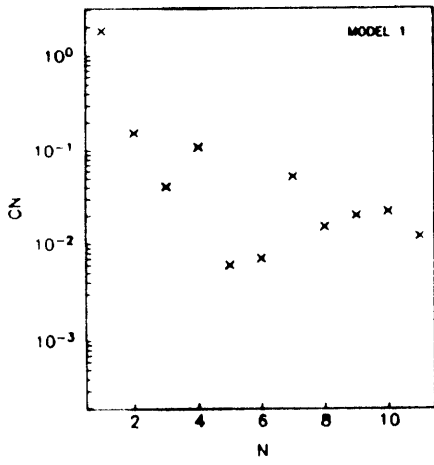


Figure 3.3

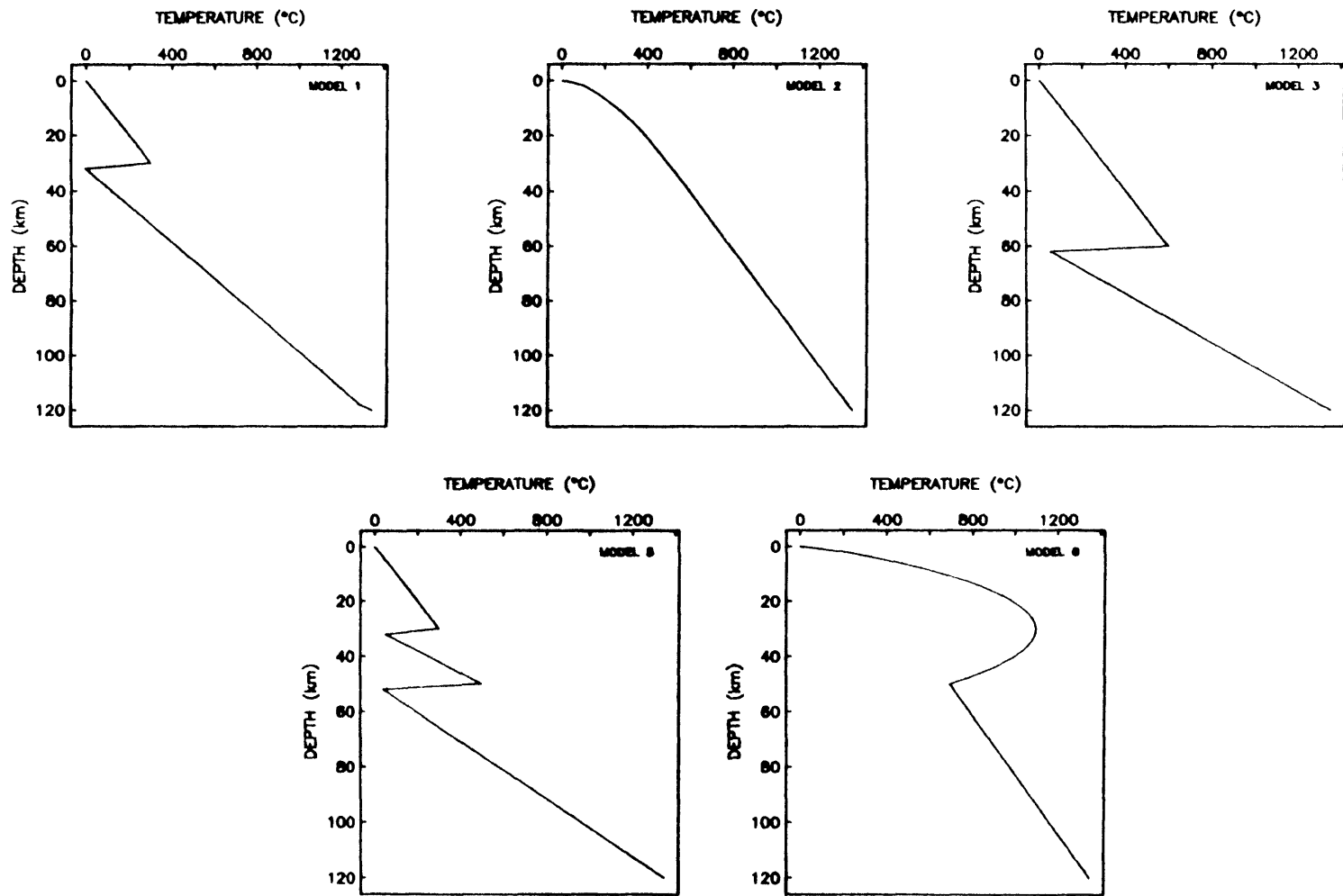


Figure 3.4

TRUNCATION OF SERIES

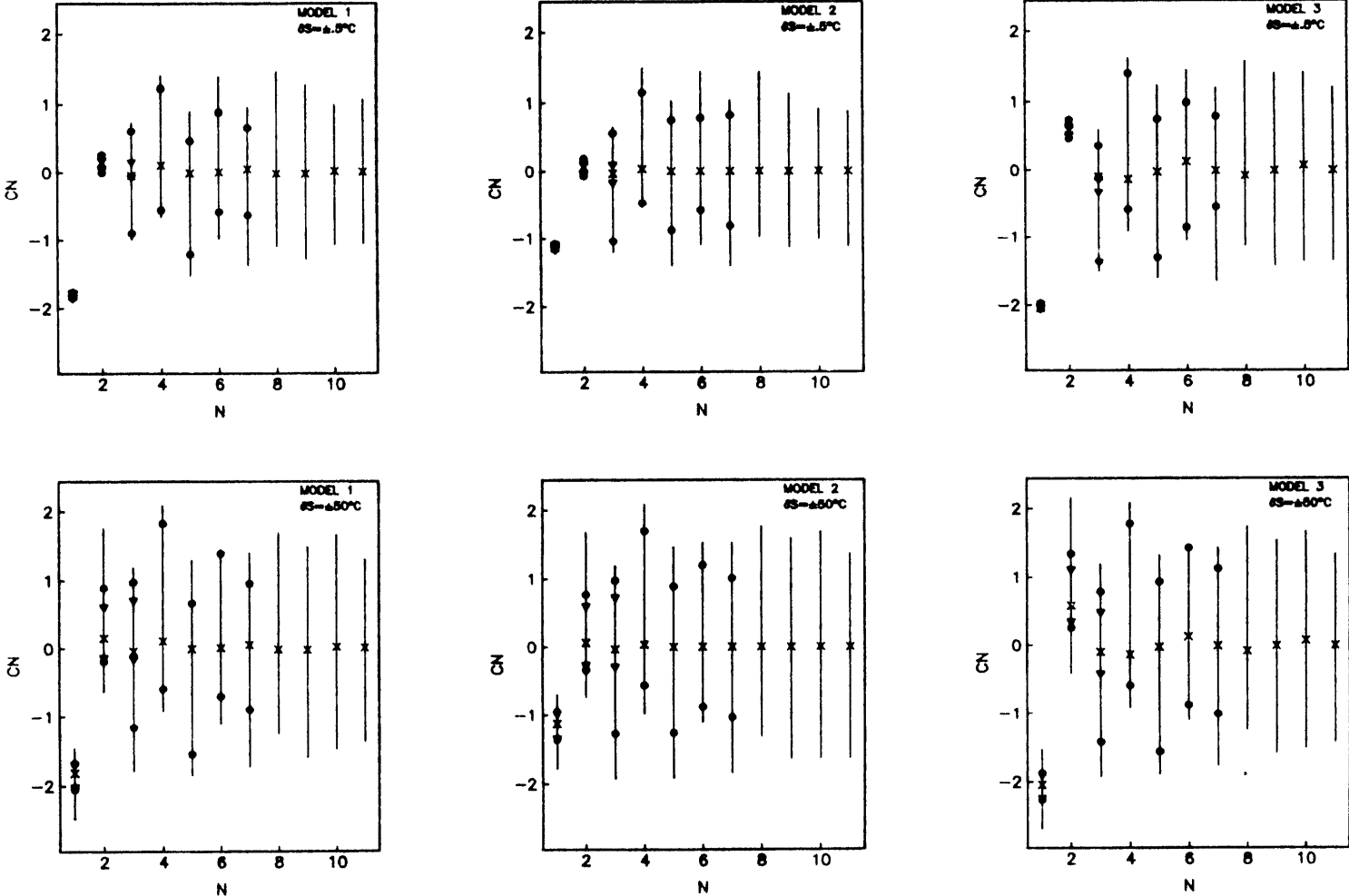


Figure 3.5

Tz DATA

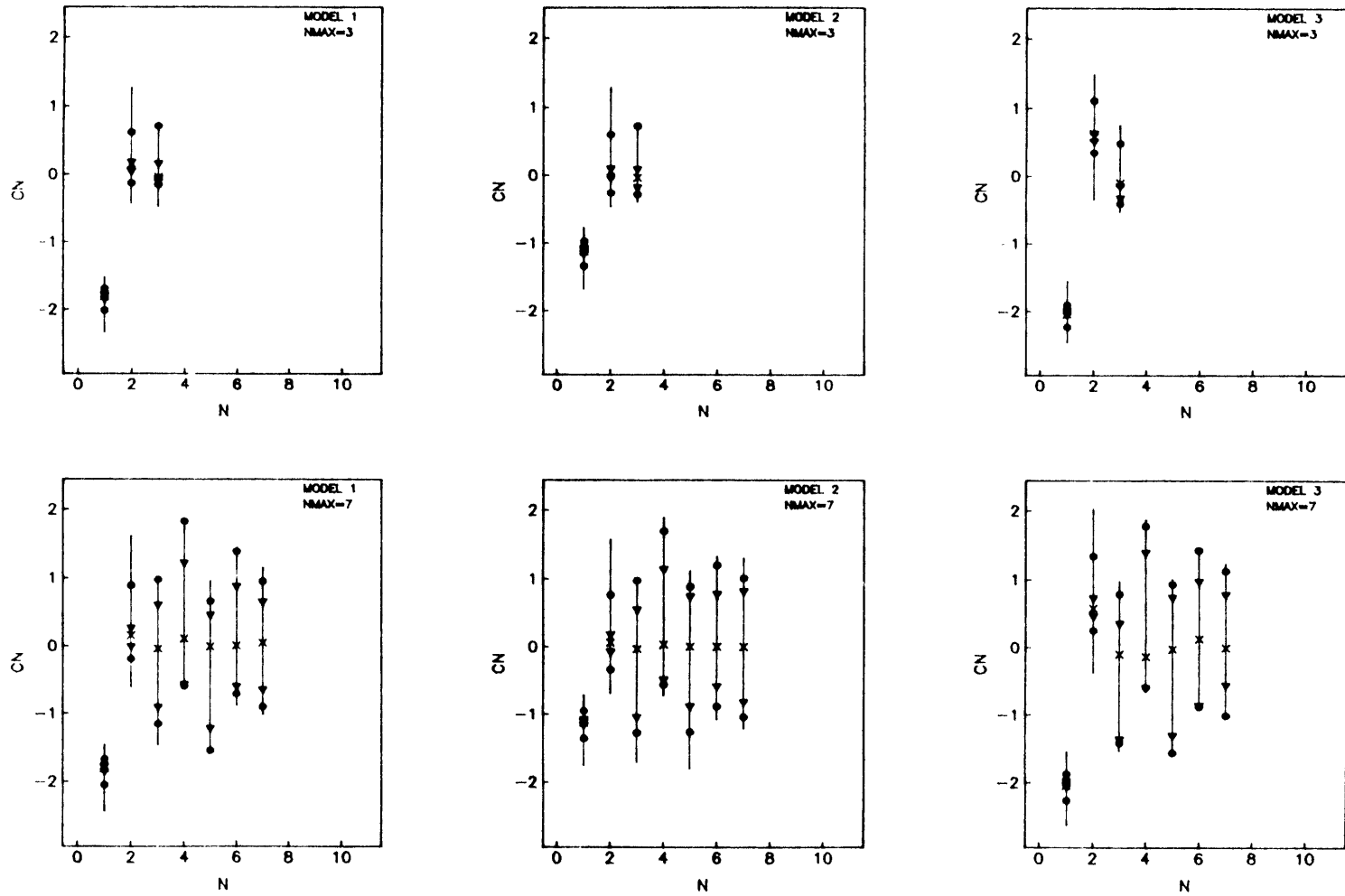


Figure 3.6

Tz DATA

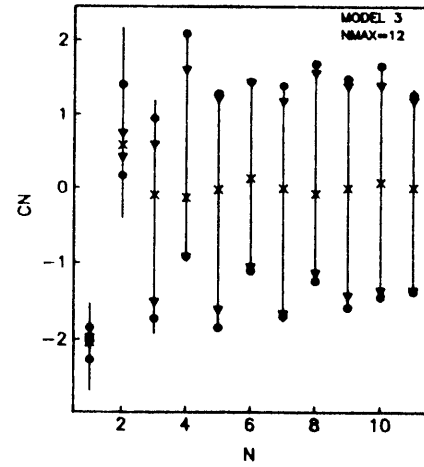
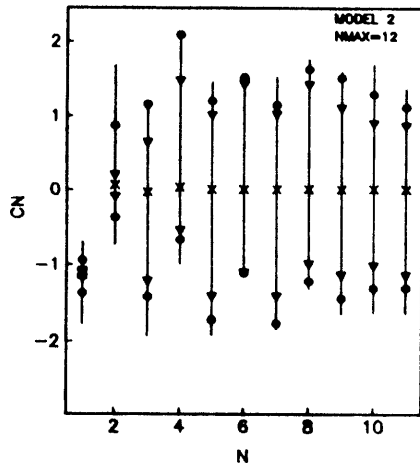
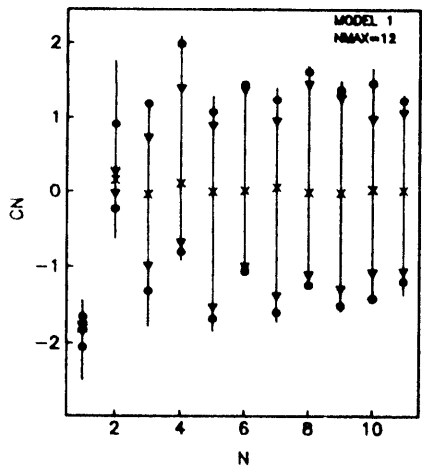


Figure 3.6
(continued)

(EXTREMAL CN / ACTUAL CN)

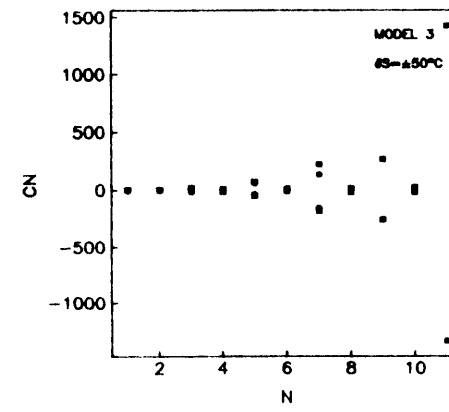
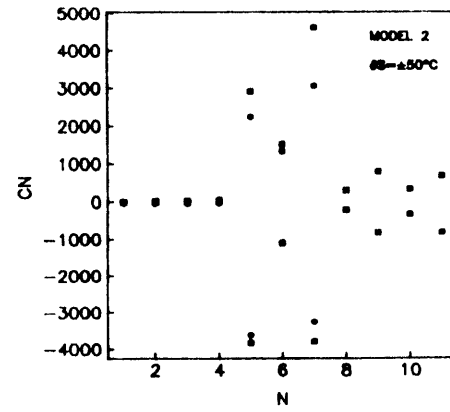
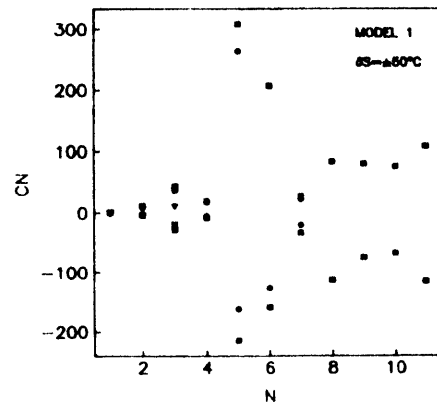
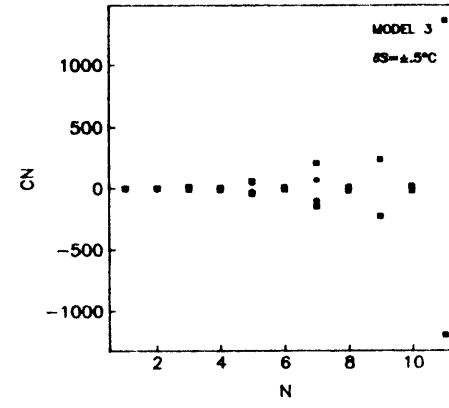
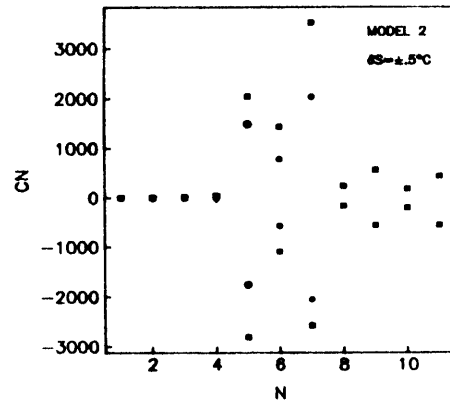
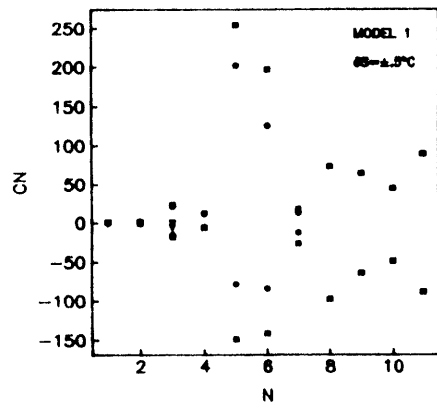


Figure 3.7

C1 - MODEL 1

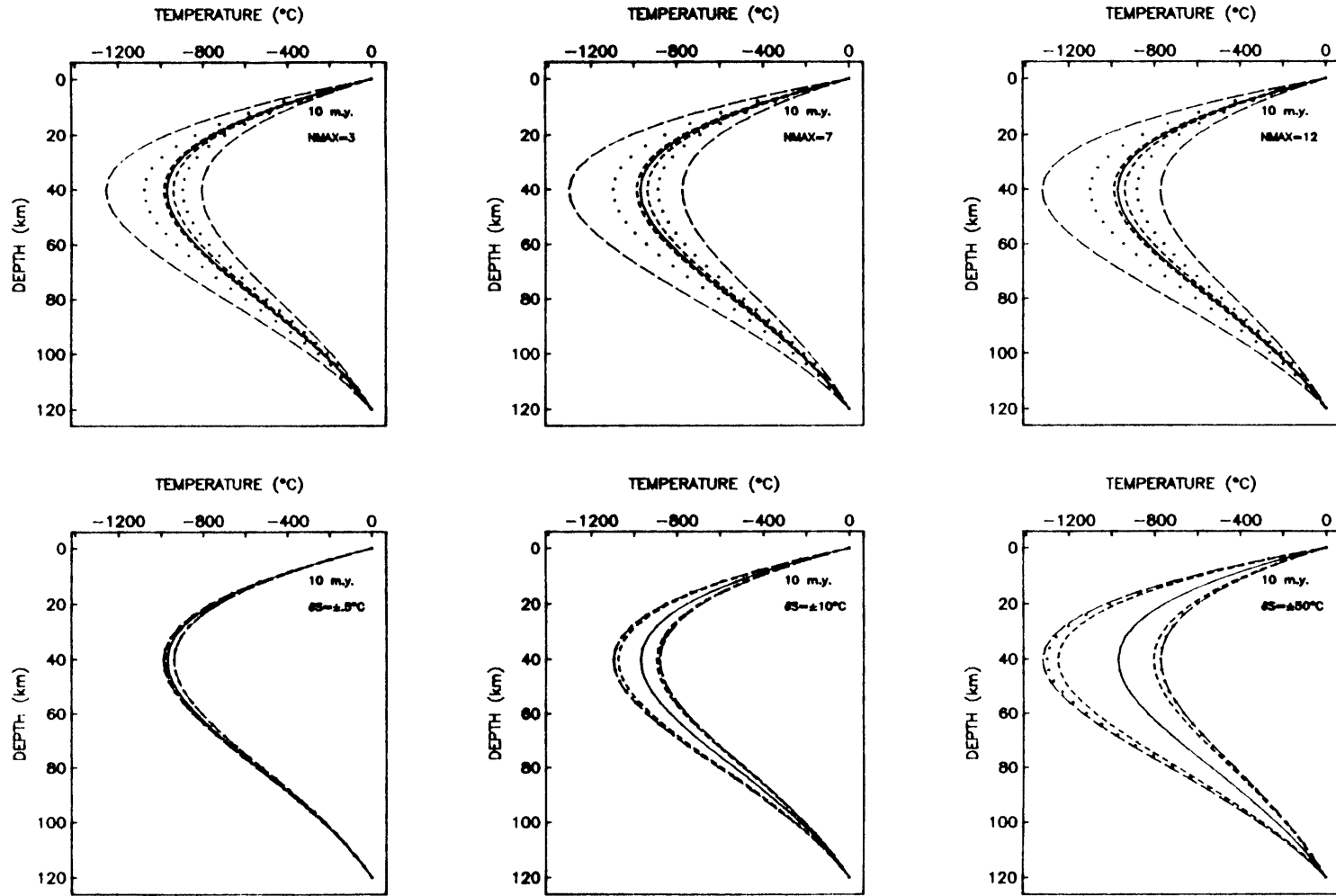


Figure 3.8

C2 - MODEL 1

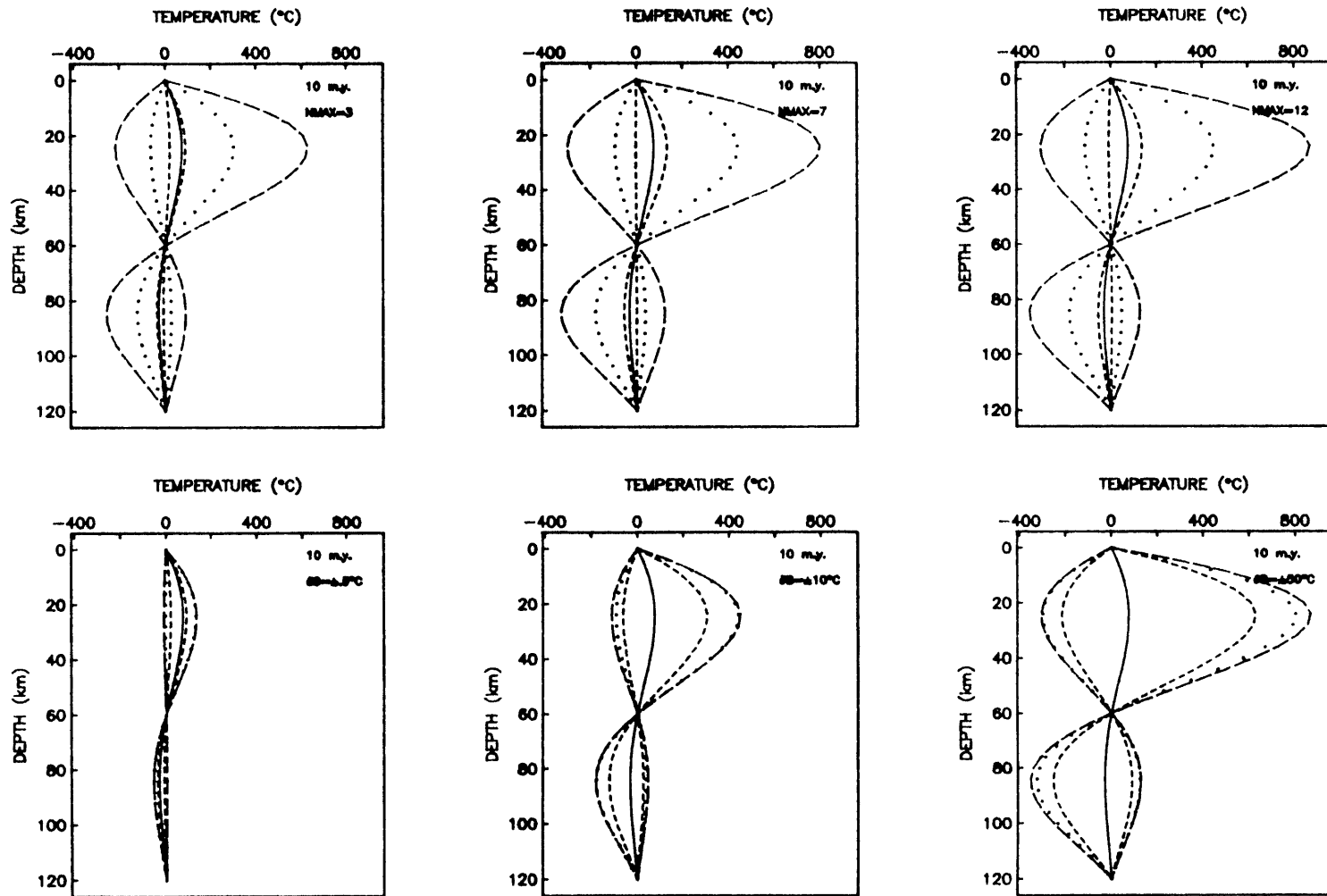


Figure 3.9

C3 - MODEL 1

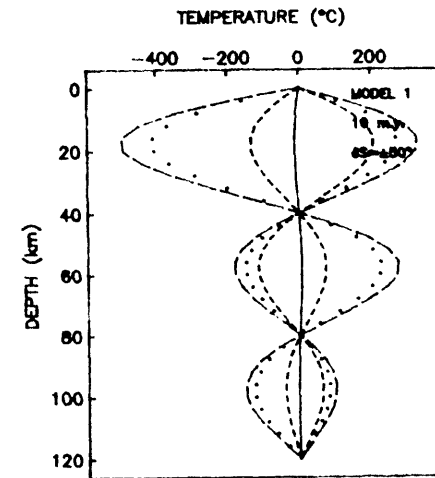
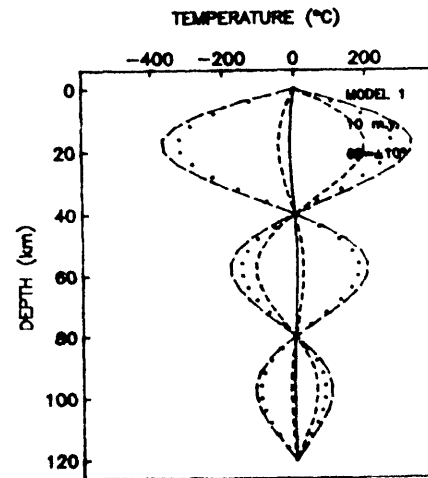
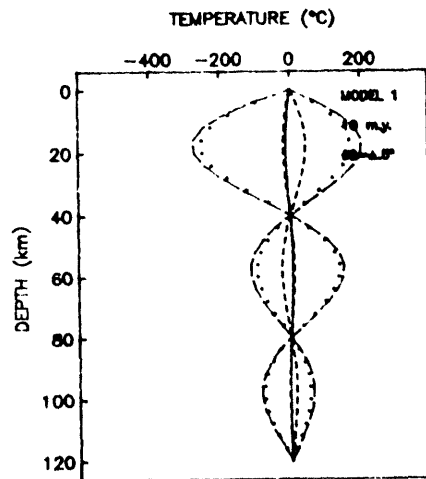
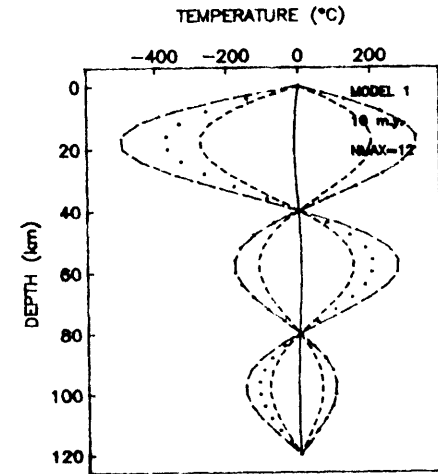
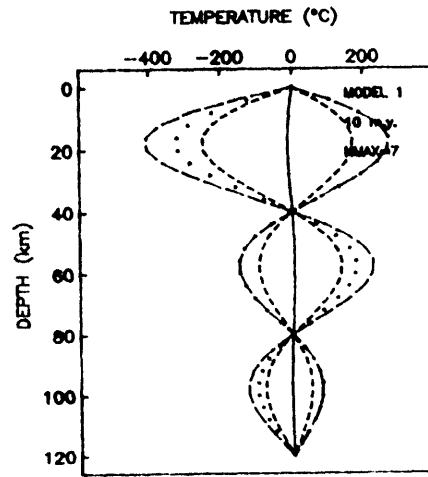
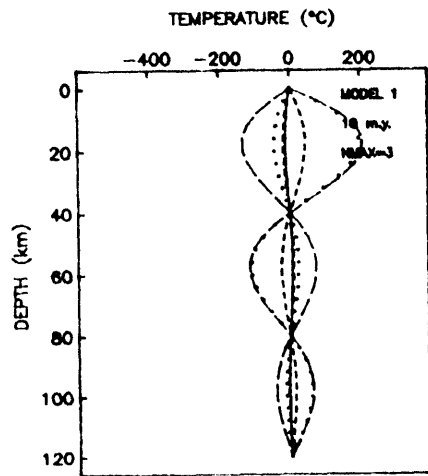


Figure 3.10

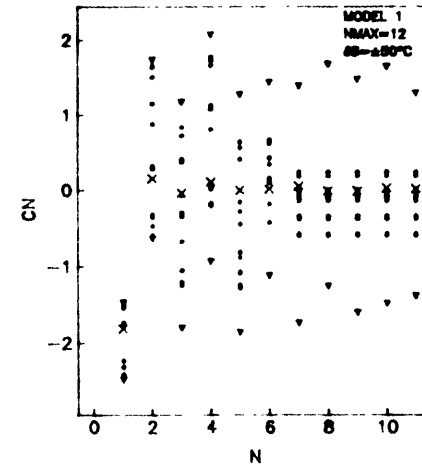
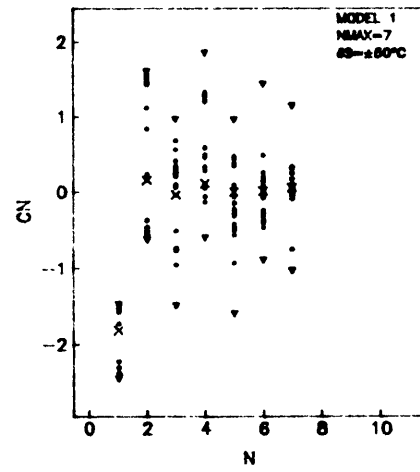
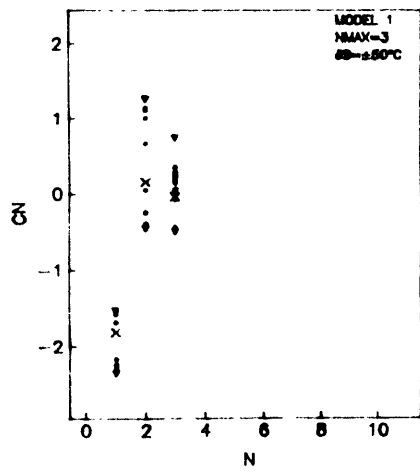
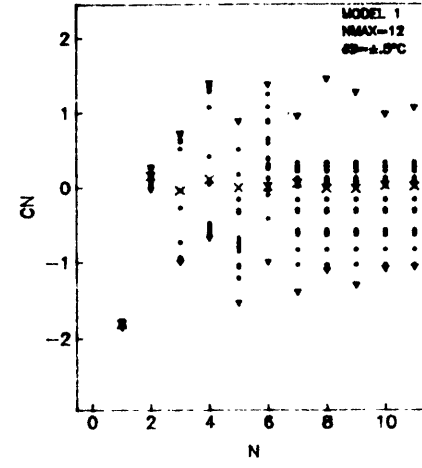
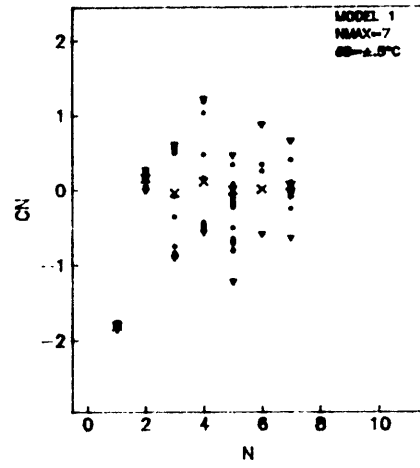
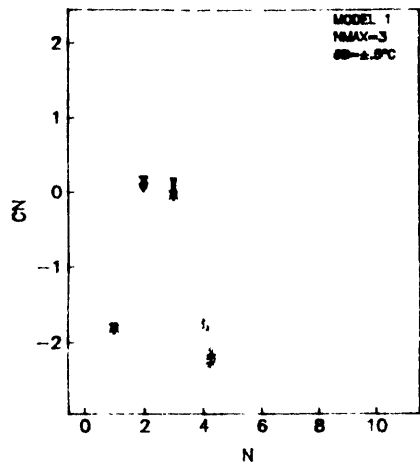


Figure 3.11

C1 - MODEL 1

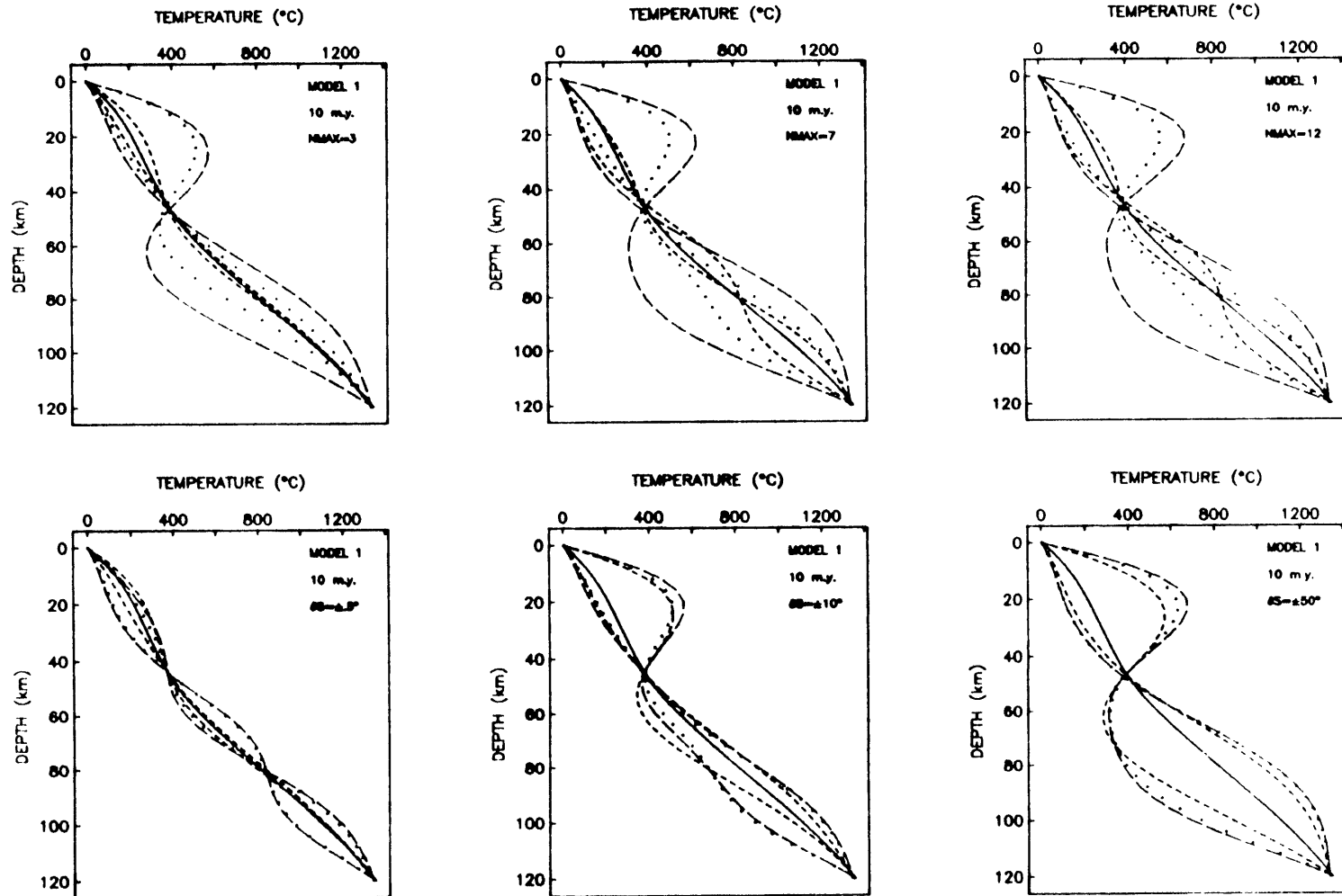


Figure 3.12

DISCUSSION

The extremal bound linear-programming technique can be used to constrain geotherms recovered from synthetic Tz data. Hence, it should also be a useful tool in constraining ancient geotherms in orogenic belts based on PTt paths determined from metamorphic rocks. The strengths and weaknesses of such an inversion scheme in handling various uncertainties in the Tz data and in the parameters of the physical model are examined in this thesis. However, other uncertainties associated with the data and the effects of possible breakdown of the physical model, such as those resulting from finite emplacement time of thrust sheets, lateral temperature gradients, and either lateral or vertical variations in any of the other physical parameters, remain to be investigated. In addition, the simultaneous inversion of Tz data from two or more crustal horizons was not attempted, although it seems likely that this would yield tighter bounds on the coefficients or, equivalently, on the total temperature structure of the lithosphere. Neither was consistency of the method checked by the inversion of data generated for two different structural levels. Clearly, these are problems which need to be investigated.

Resolution of the permissible temperature structure depends on many parameters, such as uncertainty in the Tz data and in the physical parameters of the model as well as truncation of the mathematical model; however, of these, uncertainty in the data is the most important in the resolution of ancient geotherms. Next in importance are uncertainties in

the uplift rate and in the radiogenic heating. An incorrect assumption of the uplift rate may result in extremal bounds which do not include the true geotherm while an incorrect description of the radiogenic heat sources may significantly affect the bounds on the temperature structure of the upper lithosphere, the region of primary interest. Incorrect assumptions of values for the other physical parameters of the model are not critical. While incorrect assumptions about the lithospheric thickness and the temperature at the base of the lithosphere primarily affect the bounds on the temperature structure of the lower lithosphere, an incorrect assumption of the magnitude of the thermal diffusivity results in unimportant broadening or narrowing of the extremal bounds about those determined for a correct choice of the thermal diffusivity. Because the high order transient terms in the temperature structure decay quickly with time, errors introduced into the inversion scheme through truncation of the infinite sum of the mathematical model become increasing less important through time. For example, truncation of the model to seven terms appears sufficient for convergence of the extremal bounds 10 m.y. after the onset of uplift and erosion, while at most three terms are required for convergence of the extremal bounds 30 m.y. after the onset of erosion.

Forward modelling techniques were used to investigate the contributions of the temperature structure at various wavelengths to the total temperature structure. They revealed that high order transient terms in the temperature structure decay so quickly with time that terms of order $n > 2$ become negligible within 20 m.y. of time zero. In addition,

the coefficients of most terms of expansion (1.2) have initial values which are less than 10% of that of the first coefficient. Hence, because of their relatively small initial values and their rapid decay, within 10 m.y. of the onset of uplift and erosion, only the two longest wavelength contributions to the temperature structure are significant.

The linear-programming technique was also used to bound the temperature structure at various wavelengths. The temperature contribution of the first term of the infinite sum of expansion (1.2) could be determined extremely well while the temperature contribution of the second term of the sum could be well determined only if the data were of good quality. The temperature contribution of the third term could only be well determined if the data were of excellent quality and only three terms of the sum were kept in the inversion. In general, resolution of shorter wavelength contributions to the temperature structure was not possible even if the data were of excellent quality. Because resolution of the temperature contributions for terms of $n \geq 4$ is so poor, and because it was shown that contributions of the terms of the sum of order $n \geq 4$ are negligible relative to lower order terms, it might be wise to set the temperature contributions of shorter wavelength terms to zero. This will preclude adding additional unwarranted uncertainty to the extremal bounds on the temperature structure of the lithosphere without jeopardizing the ability of the inversion scheme to recover the actual temperature structure. In addition, it is significantly more efficient computationally to bound the temperature structure at long wavelengths ($n \leq 3$) than to bound the total temperature structure of the

lithosphere.

REFERENCES

- Albarède, F., Thermal models of post-tectonic decompression as exemplified by the Haut-Allier granulites (Massif Central, France), Bull. Soc. Geol. Fr., 18, 1023-1032, 1976.
- Carslaw, H. S., and J. C. Jaeger, Conduction of Heat in Solids, Clarendon, Oxford, 1959.
- Chung, A., Linear Programming, Charles E. Merrill Books, Columbia, OH, 1963.
- Dantzig, G.B., Computational Algorithm of the Revised Simplex Method, RAND Report RM-1266, The RAND Corporation, Santa Monica, CA, 1953.
- Dantzig, G. B., A. Orden, and P. Wolfe, The Generalized Simplex Method for Minimizing a Linear Form under Linear Inequality Restraints, Pacific J. Math., 5, 183-195, 1955.
- England, P. C., and S. W. Richardson, The influence of erosion upon the mineral facies of rocks from different metamorphic environments, J. Geol. Soc. Lond., 134, 201-213, 1977.
- England, P. C., and A. B. Thompson, Pressure-temperature-time paths of regional metamorphism, Part I: Heat transfer during the evolution of regions of thickened continental crust, J. Petrology, 25, 894-928, 1984.
- Gass, S. I., Linear Programming. Methods and Applications, 5th ed., McGraw-Hill, NY, 1985.
- Hubbard, M. S., Effects of unknowns on thermal history reconstruction of orogenic belts, unpublished manuscript.
- McNutt, M. K., and L. H. Royden, Extremal bounds on geotherms in uplifting and eroding mountain belts from metamorphic pressure-temperature conditions, Geophys. J. R. Astron. Soc., 1987, (in press).
- Orchard-Hays, W., Background, Development, and Extensions of the Revised Simplex Method, RAND Report RM-1433, The RAND Corporation, Santa Monica, CA, 1954.
- Orden, A., Application of the Simplex Method to a Variety of Matrix Problems, in A. Orden and L. Golstein (eds.), Directorate of Management Analysis: Symposium on Linear Inequalities and Programming, DCS/Comptroller, Headquarters, U.S. Air Force, Washington, DC, 1952.
- Oxburgh, E. R., and D. L. Turcotte, Origin of paired metamorphic belts

- and crustal dilation in island arc regions, J. Geophys. Res., 76, 1325-27, 1971.
- Oxburgh, E. R., and D. L. Turcotte, Thermal gradients and regional metamorphism in overthrust terrains with special reference to the Eastern Alps, Schweiz. Miner. Petrogr. Mitt., 54, 641-62, 1974.
- Parsons, B., and J. G. Sclater, An analysis of the variation of ocean floor bathymetry and heat flow with age, J. Geophys. Res., 82, 803-827, 1977.
- Richtmyer, R. D., Difference Methods for Initial Value Problems, Interscience Publishers, NY, 1957.
- Royden, L. H., and K. V. Hodges, A technique for analyzing the thermal and uplift histories of eroding orogenic belts: A Scandinavian example, J. Geophys. Res., 89, 7091-7106, 1984.
- Selverstone, J., Pressure-temperature-time constraints on metamorphism and tectonism in the SW Tauern Window, eastern Alps, Ph.D. Thesis, Massachusetts Institute of Technology, Cambridge, MA, 1985.
- Zienkiewicz, O. C., and K. Morgan, Finite Elements and Approximations, John Wiley, NY, 1983.

APPENDIX A

```

c      This program uses a finite difference approximation to the heat
c      conduction equation to calculate geotherms for all depths and
c      times given an initial geotherm. This program accepts variable
c      uplift rates.
c
c      Parameters are...
c      kappa=thermal conductivity (W/(m-K))
c      alpha=thermal diffusivity (m**2/s)
c      u=uplift (km/Ma) relative to the surface (positive for uplift)
c      dz=depth increment (km)
c      dt=time increment (Ma)
c      nz=number of rows in grid
c      nt=number of columns in grid
c      st=step size for storing Tz points
c      npts=number of points from which initial geotherm is calculated
c      a0=heat productivity of a uniform layer (W/m**3)
c      ar=depth to base of heat producing layer at t=0 (km)
c      hr=scale length for exponential heat function
c
c      Input/Output arrays are...
c      zi(ic)=depth array
c      s(j,k)=temperature(depth,time)
c      a(j,k)=heat production function (W/m**3)
c
c      real kappa,1,12
c      integer ic
c      character hp*1
c      dimension zi(150),s(150,2001),a(150,2001),t(11),varu(2001)
c      dimension u(10),tu(10),arad(5),aps(150,2001),coeff(150)
c      data kappa,alpha /2.5,6.4e-7/
c      data a0 /8.4e-7/
c      open (1,file='gtherm')
c      rewind (1)
c      open (2,file='radheat')
c      rewind (2)
c
c      write (*,*) 'enter depth increment(km)'
c      read (*,*) dz
c      write (*,*) 'enter depth to base of lithosphere(km)'
c      read (*,*) l
c      write (*,*) 'enter temperature at base of lithosphere(degrees C)'
c      read (*,*) tm
c      write (*,*) 'enter time increment(Ma)'
c      read (*,*) dt
c      write(*,*) 'enter number of columns in grid'
c      read (*,*) nt
c      write (*,*) 'enter step size for storing Tz points'
c      read (*,*) st
c      write (*,*) 'enter coefficients for initial geotherm(c1 + c2*zi(j)
c      & + c3*zi(j)*zi(j) + c4*exp(-1.0*zi(j)/c5)'
c      read (*,*) c1,c2,c3,c4,c5
c      write (*,*) 'type of heat production(p=pt source,s=slab,none)'
c      read (*,5) hp
c      5 format (a1)
c
c      ic=0
c      npts=int(l/dz)

```

```

      npts=npts+1
10  do 20 i=1,npts
      ic=ic+1
      zi(ic)=(i-1)*dz
20  continue
c
      write (*,*) 'enter maximum running time(Ma)'
      read (*,*) tmax
      write (*,*) 'enter number of segments of uplift rate curve'
      read (*,*) nu
      write (*,*) 'enter uplift rate(km/Ma) at time t=0'
      read (*,*) u(1)
      nu=nu+1
      do 22 i=2,nu
        write (*,*) 'enter uplift rate(km/Ma)-if on a linear segment of
&the uplift rate curve,enter uplift rate of maximum time'
        read (*,*) u(i)
        write (*,*) 'enter maximum time for this uplift rate'
        read (*,*) tu(i)
22  continue
c
      kountu=2
      do 25 j=2,nt
        time=dt*float(j-1)
        if (time .gt. tmax) go to 25
        if (time .gt. tu(kountu)) kountu=kountu+1
        varu(j)=(u(kountu)-u(kountu-1))/(tu(kountu)-tu(kountu-1))*(time -
& tu(kountu-1)) + u(kountu-1)
25  continue
      varu(1)=u(1)
      print#,(varu(j),j=1,2001,200)
c
c      choose heat production function
c
c      if (hp .eq. 'p') then
c
c      write (*,*) 'enter number of point sources'
      read (*,*) nps
c
c      initialize heat production for point source
c
      do 85 n=1,nps
        write (*,*) 'enter depth of point source'
        read (*,*) arad(n)
        if (varu(1) .eq. 0) then
          do 30 m=2,ic
            if (arad(n) .lt. zi(m)) h=0
            if (arad(n) .ge. zi(m)) h=1
            aps(m,1)=-1.0*(arad(n)-zi(m))*h + arad(n)*(1-zi(m))/1
            aps(m,1)=(a0*dz/kappa)*1.0e6*aps(m,1)
            a(m,1)=a(m,1) + aps(m,1)
30          continue
        else
c      r=dimensionless Peclet number
        r=(varu(1)/3.15576e7)*1/(2.0*alpha)
        bh=exp(-2.0*r)
        cc=1./(1.-bh)
        cc2=cc**2

```

```

      do 40 m=2,ic
        aa=exp(-2.*r*zi(m)/l)
        if (arad(n) .lt. zi(m)) h=0
        if (arad(n) .ge. zi(m)) h=1
        aps(m,1)=-1.*(arad(n)-zi(m))*h + arad(n)*(aa-bb)*cc
      &      +zi(m)*(bb+aa)*cc + 2.*l*bb*(aa-1.)*cc2
        aps(m,1)=(a0*dz/kappa)*1.e6*aps(m,1)
        a(m,1)=a(m,1) + aps(m,1)
    40    continue
      endif

c
c      calculate heat production for all time for point source
c
c      adt1=dt*3.15576e13
      adz1=dz*1.0e3
      a1=alpha*adt1/adz1**2
      a3=(alpha*adt1*a0/kappa)
      do 80 k=2,nt
        a2=0.5*varu(k)*dt/dz
        zrad=arad(n)-float(k-1)*varu(k)*dt
        if (zrad .lt. 0) zrad=0
        az=ic-1
        call coef(az,zrad,dz,zi,coeff)
        do 70 j=2,az
          aa3=a3*coeff(j)
          aps(j,k)= aps(j,k-1) + a1*(aps(j+1,k-1) - 2.*aps(j,k-1)
      &      + aps(j-1,k-1)) + a2*(aps(j+1,k-1) - aps(j-1,k-1)) + aa3
          a(j,k)=a(j,k) + aps(j,k)
    70    continue
    80    continue
    85    continue

c
c      elseif (hp .eq. 's') then
c
c      layer of uniform heat production
c      initialize heat production for slab model
c
c      write (*,*) 'enter depth to base of slab(km)'
      read (*,*) ar
      ar=ar/l
      l2=l*l*1.0e6
      if (varu(1) .eq.0) then
        do 86 j=2,ic
          z=zi(j)/l
          if (ar .lt. z) h=0
          if (ar .ge. z) h=1
          a(j,1)=-0.5*((ar-z)**2)*h + 0.5*ar*ar*(1-z)
          a(j,1)=(a0*l2/kappa)*a(j,1)
    86    continue
        else
c      r=dimensionless Peclet number
          r=(varu(1)/3.15576e7)*l/(2.*alpha)
          bb=exp(-2.*r)
          cc=1./(1.-bb)
          cc2=cc*cc
          cc3=cc2*cc
          do 87 j=2,ic
            aa=exp(-2.*r*zi(j)/l)

```

```

      z=zi(j)/l
      if (ar .lt. z) h=0
      if (ar .ge. z) h=1
      a(j,1)=-0.5*((ar-z)**2)*h - 0.5*ar*ar*(bb-aa)*cc
&          + ar*z*(bb+aa)*cc - 0.5*z*z*(bb-aa)*cc
&          + 0.5*z*(bb+aa)*cc/r - 2.0*ar*bb*(1.0-aa)*cc2
&          + 2.0*z*bb*(1.0+aa)*cc2 - bb*(1.0-aa)*cc2/r
&          - 2.0*bb*(1.0+bb)*(1.0-aa)*cc3
      a(j,1)=(a0*I2/kappa)*a(j,1)
87  continue
endif

c
c calculate heat production for all time for slab
c

ad1=dt*3.15576e13
adz1=dz*1.0e3
ar=ar*I
a1=alpha*adt1/adz1**2
a3=alpha*adt1*a0/kappa
do 89 k=2,nt
a2=0.5*varu(k)*dt/dz
zrad=ar-float(k-1)*varu(k)*dt
if (zrad .lt. 0) zrad=0
az=ic-1
do 88 j=2,az
  if (zi(j) - 0.5*dz .gt. zrad) h=0
  if (zi(j) - 0.5*dz .le. zrad .and. zi(j) + 0.5*dz .ge. zrad)
&    h=(zrad - zi(j) + 0.5*dz)/dz
  if (zi(j) + 0.5*dz .lt. zrad) h=1
  a(j,k)= a(j,k-1) + a1*(a(j+1,k-1) - 2.*a(j,k-1) + a(j-1,k-1))
&        + a2*(a(j+1,k-1) - a(j-1,k-1)) + a3*h
88  continue
89  continue

c
elseif (hp .eq. 'n')then
  a0=0.0
endif

c
c initialize geotherm
c
90 do 100 j=1,ic
c   s(j,1)=1350
c   s(j,1)=222.0+9.4*zi(j)-168.0*exp(-1.0*zi(j)/10.0)
c   s(j,1)=c1 + c2*zi(j) + c3*zi(j)*zi(j) + c4*exp(-1.*zi(j)/c5)
c   if (zi(j) .lt. 32) then
c     s(j,1)=10*zi(j)
c   else
c     s(j,1)=15*zi(j) - 480
c     if (zi(j) .le. 60) then
c       s(j,1)=10*zi(j)
c     else
c       s(j,1)=22.5*zi(j) - 1350
c     endif
100  continue

c
c reset s(1,1) to zero
s(1,1)=0.0

```

```

c      reset initial geotherm to desired geotherm in the event of a
c      radioactive heat contribution
c
      do 110 j=2,ic
110    s(j,1)=s(j,1) - a(j,1)
c
c      geotherm at base of lithosphere(z=1) equals Tm for all time
c
      do 130 k=1,nt
120    s(ic,k)=tm
130    continue
c
c      calculate geotherms for all depths and times
c
      dt1=dt*3.15576e13
      dz1=dz*1.0e3
      b1=alpha*dt1/dz1**2
      nz=ic-1
      do 160 k=2,nt
        b2=0.5*varu(k)*dt/dz
      do 150 j=2,nz
        s(j,k)=s(j,k-1)+b1*(s(j+1,k-1)-2.*s(j,k-1)+s(j-1,k-1))+
&          b2*(s(j+1,k-1)-s(j-1,k-1))
150    continue
160    continue
      do 162 k=1,nt
      do 161 j=1,ic
        s(j,k)=s(j,k)+a(j,k)
161    continue
162    continue
      write (2,*) 'T(z=1)=',s(ic,nt)
      write (2,*) 'l=',l
      write (2,*) 'hp=',hp
      do 165 i=1,nt,st
        t(i)=dt*float(i-1)
165    continue
      write (2,166) (t(i),i=1,nt,st)
166    format (7x,11f8.2)
      write (2,167) (varu(i),i=1,nt,st)
167    format (2x,'varu',1x,11f8.2,/)
      do 180 j=1,ic
        write (2,171) zi(j), (a(j,k),k=1,nt,st)
171    format (1x,f5.1,1x,11f8.2)
180    continue
      write (1,*) 'T(z=1)=',s(ic,nt)
      write (1,*) 'l=',l
      write (1,*) 'hp=',hp
      write (1,181) (t(i),i=1,nt,st)
181    format (7x,11f8.2)
      write (1,182) (varu(i),i=1,nt,st)
182    format (2x,'varu',1x,11f8.2,/)
      do 200 j=1,ic
        write (1,191) z (j), (a(j,k),k=1,nt,*)
191    format (1x,f5.1,1x,11f8.2)
200    continue
      close (1)
      close (2)
      stop
      end

```

```
r   **subroutine coef**  
c  
   subroutine coef(az,zrad,dz,zi,coeff)  
     dimension zi(150),coeff(150)  
     do 5 j=1,az  
       coeff(j)=0.0  
5    continue  
     if (zrad .eq. 0.0) go to 20  
     do 10 j=1,az  
       if (zi(j) - 0.5*dz .gt. zrad) then  
         coeff(j)=0.0  
       elseif (zi(j) + 0.5*dz .lt. zrad) then  
         coeff(j)=0.0  
       elseif (zi(j) - 0.5*dz .le. zrad .and. zi(j) .ge. zrad) then  
         if (j-1 .ne. 0) coeff(j-1)=(zi(j)-zrad)/dz  
         if (j-1 .ne. 0) coeff(j)=1.0 - coeff(j-1)  
         if (j-1 .eq. 0) coeff(j)=(zrad - zi(j))/dz  
       elseif (zi(j) .le. zrad .and. zi(j) + 0.5*dz .ge. zrad) then  
         coeff(j)=1.0 - (zrad - zi(j))/dz  
         coeff(j+1)=1.0 - coeff(j)  
         j=j+1  
       endif  
10    continue  
20    return  
     end
```

ACKNOWLEDGEMENTS

This research was supported by a National Science Foundation Graduate Fellowship and a NASA geodynamics grant.